

Redshift of photons penetrating a hot plasma

Ari Brynjolfsson ^{*}

Applied Radiation Industries, 7 Bridle Path, Wayland, MA 01778, USA

Abstract

A new interaction is derived, which is important only when photons penetrate a hot, sparse electron plasma. When photons penetrate a cold and dense electron plasma, they lose energy through ionization and excitation, through Compton scattering on the individual electrons, and through Raman scattering on the plasma frequency. But when the plasma is very hot and has low density, such as in the solar corona, the photons lose energy also in a newly derived collective interaction with the electron plasma. This energy loss per cm of a photon's path is about $\hbar\omega(\Phi_C/2)N_e$, where $\hbar\omega$ is the photon energy, Φ_C the Compton cross section and N_e the electron density. This energy loss ("plasma redshift" of the photons) consists of very small quanta, which are absorbed by the plasma and cause significant heating. In quiescent solar corona, this heating starts in the transition zone to the solar corona and is a major fraction of the coronal heating. Plasma redshift also contributes to the heating of interstellar plasma and to the galactic corona. It explains the solar redshift, the galactic corona, the cosmological redshift, and the cosmic microwave background. Plasma redshift also leads to repulsion of photons in a gravitational field and, thereby, causes fundamental changes in the theory of general relativity.

Keywords: Plasma, redshift, heating of solar corona, solar redshift, gravitational redshift, galactic corona, intergalactic matter, cosmological redshift, cosmic microwave background.

PACS: 52.25.Os, 52.40.-w, 97.10.Ex, 04.60.-m, 98.80.Es, 98.70.Vc

Contents

1	Introduction	2
2	Energy loss of photons as they penetrate a plasma	3
3	Damping factor β and the cut-off wavelength	5
4	Effect of magnetic fields	8
5	Comparing plasma-redshift theory with experiments	10
5.1	Transition zone to solar corona and the region of spicules	10
5.2	Solar corona	13
5.3	Solar wind	17
5.4	Far-reaching solar streamers	20
5.5	Solar flares	20
5.6	Plasma redshift of spectral lines and gravitational redshift	22
5.6.1	Plasma redshift of solar Fraunhofer lines	22
5.6.2	Gravitational redshift	26
5.6.3	Results of solar redshift experiments compared with theory	29
5.6.4	Redshifts of stars	31
5.7	Galactic corona	31
5.8	Cosmological redshift	40
5.9	Cosmic microwave background radiation	43

^{*}Corresponding author: aribrynjolfsson@comcast.net

6	Repulsion of photons	47
7	Possible future experiments	50
8	Summary and conclusions	51

1 Introduction

Compton scattering consists of scattering of one incident photon on one electron, and it results in only one out-going photon. Its cross section is about $\Phi_C = 6.65 \cdot 10^{-25} \text{ cm}^2$. Only a very small amount of recoil energy is transferred to the electron. Double Compton scattering consists of one incident photon scattered on one electron and results in two out-going photons. The cross section is very small, or about $\Phi_C/137$. ‘Multiple Compton scattering’ is also very small and consists of one incident photon scattered on one electron and results in multiple (three or more) out-going photons. Both double and multiple Compton scattering cross sections are quantum mechanical effects, and could not be deduced in classical physics. Coherent scattering on the electrons of atoms is usually called Rayleigh scattering when the initial and final states of the electrons are the same. But if the initial and final electronic states differ, the corresponding incoherent scattering is often called either Raman scattering or Stokes scattering. All these processes are well known, and not a subject of this article. When the photons scatter on the plasma electrons in thermal equilibrium, the redshifts produced by these processes are small and usually insignificant. If the scattering electron moves relative to the observer, we get a Doppler shift, but that does not change the nature of the interactions.

The plasma-redshift theory, deduced in this article, distinguishes itself from all the processes mentioned above. It is about the interaction of one incident photon with great many electrons in the plasma. The theory for this scattering has never been dealt with before. The plasma redshift is related to ‘double Compton scattering’ and ‘multiple Compton scattering’, but it distinguishes itself from these processes, because it is a new multiple scattering process on a great many electrons (not only one electron, as in double and multiple Compton scattering). Although incoherent, it is not related to Raman scattering, or incoherent scattering on the plasma frequency. The plasma redshift can usually be deduced using classical physics methods, but it requires quantum mechanics to derive the relevant damping. If classical physics damping were used, the cross section would be zero.

In Compton scattering, an incident photon with wavelength of 500 nm transfers energy of about $1.6 \cdot 10^{-30} h\nu$ to the plasma per electron. The corresponding energy transferred to the plasma in the plasma redshift is about 200,000 times larger, or $3.3 \cdot 10^{-25} h\nu$ per electron. Compared with heating by Compton scattering, the heating by plasma redshift is very large and important for explaining the heating of the solar corona, the corona of galaxies and the intergalactic plasma. This interaction is very important although it has been overlooked in the past.

Heitler (see, in particular, Sections 23 and 33 of [1]) has shown that when one of the photons emitted in ‘double Compton scattering’ (or ‘multiple Compton scattering’) is far in the infrared, the cross section becomes large and approaches infinity as infrared photon energy approaches zero. When higher order effects are taken into account, Heitler found the integrated cross section to be finite. Gould [2] has made refined calculations with essentially the same result. Their result is based on the assumption that the photon interacts with only one electron. However, when one of the outgoing infrared photons is far in the infrared, the interaction in a hot, sparse plasma involves many electrons. Collective effects are then very important and make this cross section much larger and significant in hot, sparse plasmas, such as those in the coronas of stars, while it is insignificant in cold, dense laboratory plasmas and in the denser and colder chromospheres of stars. The fact that this cross section is usually insignificant is likely the reason that it has been overlooked.

In the hot, sparse plasmas of stars’ coronas, the electrons keep each other at distances, which are very long compared with their de Broglie wavelengths. The exchange effects, which play a role only over distances shorter or comparable to the de Broglie wavelength, are therefore of little or no importance in the hot, sparse plasmas that we are dealing with in the following discussion. Within reasonable boundaries all the electrons have different energy levels. The quantum numbers of angular

moments in the interactions between the electrons are large. We may, therefore, treat these sparse and hot plasmas either quantum mechanically or semiclassically. The quantum-mechanical equation for polarization of the plasmas by light is for $\hbar\omega \ll m_e c^2$ identical with the semiclassical equation.

In Section 2, we deduce the cross section for the redshift in a plasma free of magnetic fields. Some of the details of the theory are shown in Appendix A. The cross section for the plasma redshift depends on the photon width and the damping in the plasma. In Section 3, we elaborate on how the damping in the electron plasma varies with plasma temperature, and how the damping and the density affect both the coherence effects and the cross section for the plasma redshift of photons penetrating the plasma. It is shown how the plasma redshift varies with the wavelength, plasma temperature, and plasma density. Only when the wavelength is less than a certain cut-off wavelength, which depends on the plasma temperature and the plasma density, is the plasma redshift significant. In Section 4, we give examples of how the magnetic field affects the plasma redshift and the cut-off wavelength for the redshift. This is especially important for explaining some of the phenomena in the Sun, such as the flares, loops and arches. Also important for explaining the phenomena is the theory for transforming magnetic field energy to heat. This theory is developed in Appendix B. The transformation is often initiated and accelerated by the plasma-redshift heating. In Sections 5.1 to 5.9, we compare the plasma-redshift theory with observations in the Sun, Milky Way, and intergalactic space. These comparisons lead to fundamental changes in the theory of general relativity, as well as in the cosmological perspective. The changes in the theory of general relativity include a repulsion of photons in a gravitational field, and a significant modification of the equivalence principle. Independent evidences for the consequences of photons' repulsions are discussed in Section 6. The changes in the cosmological perspective include replacing the "Big Bang" model (or the standard model) with a seemingly static model, because the plasma redshift leads to a hot intergalactic plasma, which can explain the entire cosmological redshift and the microwave background. Furthermore, the repulsion of photons by the gravitational field makes it possible that the universe is seemingly static without Einstein's Lambda term. In Section 7, we suggest additional experiments for confirming the findings. In Section 8, we give a summary and conclusions.

2 Energy loss of photons as they penetrate a plasma

For a photon's field moving along the x-axis, we can at x equal to 0 normalize the Poynting vector, S , to the energy flux of one photon, $\hbar\omega_0 = h\nu_0$, per second and per square cm in vacuum, where h is the Planck constant. Even in a vacuum, the photon is never infinitely sharp but consists of a distribution of frequency components as indicated by

$$S = \hbar\omega_0 = \hbar\omega_0 \frac{\gamma}{2\pi} \int_{-\infty}^{\infty} \frac{d\omega}{((\omega - \omega_0)^2 + \gamma^2/4)}, \quad (1)$$

where γ is the photon width [1]. When the photon penetrates a plasma, the photon's virtual field will be modified by the dielectric constant $\varepsilon = (n - i\kappa)^2$, where n is the refraction index, κ the absorption coefficient, and i the notation for the imaginary component. From Eq. (A12) of Appendix A, we derive for the binding-energy frequency $\omega_q = 0$ and the collision damping $\alpha = 0$ that

$$\varepsilon = \left(1 - \frac{\omega_p^2}{\omega^2 + \beta^2\omega^4}\right) - i\frac{\beta\omega\omega_p^2}{\omega^2 + \beta^2\omega^4}, \quad (2)$$

where $\omega_p = \sqrt{4\pi e^2 N_e / m_e}$ is the plasma frequency, and where $\beta\omega^2$ is the radiation damping in the hot sparse plasma.

We set the magnetic permeability equal to 1. As shown in Eq. (A21) of Appendix A, we get from Eq. (1) and Eq. (2) at distance x that

$$S = \hbar\omega_0 \frac{\gamma}{2\pi} \int_{-\infty}^{\infty} \frac{n}{\varepsilon\varepsilon} \frac{[\exp(-2\kappa\omega x/c)] d\omega}{(\gamma^2/4 + (\omega - \omega_0)^2)}, \quad (3)$$

where $\bar{\varepsilon}$ is the complex conjugate of ε .

We differentiate this expression with respect to x and get that the photon's energy loss per cm is given by

$$\frac{dS}{dx} = -\frac{\hbar\omega_0\gamma}{2\pi c} \int_{-\infty}^{\infty} \frac{2\kappa\omega n}{\varepsilon\bar{\varepsilon}} \frac{[\exp(-2\kappa\omega x/c)] d\omega}{\left(\gamma^2/4 + (\omega - \omega_0)^2\right)}.$$

For x equal to 0, the energy loss per cm is then

$$\frac{dS}{dx} = -\frac{\hbar\omega_0\gamma}{2\pi c} \int_{-\infty}^{\infty} \frac{2\kappa\omega n}{\varepsilon\bar{\varepsilon}} \frac{d\omega}{\left(\gamma^2/4 + (\omega - \omega_0)^2\right)}. \quad (4)$$

From Eq. (2), we derive that

$$\frac{2\kappa\omega}{\varepsilon\bar{\varepsilon}} = \frac{\beta\omega^4\omega_p^2}{(\omega_p^2 - \omega^2)^2 + \beta^2\omega^6},$$

and when we insert this expression into Eq. (4), we get that the photon's energy loss per cm

$$\frac{dS}{dx} = -\frac{\hbar\omega_0\gamma}{2\pi c} \int_{-\infty}^{\infty} \frac{\beta\omega_p^2\omega^4}{\left[(\omega_p^2 - \omega^2)^2 + \beta^2\omega^6\right]} \frac{d\omega}{\left[\gamma^2/4 + (\omega - \omega_0)^2\right]}. \quad (5)$$

The right side of Eq. (5) can be integrated in the complex plane along the x-axis from $-\infty$ to $+\infty$ and then counterclockwise along the semicircle in the upper half plane. The integral along the semicircle is zero. The integral in Eq. (5) is then equal to $2\pi i$ times the sum of the residue of the poles in the upper half-plane, where i is the notation for the imaginary component. For

$$\omega_q = 0, \quad \alpha = 0, \quad \beta \gg \beta_0, \quad \omega_0 \gg \omega_p, \quad \beta\omega_p \ll 1, \quad \gamma \ll \omega_0,$$

the four poles in the upper plane are given by (see Eq. (A25) of Appendix A)

$$\omega = \left\{ \begin{array}{l} a = +\omega_p + i\frac{\beta\omega_p^2}{2} \\ b = -\omega_p + i\frac{\beta\omega_p^2}{2} \\ c = \quad \quad + i\frac{1}{\beta} \left[1 + (\beta\omega_p)^2 \right] \\ d = +\omega_0 + i\frac{\gamma}{2} \end{array} \right\}. \quad (6)$$

From Eqs. (5) and (6), we get that

$$\frac{dS}{dx} = -\hbar\omega_0 \frac{8\pi}{3} r_e^2 N_e \left[\frac{\gamma}{4\gamma_0} + \frac{\gamma}{4\gamma_0} + \frac{\gamma}{2\gamma_0} \cdot \frac{\left(1 - 1/(\beta\omega_0)^2\right)}{\left(1 + 1/(\beta\omega_0)^2\right)^2} + \frac{1}{\left(1 + (\beta_0\omega_0)^2\right)} \right], \quad (7)$$

where $\beta_0\omega_p^2/c = (8\pi/3) r_e^2 N_e = 6.65 \cdot 10^{-25} N_e$ is the Compton cross section per cm of photon path when N_e is the electron density per cubic cm, and where $\beta_0 = 2e^2/(3m_e c^3) = 6.266 \cdot 10^{-24}$ is the classical damping constant and $\gamma_0 = \beta_0\omega_0^2$ the classical damping for the incident photon.

The last term inside the brackets, corresponding to the pole d in Eq. (6), is identical to the quantum mechanical Compton scattering cross section for soft photons [1]. In the Compton scattering, we set damping constant equal to the classical damping constant and the dielectric constant equal to 1, because in the sparse plasmas of our interest the incident photon interacts with only one electron.

The two first terms inside the brackets, correspond to the poles a and b in Eq. (6). These poles correspond to Raman scattering on the plasma frequency, ω_p . In the treatment above, the oscillator

strengths are positive as we assumed that they were in the ground state. In the actual hot plasma of our interest the plasma oscillators are usually in thermodynamic equilibrium, and we have then about equal number of positive and negative oscillator strengths. In thermodynamic equilibrium the emission and absorption cancel each other. Nevertheless, these interactions cause small angular scatterings, which are insignificant in practically all experiments of our interest, because the densities of the plasmas of our interest are usually very low. However, they can affect the observations of most distant supernovas.

The third term inside the brackets, the plasma-redshift term, corresponds to pole c, the pole on the imaginary axis. The plasma-redshift term is a new cross section term and the focus of our interest in this article. It is due to loss (emission and absorption) of very low frequency components in the photon field. This cross section has been overlooked in the past, most likely because when the damping factor β in the radiation damping, $\beta\omega_0^2$, is close to the classical value β_0 , as it is in an ordinary laboratory plasma, this third term is practically zero and the cross section insignificant. However, in a hot, sparse plasma both the damping factor and the collective effects are very large; and this plasma-redshift term becomes significant. As mentioned in the introduction, this term is also related to the emission of very soft quanta in double and multiple Compton scattering. The classical mechanics cannot treat properly the radiation damping terms. We must therefore use quantum mechanics to determine the damping. It then can be seen that β can be very large in a hot, sparse plasma. In the third term inside the brackets of Eq. (7), the value of $1/(\beta\omega_0)$ is then very small. The plasma-redshift cross section becomes then equal to $3.326 \cdot 10^{-25} (\gamma/\gamma_0) N_e$ per cm of the photon path. In the following Section 3, we will see how β changes with temperature and density of the plasma, and with the wavelength of the incident light.

3 Damping factor β and the cut-off wavelength

For the electrons in a hot plasma the Hamiltonian is

$$H_0 = H_0^0 + \frac{1}{2}m_e\omega_q^2\bar{r}r = -\frac{\hbar^2}{2m_e}\nabla^2 + \frac{1}{2}m_e\omega_q^2\bar{r}r, \quad (8)$$

where ω_q is principally any frequency in the plasma and r is given by Eq. (A7). The plasma frequency ω_p is the dominant frequency, however, and we will usually replace ω_q by ω_p . This non-relativistic Hamiltonian does not take into account the effects of magnetic fields, which will be treated subsequently.

The solutions corresponding to the Hamiltonian given by Eq. (8) are well known. The energy levels when we include the finite lifetime of the states are

$$E_\Lambda = E_{n,l} = \left(\Lambda + \frac{3}{2}\right)\hbar\left(\omega_q - i\frac{\beta\omega_q^2}{2}\right), \quad (9)$$

where $\Lambda = 2n + l$ and where n and l can be any of the whole numbers: 0, 1, 2, .., .. The imaginary part of the frequency is included to indicate the finite lifetime of the states and the magnitude of the damping. In the case of magnetic fields, we must, in addition to the radial quantum number n and the angular quantum number l , take into account the third quantum number m .

When the magnetic field is zero, the states are degenerate; that is, several states can have the same energy for $\Lambda \geq 1$. For example, for the states $\Lambda = 4$, we have $(n, l) = (2, 0), (1, 2)$, or $(0, 4)$. These three states in turn have the multiplicity of 1, 5, and 9, respectively, for a total of 15 states. More generally, for each quantum number Λ , the total number of states is $(\Lambda + 1)(\Lambda + 2)/2$, all with the same energy.

The radiation-damping factor β may deviate significantly from the classical value β_0 . In the transitions from a state Λ to all final states, the energy emitted is given by

$$\begin{aligned} I(\omega_q) &= \hbar\omega_q A_{n,l} = \frac{4e^2\omega_q^4}{c^3} \frac{\hbar}{2m_0\omega_q} \left[\frac{n_x + n_y + n_z}{3} \right] \\ &= \hbar\omega_q \frac{2e^2\omega_q^2}{3m_0c^3} \Lambda = \hbar\omega_q \Lambda \beta_0 \omega_q^2 = \hbar\omega_q \beta \omega_q^2, \end{aligned} \quad (10)$$

Table 1 $F_1(a)$ as a function of a , see Eq. (14).

a	$F_1(a)$	a	$F_1(a)$	a	$F_1(a)$	a	$F_1(a)$
0.0	1.000	1.0	0.571	2.0	0.228	6.0	-0.070
0.1	0.990	1.1	0.527	2.2	0.183	7.0	-0.073
0.2	0.962	1.163	0.500	2.4	0.144	8.0	-0.071
0.3	0.921	1.2	0.485	2.6	0.111	9.0	-0.067
0.344	0.900	1.3	0.445	2.671	0.100	10.0	-0.061
0.4	0.872	1.4	0.407	2.8	0.082	20.0	-0.024
0.5	0.821	1.5	0.372	3.0	0.057	40.0	-0.0071
0.6	0.769	1.6	0.339	3.5	0.010	50.0	-0.0047
0.7	0.717	1.7	0.309	3.633	0.000	100.0	-0.0012
0.8	0.667	1.8	0.280	4.0	-0.022	200.0	-0.0008
0.9	0.618	1.9	0.253	5.0	-0.057	∞	-0.0000

where $\beta = \Lambda\beta_0$ can be very large. In hot plasmas, practically all the oscillators are highly excited. Their average Λ values are about $\Lambda = 3kT/(\hbar\omega_q)$, and Einstein's A coefficients, $A_{\Lambda \rightarrow \Lambda-1} = \beta\omega_q^2 = \Lambda\beta_0\omega_q^2$, are therefore large. The radiation loss given by the redshift term in Eq. (7) then becomes relatively large and significant. In good plasmas ω_p is the dominant frequency and we can therefore replace ω_q by ω_p .

For evaluating the value of this redshift term we need to average it over all states in the hot plasma. The number of possible states in a hot plasma with quantum number Λ is

$$g_\Lambda = \frac{(\Lambda+1)(\Lambda+2)}{2} \approx \frac{\Lambda^2}{2}. \quad (11)$$

The statistical energy distribution of the oscillators in thermal equilibrium is given by

$$n_\Lambda = \frac{g_\Lambda}{\exp(\alpha + \Lambda\hbar\omega_p/(kT)) - 1} \approx \frac{g_\Lambda \exp(-\alpha)}{\exp(\Lambda\hbar\omega_p/(kT))}. \quad (12)$$

The last approximation is valid because $\exp(\alpha)$ is very large in hot and sparse plasmas, which in turn means that the Boltzmann, Fermi-Dirac, and Bose-Einstein statistics all render the same result. The normalized distribution function for the oscillator strengths is then given by

$$P(n_\Lambda) d\Lambda = \left(\frac{\hbar\omega_p}{kT}\right)^3 \frac{\Lambda^2}{2} \exp\left(-\frac{\Lambda\hbar\omega_p}{kT}\right) d\Lambda. \quad (13)$$

The cut-off frequency for the plasma redshift can be determined by weighing the third term inside the brackets of Eq. (7) by the normalized distribution function, Eq. (13). For $\beta\omega_0 = \Lambda\beta_0\omega_0 = x$, and $a = \hbar\omega_p/(\beta_0\omega_0 kT) = 3.65 \cdot 10^5 \lambda_0 \sqrt{N_e}/T$, we get

$$F_1(a) = a^3 \int_0^\infty \frac{(x^2 - 1)}{(x^2 + 1)^2} \frac{x^4}{2} \exp(-ax) dx. \quad (14)$$

The numerical values for this function are shown in Table 1.

The redshift is proportional to $\Delta N_2 = N_e F_1(a)$, which is thus a measure of the oscillator strength of the redshift term, the third term inside the brackets in Eq. (7). Table 1 shows that $F_1(a)$ is close to 1 for small values of a , or for small wavelengths in cm given by

$$\lambda_0 = \frac{c}{\nu_0} = 2.74 \cdot 10^{-6} a \frac{T}{\sqrt{N_e}}. \quad (15)$$

From Table 1, we can find the oscillator strength for a given value of a . For example, for a less than or equal to 1.163, the oscillator strength is 50% or more of the maximum oscillator strength,

N_e , if the wavelengths $\lambda \leq \lambda_{0.5}$, where the 50% cut-off wavelength in cm, $\lambda_{0.5}$, for the redshift is determined by inserting 1.163 for a into Eq. (15). We get

$$\lambda_{0.5} = 2.74 \cdot 10^{-6} \cdot 1.163 \frac{T}{\sqrt{N_e}} = 3.18 \cdot 10^{-6} \frac{T}{\sqrt{N_e}}. \quad (16)$$

The 90% and 10% oscillator strengths are obtained for a equal to 0.344 and 2.671, respectively. The corresponding 90% and 10% cut-off wavelengths are obtained by inserting the corresponding values for a into Eq. (15).

When we in Eq. (7) replace dS by $d\hbar\omega$ and focus on the redshift term, the third term within the brackets, while disregarding the first, second, and fourth term within the brackets, we get

$$-\frac{d\hbar\omega}{\hbar\omega} = \frac{4\pi}{3} r_e^2 N_e \frac{\gamma}{\gamma_0} \frac{1 - 1/(\beta\omega)^2}{\left(1 + 1/(\beta\omega)^2\right)^2} dx. \quad (17)$$

We weigh the oscillator strength by Eq. (13), which results in Eq. (14). When we then integrate each side and set $\lambda - \lambda_0 = \Delta\lambda$, we get

$$-\int_{\omega_0}^{\omega} \frac{d\omega}{\omega} = \ln\left(\frac{\omega_0}{\omega}\right) = \ln\left(1 + \frac{\Delta\lambda}{\lambda_0}\right) \approx \frac{\Delta\lambda}{\lambda_0} = 3.326 \cdot 10^{-25} \int_0^R F_1(a) \frac{\gamma}{\gamma_0} N_e dx. \quad (18)$$

The approximation $\ln(1 + \Delta\lambda/\lambda) \approx \Delta\lambda/\lambda = z$ is valid only for small redshifts z , such as those in the Sun and most stars, while for large cosmological redshifts and quasars' redshifts, we must use the logarithmic expression.

Once the redshift is initiated in the cut-off region in the plasma, the redshift heating (due to absorption of the far infrared components of the photon) causes relatively rapid temperature increase and density decrease. Below 50% cut-off for a given wavelength in the transition zone, the oscillator strength function in Eq. (14) is less than 50% and above this cut-off it is more. By averaging, we can often for each wavelength set the oscillator strength function equal to 1 above the 50% cut-off and equal to zero below the 50% cut-off.

In the middle of the transition zone to the solar corona, we may have (see the discussion in Section 5.1 and Vernazza et al. [3]) that the temperature is equal to 500,000 K and the value of $T N_e \approx 5 \cdot 10^{14} \text{ K cm}^{-3}$. From Eq. (16) we get for these values that the 50% cut-off wavelength is 500 nm; that is, photons with wavelength shorter than 500 nm will be redshifted more than 50% of the maximum redshift. Above the cut-off limit the temperature usually increases sharply and the density continues to decrease until, usually, the entire solar spectrum is redshifted. For a quiescent corona, detailed analysis shows that above the cut-off limit for the main portion of the solar spectrum the redshift heating exceeds the x-ray and recombination cooling, causing the temperature to increase to about two million degrees (see Sections 5.1 and 5.2). Below this maximum temperature, a significant fraction of the heating leaks by conduction into the transition zone and helps compensate the recombination cooling. For shorter frequencies, the cut-off zone penetrates deeper into the transition zone. For example, for the same pressure or the same product of temperature and density, and for the 50% cut-off wavelength equal to 121.5 nm, the cut-off zone is at a temperature of about 200,000 K.

Different effects, including collisions' effects, broaden the photon width. For example, at the center of the solar disk, the measured photon-width, $\gamma = \gamma_i$, of the Na I 589.592 nm resonance-line is about 20 times the classical width, γ_0 , which in this case is about equal to the quantum mechanical width of the photons from the undisturbed sodium atom. However, we also have that when a photon penetrates and interacts with the electron plasma, the photon's initial width should approach the photon width, γ_0 , which is the natural quantum mechanical and classical width of photons interacting with an electron plasma. We do not know exactly how fast the redistribution takes place or how fast the photon width approaches the classical width; but we assume that the small incremental change in the width is proportional to the difference in the actual width and the

final classical width and proportional to the plasma redshift. We set

$$d\gamma = -\xi \frac{(\gamma - \gamma_0) \omega}{\gamma_0} \frac{4\pi r_e^2}{3} N_e dx, \quad (19)$$

where $\gamma_0 = \beta_0 \omega^2 = 6.266 \cdot 10^{-24} \omega^2$ is the classical width as well as the quantum mechanical width of photons penetrating and interacting with the electron plasma. In Eq. (19), ξ is an adjustment factor, and its value is to be determined experimentally. (When we have a better theory for the forces within the photon, we may be able to determine this factor theoretically, but at this stage we suggest that it be determined experimentally. A rough estimate for the resonance line of Na-I in the Sun indicates that ξ is about 0.25). From Eq. (19) we determine γ as a function of x , and insert that value into Eq. (18). For oscillator strength function $F_1(a)$ equal to 1, Eq. (18) takes the form

$$\frac{\Delta\lambda}{\lambda} \approx 3.326 \cdot 10^{-25} \int_0^R N_e dx + \frac{\gamma_i - \gamma_0}{\xi \omega}, \quad (20)$$

where γ_i is the initial photon width and γ_0 is the final photon width. The latter term in Eq. (20) is usually a small correction to the first term.

4 Effect of magnetic fields

In Sections 2 and 3, we disregarded magnetic fields mainly because exact calculations that include their effects lead to significant complications. Had we included the magnetic fields from the start, we might have lost sight of the simplicity and basic nature of the plasma redshift. When the photon's polarization is in the direction of the magnetic field, the dielectric constant is largely unchanged; however, when it is in a plane perpendicular to the magnetic field, the dielectric constant is affected significantly. Polarization produced by an external force in one direction may then cause a force on the charge in other directions. The isotropic dielectric constant can be replaced by an anisotropic dielectric tensor. This tensor complicates the mathematical treatment. We must then solve Maxwell's equations together with the constitutive relations for current and magnetization in three dimensions.

We are mainly interested in phenomena involving exchange of small energy quanta or low frequencies. From Maxwell equations and plane wave equations for the fields, we derive the homogeneous wave equation $\mathbf{k} \times (\mathbf{k} \times \mathbf{e}) + k_0^2 \varepsilon \mathbf{e} = 0$, where \mathbf{k} is the wave vector, \mathbf{e} the polarization vector of the electromagnetic wave and ε is the dielectric tensor (see, for example, Sturrock 1994 [4]). The dispersion relation for waves propagating parallel to the magnetic field in the z direction is

$$\begin{vmatrix} \varepsilon_{xx} - k^2/k_0^2 & \varepsilon_{xy} & \varepsilon_{xz} \\ \varepsilon_{yx} & \varepsilon_{yy} - k^2/k_0^2 & \varepsilon_{yz} \\ \varepsilon_{zx} & \varepsilon_{zy} & \varepsilon_{zz} \end{vmatrix} = 0. \quad (21)$$

Due to the rotational symmetry and definition of the axes, and because an electric field when in the direction of the z -axis produces no coupling to the other axes, we have that: $\varepsilon_{xx} = \varepsilon_{yy}$, $\varepsilon_{xy} = -\varepsilon_{yx}$, $\varepsilon_{xz} = \varepsilon_{zx} = 0$, and $\varepsilon_{yz} = -\varepsilon_{zy} = 0$. In the very long wavelength limit, we make the approximation that the wave vector k is independent of the dielectric constant. We can then write the dielectric tensor on the form

$$\begin{Bmatrix} 1 - \frac{\omega_p^2 \tilde{\omega}}{\omega(\tilde{\omega}^2 - \omega_c^2)}, & i \cdot \frac{\omega_p^2 \omega_c}{\omega(\tilde{\omega}^2 - \omega_c^2)}, & 0 \\ -i \cdot \frac{\omega_p^2 \omega_c}{\omega(\tilde{\omega}^2 - \omega_c^2)}, & 1 - \frac{\omega_p^2 \tilde{\omega}}{\omega(\tilde{\omega}^2 - \omega_c^2)}, & 0 \\ 0, & 0, & 1 - \frac{\omega_p^2}{\omega \tilde{\omega}} \end{Bmatrix}, \quad (22)$$

where $\omega_c = eB / (m_e c)$ is the cyclotron frequency, and where $\tilde{\omega} = \omega - i\beta\omega^2$. From Eq. (21) we have that

$$\left[(\varepsilon_{xx} - k^2/k_0^2)^2 - \varepsilon_{xy}\varepsilon_{yx} \right] \varepsilon_{zz} = 0. \quad (23)$$

The root $\varepsilon_{zz} = 1 - \omega_p^2 / (\omega\tilde{\omega}) = 0$, or $\omega_p^2 = \omega^2 - i\beta\omega^3$ corresponds to the plasmon oscillation along the z-axes. For the other roots we have

$$\left(\frac{k}{k_0} \right)^2 \approx \varepsilon_{xx} \pm \sqrt{\varepsilon_{xy}\varepsilon_{yx}} \approx 1 - \frac{\omega_p^2}{\omega(\tilde{\omega} \pm \omega_c)}. \quad (24)$$

In the case when the minus sign in the denominator is valid, we have for $0 < \omega \ll \omega_c$ and for $\omega\omega_c \ll \omega_p^2$, that $v_{ph}/c = k_0/k \approx \sqrt{\omega\omega_c/\omega_p^2} \approx \sqrt{\omega}\sqrt{B/(4\pi e c N_e)}$, where v_{ph} is the phase velocity of the helicons traveling along the magnetic field lines or of the whistler waves in the ionosphere. Our main interest, however, is the photon's attenuation factor. We get:

$$\frac{2n\kappa\omega}{\varepsilon\tilde{\varepsilon}} = \frac{\beta\omega^4\omega_p^2}{(\omega_p^2 - \omega^2 \pm \omega_c\omega)^2 + \beta^2\omega^6}. \quad (25)$$

The main result is that the magnetic field splits each of the poles for the dielectric constant in the complex plane into two poles if the photon's polarization is perpendicular to the field. In the upper plane, seven poles would then replace the four poles given by Eq. (6). But the sum of the oscillator strengths and the sum of the residues is the same as in a plasma free of magnetic fields.

At lower temperatures it often can be assumed that the dielectric constant is constant and equal to one. We can set the magnetic field \mathbf{H} equal to a rotation of a vector potential, $\mathbf{H} = \text{curl } \mathbf{A}$. To the Hamiltonian operator (8), we must add two terms given by

$$\frac{ie\hbar}{mc} \mathbf{A} \cdot \mathbf{grad} + \frac{e^2}{2mc^2} \mathbf{A}^2 = -\frac{e}{2mc} \mathbf{H} \cdot \mathbf{L} + \frac{e^2}{8mc^2} \mathbf{H}^2 r^2 \sin^2\theta, \quad (26)$$

where $\mathbf{A} = (1/2) \mathbf{H} \times \mathbf{r}$ and $\mathbf{L} = \mathbf{r} \times \mathbf{p}$ are the vector potential and the angular momentum of a centrally bound electron, respectively, and θ is the angle between \mathbf{r} and \mathbf{H} . The charge e of the electron is a negative number. We could in the usual way also add the electron spin term $-e\mathbf{H} \cdot \mathbf{S}/(mc)$. At very low field strengths and low temperatures, the usual quantum mechanical calculations for bound electrons show that the angular momentum term and the spin dominate the second term. The energy levels given by Eq. (9) will then split up into many very close states defined by the quantum number m , and the states become nondegenerate.

For strong fields in plasmas at high temperatures (large \mathbf{r}), the second term on the right side of Eq. (26) dominates. In hot plasmas the first term and the spin term can then usually be disregarded. The displacement and the line widths are then proportional to B^2 . For large \mathbf{B} and \mathbf{r} in hot plasmas, the problems can also be treated semiclassically. The electrons lose energy as they encircle the magnetic field lines. This energy loss corresponds to an increase in the transition rates in the usual way. The corresponding increase in the damping factor β can be taken into account by multiplying Eq. (16) by a factor given by

$$F_B = \left(1 + b \frac{\omega_c^2}{\omega_p^2} \right) \approx \left(1 + 1.3 \cdot 10^5 \frac{B^2}{N_e} \right), \quad (27)$$

where in the nonrelativistic approximation, we have set $b = 4/3$, and where ω_c and ω_p are the cyclotron and plasma frequencies, respectively, B the field in gauss units, and N_e is the electron density in cm^{-3} . When applying this factor to Eq. (16) we get for the 50% cut-off wavelength that

$$\lambda_{0.5} = 3.185 \cdot 10^{-6} \left(1 + 1.3 \cdot 10^5 \frac{B^2}{N_e} \right) \frac{T}{\sqrt{N_e}}. \quad (28)$$

At extremely high temperature, we must include a factor that takes into account relativistic effects. However, for the redshift in the solar corona and in most astrophysical plasmas, this factor, which is about $\left[1 + (1 - v^2/c^2)^{-1/2} \right] / 2$, is not important.

5 Comparing plasma-redshift theory with experiments

Comparison of the plasma-redshift theory with an experimental finding often requires a thorough review of the experimental design and extensive calculations. In Sections 5.1 to 5.9, we will discuss briefly a few applications of the plasma-redshift theory.

5.1 Transition zone to solar corona and the region of spicules

The plasma redshift is significant for light with a wavelength less than a certain wavelength $\lambda_{0.5}$, which depends on the temperature, density and the magnetic field in accordance with Eq. (28). According to Vernazza et al. [3], the product of density and temperature in the transition zone to the solar corona is $N_e T \approx 5 \cdot 10^{14} \text{ cm}^{-3} \text{ K}$. When the temperature is 500,000 K, the electron density $N_e \approx 10^9 \text{ cm}^{-3}$, and the magnetic field B equal to zero, we get from Eq. (28) that photospheric light with wavelength less than cut-off wavelength $\lambda_{0.5} = 500 \text{ nm}$ is plasma redshifted. If the magnetic field B is 20 gauss the cut-off wavelength increases by 5%; and if B is 100 gauss the cut-off wavelength increases by 130%. That is, the cut-off wavelength increases as the magnetic field increases. We have also that the cut-off wavelength $\lambda_{0.5} = 500 \text{ nm}$ reaches deeper into the transition zone, as the magnetic field increases.

The notation $\lambda_{0.5}$ means that the redshift is 50% of its maximum value. Shorter wavelengths will be redshifted more than 50% and longer wavelengths less than 50%. A more detailed evaluation is obtained by using Eq. (18) and by determining for each wavelength the value of the function $F_1(a)$, which is given by Eq. (14) and Table 1. The plasma redshift of a photon means that the photon loses energy. This energy loss consists of low energy quanta, which are immediately absorbed (evanescent) in the plasma and cause a corresponding increase in the plasma temperature. According to Eq. (28), shorter wavelengths can be redshifted at lower temperature and or at higher densities. For the magnetic field \mathbf{B} about equal to zero, the cut-off for the shorter wavelengths is deep in the transition zone, and the cut-off for the longer wavelengths is high in the transition zone. For this reason we have that short-wavelength light is plasma redshifted slightly more than the long-wavelength light. However, the transition zone is short so usually this is a small effect on the measured redshift, except for the very short-wavelength light. Thus, the cut-off zone for the photospheric light is not sharp. Besides the external light from the photosphere, we must sometimes take into account also the internal short wavelength light in the plasma. This internal light in the plasma, mostly short wavelength light, below the L_α -limit, often has high intensity and high optical density.

The region of spicules covers the upper chromosphere, where $2 \cdot 10^4 \leq T \leq 2 \cdot 10^5 \text{ K}$, and the transition zone, where $2 \cdot 10^5 \leq T \leq 7 \cdot 10^5 \text{ K}$. The height of the spicules region is from about 2,150 km to about 15,000 km above the photosphere. As described by Feldman et al. [5], Friedman [6], Hollweg [7], and Goodman [8], this region is broader than the corresponding region in the models by Vernazza et al. [3]. The models by Vernazza et al. assume that the isothermal surfaces are stratified horizontally, while in fact they may sometimes be nearly vertical and roughly parallel to the surfaces of the spicules between huge plasma-redshift heated “bubbles”, as described in the following paragraphs.

The upper chromosphere is highly ionized and contains internally rather high intensity short-wavelength radiation emitted from highly excited states, including those of hydrogen and helium. The pressures, temperatures, and densities in the plasma fluctuate. In a small hot spot, a “bubble”, the temperature may be about 100,000 K and the electron density $N_e \approx 4 \cdot 10^9 \text{ cm}^{-3}$, while the surrounding regions, the “walls” of the “bubble”, contain slightly denser and colder plasma. The denser “walls” may emit more of the internal light, which may bounce back and forth across the hot region. The plasma-redshift heating is a first-order process in density, while the cooling processes are second order in density. The plasma redshift causes, therefore, the short-wavelength photons to deposit some of their energy in the less dense hot spots, the bubbles. The cooling due to recombination emission in the denser and colder “walls” is compensated to a lesser extent by the redshift heating. The plasma redshift enhances therefore temperature inhomogeneity and makes the hot low-density region, the “bubble”, hotter, while the denser surrounding regions, the “walls”, become

colder. According to Eqs. (16) and (28), the 50% cut-off wavelength for the above mentioned density and temperature and for low magnetic fields is initially in the hot low-density region about 50.3 nm; and the analogous 10% cut-off wavelength, corresponding to $a = 2.671$ in Table 1, is about 116 nm. A magnetic field will increase the cut-off wavelength. In the bubbles, the very short wavelength internal light in the plasma may then initiate significant plasma-redshift heating.

The magnetic field enhances therefore the temperature inhomogeneity. In addition, the conversion of field energy to heat is strongest in the hot regions (see Appendix B). As the kinetic energy of a particle increases, its diamagnetic moment increases. This fact in turn reduces the H-field inside the hot low-density region and partially transforms the field energy to heat, while the field from the diamagnetic moments inside the bubble combine to strengthen the H-field in the colder high-density region, the “walls”.

As the temperature in the hot region increases, some of the light from the photosphere will also be plasma redshifted, first the short-wavelength light, and then the longer-wavelength light. The plasma redshift deposits then a fraction of the photospheric photon energy in the “bubbles” in the transition zone, and accelerates conversion of magnetic field energy to heat.

A rough estimate of the plasma-redshift heating from the photosphere is obtained from the integrated intensity $I(R)$ over all directions of solar light penetrating each location in the transition zone and the corona. The light intensity from the photosphere decreases with R as

$$\begin{aligned} I(R) &\approx I_0 2\pi \left(1 - \sqrt{1 - R_0^2/R^2} \right) \\ &= 2\sigma T^4 \left(1 - \sqrt{1 - R_0^2/R^2} \right) = 1.29 \cdot 10^{11} \left(1 - \sqrt{1 - R_0^2/R^2} \right) \text{ erg cm}^{-2} \text{ s}^{-1}, \end{aligned} \quad (29)$$

where R_0 is the solar radius. Low in the transition zone, we have that the parenthetical factor is close to 1, but farther away it approaches $0.5(R_0/R)^2$. In the transition zone, we can multiply Eq. (29) by the redshift given by Eq. (18) per cm of integration, and get for the photospheric light that

$$\begin{aligned} \frac{dQ_{heat}}{dt} &= I(R) \frac{\delta\lambda}{\lambda} = 1.29 \cdot 10^{11} \left(1 - \sqrt{1 - R_0^2/R^2} \right) 3.326 \cdot 10^{-25} F_1(a) \frac{\gamma}{\gamma_0} N_e \\ &= 4.29 \cdot 10^{-14} \left(1 - \sqrt{1 - R_0^2/R^2} \right) F_1(a) \frac{\gamma}{\gamma_0} N_e \text{ erg cm}^{-3} \text{ s}^{-1}, \end{aligned} \quad (30)$$

where $\delta\lambda/\lambda$ is the redshift per cm of the plasma. This redshift heating density can be compared with net cooling density from recombination emission and x-ray emission, which according to Sutherland and Dopita [9] has a maximum cooling density of about $4.5 \cdot 10^{-22} N_t N_e \text{ erg cm}^{-3} \text{ s}^{-1}$ at a temperature of about 180,000 K, where $N_t = 0.917 N_e$ is the number density of positive ions. At lower and higher temperatures the cooling rate is lower. Below the temperature of about 30,000 K, and above about 800,000 K, the rate of cooling is less than $10^{-22} N_t N_e$. We will see later that the excess redshift heating in the corona leaks into the transition zone and that the conversion of magnetic heating is significant and may double the redshift heating in the transition zone. However, even when we disregard this additional heating, we see that the redshift heating given by Eq. (30) about balances the recombination emission and x-ray cooling, when the temperature is about one million degrees and the electron density $4.7 \cdot 10^8 \text{ cm}^{-3}$ and $(\gamma/\gamma_0) F_1(a) \approx 1$.

The initial photon width γ_i is often large due to broadening by collisions with neutral atoms, Fourier field components of charged particles, the Stark effect, and stimulated emissions. Holweger [10] found that the initial photon widths of the sodium resonance lines 588.995 and 589.592 nm, which are formed high in the photosphere, are about 0.202 pm. This width is about 17 times the classical photon width of 0.0118 pm. We do not know the average photon width, but for many lines it is between 1 and 20 times the classical width. The second electron in the important H⁻-species is loosely bound and sensitive to collision broadening by neutral atoms, by the Fourier field harmonics of the fast moving electrons, and by stimulated emissions and absorptions. Many of the Ca-II and Mg-II lines have very broad photon widths, while some weak lines have small photon widths. In the balance of heating and cooling, we should consider also other processes, and different modes of heat transport. However, other authors, such as Vernazza et al. [3], have done so. The present focus is to

evaluate only the photon-width portion directly related to the plasma redshift, which has not been considered by others.

The increase in redshifts due to broadenings of photon widths is significant in the transition zone, but less in the corona, because in the corona the photon width is close to the classical width. This estimate is based on comparison of observed redshifts of Fraunhofer lines with Eq. (20). Presently, this estimate is imprecise and will have to be improved as the photon widths become better determined. The heating by conversion of the magnetic field is most important in the spicules region, as discussed in Appendix B, because the field is stronger and because the mutual induction between the diamagnetic moments of the charged particles and the currents creating the magnetic field is larger low in the transition region than high in the corona.

The redshift experiments indicate that the second term on the right side of Eq. (20) is on the order of 10^{-6} . The integrated heating derived from this second term is then on the order of $1.29 \cdot 10^{11} \cdot 10^{-6} = 1.3 \cdot 10^5 \text{ erg cm}^{-2}\text{s}^{-1}$, which is deposited mainly in the transition zone. In addition, we have the heating from the first term, which can be obtained by integrating the first term on the right side of Eq. (20) along the line of sight from the observer to the different points on the solar disk. Much of the heating by this term, about $1.1 \cdot 10^5 \text{ erg cm}^{-2}\text{s}^{-1}$, leaks by conduction into the transition zone, as we show in Section 5.2. The total plasma-redshift heating in the spicules region and in the corona is then about $2.4 \cdot 10^5 \text{ erg cm}^{-2}\text{s}^{-1}$.

In addition to this direct plasma-redshift heating, we have heating by conversion of the magnetic field to heat, which is often initiated by the plasma redshift, as described in Appendix B. The magnetic heating consists of two major contributions:

1. The conversion of magnetic field energy to heat. This conversion is often induced by the increase in the diamagnetic moments caused by the redshift heating. The increase in the diamagnetic moments induces electromotive forces that oppose the magnetic field and the currents that generate it. This effect is most prominent in the hot bubbles between the spicules in the transition zone.
2. The repulsion of the diamagnetic moments by the outward decreasing magnetic field. This repulsion is important for accelerating the solar wind, as shown in Section 5.3.

The plasma redshift has a tendency to create “bubble” like structures in the upper chromosphere, because the plasma redshift is a first-order process in the electron density, while the cooling processes are second (or higher) order processes in the density. The plasma redshift therefore enhances the inhomogeneity in temperature. Initially, the “internal” light in the plasma in the upper chromosphere contributes to the plasma redshift and the unevenness in temperature. This “internal” light is rich in high-energy short-wavelength photons from the Lyman series in hydrogen and helium transition lines, as hydrogen and helium are highly ionized in the upper chromosphere. Subsequently, as the temperature in the hot “bubbles” increases, also the light from the photosphere is redshifted in the “bubbles”. If for a moment, we disregard the recombination cooling, and the heating by the magnetic field, the plasma-redshift heating in the transition zone according to Eq. (30) is for $(\gamma/\gamma_0) F_1(a) \approx 10$ about equal to $dQ_{heat}/dt \approx 4.3 \cdot 10^{-13} N_e \text{ erg cm}^{-3}\text{s}^{-1}$. The rate of heating is then about

$$\frac{dT}{dt} \approx \frac{4.3 \cdot 10^{-13}}{1.917 \cdot \frac{3}{2}k} \approx 1000 \text{ K s}^{-1}, \quad (31)$$

where k is the Boltzmann constant. The “bubble” temperature would then reach 500,000 K in about 500 seconds, which is on the order of the time for the formation of the spicules (see p. 124 of reference [6]). It takes the spicules about 270 seconds to fall freely 10,000 km. During the latter part of the “bubble” formation, the conversion of magnetic field energy to heat is relatively large, and the rate of heating of the “bubbles” increases exponentially as the “bubbles” explode to the surface and into the corona. A spicule consists of the colder plasma in the walls of the bubbles. This colder plasma is squeezed 5 to 15 km out into the transition zone and the lower corona by the expanding “bubbles” [6]. The spicule then falls down, which causes significant pressure variations and turbulence in this region. The “bubbles” are filled with a hot, fully ionized plasma as they open

up into the corona. The heating produced by the conversion of magnetic field varies with strength of the field. If a field of 10 gauss is embedded in the plasma with a density of $N_e = 10^{10} \text{ cm}^{-3}$, it could heat the plasma to about million degrees. If such a field in a bubble with a height of 10,000 km is destroyed every 1000 seconds the heating would be about $4 \cdot 10^6 \text{ erg cm}^{-2} \text{ s}^{-1}$. The magnetic field in the transition zone is estimated to be usually in the range of 1 to 10 gauss. Similarly, if a field of 2 gauss in a bubble with a height of 10,000 km is embedded in the plasma density of $N_e = 10^{10} \text{ cm}^{-3}$, and converted to heat every 1000 seconds, it would correspond to an energy flux of $1.6 \cdot 10^5 \text{ erg cm}^{-2} \text{ s}^{-1}$. The conversion of magnetic energy is likely to fluctuate, and to correspond to an energy flux, which is usually between $1.6 \cdot 10^5$ and $4 \cdot 10^6 \text{ erg cm}^{-2} \text{ s}^{-1}$.

The repulsion of a diamagnetic moment in outward decreasing magnetic field is pronounced throughout the transition zone and the corona; and at high altitudes, it is primarily responsible for the outward acceleration of the solar wind. If the solar wind at the distance of the Earth is $S_{215R_0} = N_p v_p = 3 \cdot 10^8 \text{ cm}^{-2} \text{ s}^{-1}$, the energy flux at the solar surface required for overcoming the gravitational potential is about $0.53 \cdot 10^5 \text{ erg cm}^{-2} \text{ s}^{-1}$. This assumes that helium and trace elements account for 20% of the proton energy requirements. If the solar wind has helium and trace elements equal to their concentration in the Sun, the required energy flux would be 17% higher. Usually, the kinetic energy of the particles in the solar wind increases. When the proton velocity has increased to about 600 km per second, the kinetic energy flux corresponds to about $0.53 \cdot 10^5 \text{ erg cm}^{-2} \text{ s}^{-1}$. The total of potential and kinetic energy in the solar wind is then about $1.1 \cdot 10^5 \text{ erg cm}^{-2} \text{ s}^{-1}$. In the quiescent corona, the total energy flux from the redshift heating, the magnetic heating (corresponding to conversion of 2 gauss of field energy to heat), and from the input into the solar wind is about $(2.4 + 1.6 + 1.1) \cdot 10^5 = 5.1 \cdot 10^5 \text{ erg cm}^{-2} \text{ s}^{-1}$. During flares the conversion of magnetic field energy to heat can be much greater, as described in Section 5.5.

According to McWhirter et al. [11] and Withbroe [12, 13] the estimated energy input for the quiescent corona, including the energy needed to drive the solar wind, is about $4 \cdot 10^5$ to $6 \cdot 10^5 \text{ erg cm}^{-2} \text{ s}^{-1}$.

5.2 Solar corona

The energy transport from the lower and cooler solar atmosphere to the hotter transition zone and corona has remained a puzzle, as the plasma-redshift theory has not been available. Several papers have dealt with the subject, see, for example, references [11-25], but failed to find a satisfactory explanation of the coronal heating. For explaining the observations, the different authors have tried to assume that some mechanisms deposited energy. They have suggested that sound waves or acoustic flux, Alfvén waves, electrical currents, magneto-hydrodynamic turbulence, etc. transferred energy to the corona. These explanations may be partially correct and do not necessarily conflict with the present explanation. For example, the turbulence created by the redshift-heated bubbles produces shocks and acoustic fluxes that transplant some of the energy. However, these acoustic fluxes should not be considered the primary cause, but ancillary to the primary cause, which is the plasma-redshift heating followed by conversion of magnetic field energy to heat. Recently, reconnection of the field lines has also been mentioned. Also this is more a phenomenological description than a causal description. The reconnection is due to the redshift heating of the plasma followed by conversion of the magnetic field energy to heat as described in Appendix B.

We will for a moment assume that in the transition layer and lower corona the densities are diffusion controlled and determined mainly by the gravitational potential and the temperature. We have then that

$$N_e = \frac{N_0 T_0 R_0}{T R} \exp \left[\frac{GM_S \mu m_H}{k T R_0} \left(\frac{R_0}{R} - 1 \right) \right] = \frac{N_0 T_0 R_0}{T R} \exp \left[\frac{1.41 \cdot 10^7}{T} \left(\frac{R_0}{R} - 1 \right) \right], \quad (32)$$

where N_e in cm^{-3} , T in K, and R in cm are the electron density, temperature, and radius to the solar center. At the bottom of the corona, the same quantities are indicated with subscript zero. G is the gravitational constant, M_S is the solar mass, and $\mu = 0.61$ the average molecular weight relative to the proton mass. The exponential factor accounts for the effect of the gravitational potential. The dependence of R in the factor before the exponential factor is derived from the diffusion equation

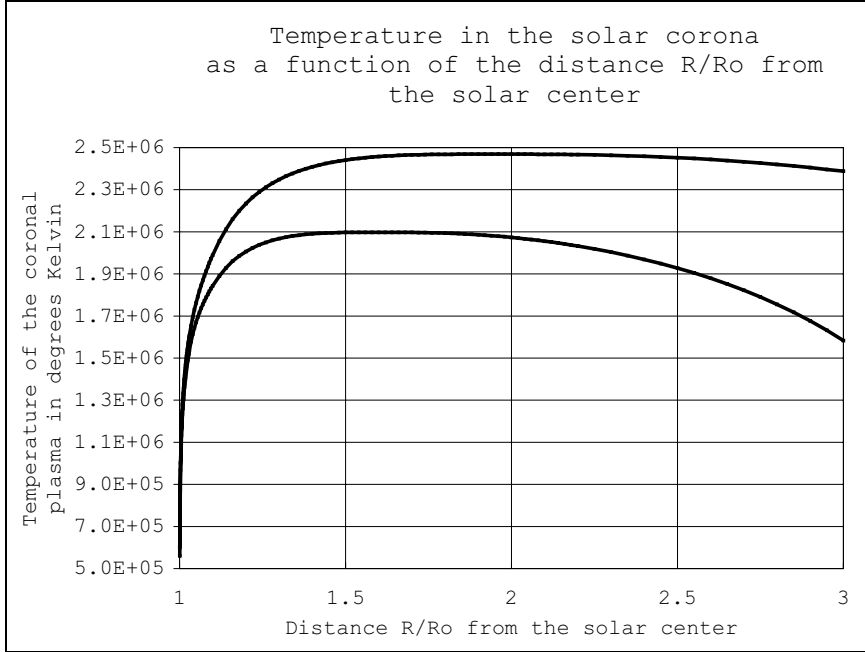


Figure 1: The lower and upper curves correspond to different pressure in the transition zone, $N_e T = 4 \cdot 10^{14}$ and $5 \cdot 10^{14} \text{ cm}^{-3} \text{ K}$, respectively. The solar wind flux at the distance of the Earth is assumed to be $N_e v_p = 3.2 \cdot 10^8 \text{ cm}^{-2} \text{ s}^{-1}$. The magnetic field in the transition zone is assumed to be 5.5 and 6.3 gauss, and to decrease nearly inversely with the square of the radius to solar center.

with proper boundaries. Other authors usually disregard this R dependence, but it is significant. (When we discuss the solar wind in Section 5.3, we will see that we must modify this equation and take into account the outward force on the diamagnetic moments. But for the moment we use this equation to help us analyze the phenomena.) For deriving the electron distribution from Eq. (32), we must know the temperature as a function of R . We can use the temperature distribution as measured by Sturrock, Wheatland and Acton [20, 21] in the most important region from 1.01 to 2 solar radii; or we can use the temperature as derived from redshift and magnetic heating.

Fig. 1 shows how the electron temperature varies below 3 solar radii when the pressure in the transition zone corresponds either to $N_e T = 4 \cdot 10^{14}$, or to $5 \cdot 10^{14} \text{ cm}^{-3} \text{ K}$. Most of the measured temperatures by Sturrock, Wheatland and Acton are between the two curves.

In models A to F of the solar atmosphere by Vernazza et al. [3], the product of temperature and electron density varies from $2.4 \cdot 10^{14}$ to $1.1 \cdot 10^{15}$ at $T = 447,000 \text{ K}$. In the model C the product is $5.4 \cdot 10^{14}$ at the same temperature. These values, especially the ones for model C, are consistent with measurements of temperatures and densities low in the corona as determined by Sturrock et al. [20] and Wheatland et al. [21], who for two points low in the quiescent corona found the product to be $4.79 \cdot 10^{14}$ at a temperature of $1.33 \cdot 10^6$ and $4.26 \cdot 10^{14}$ at a temperature of $1.64 \cdot 10^6 \text{ K}$.

In Table 2, we list the electron temperature and density values for the entire corona. We have assumed that in the middle of the transition zone $T = 475,000 \text{ K}$, and $N_e = 10^9 \text{ cm}^{-3}$. We also assumed that the magnetic field B is so low that it does not affect the cut-off wavelength as given by Eq. (28), but it contributes to the heating. In these examples, Spitzer's conductivity [26] is assumed to be $\kappa = 10^{-6} T^{5/2}$. The electron densities in Table 2 are also shown in Fig. 2. The calculations can be refined. The values listed in Table 2 are approximate values for the temperatures and electron densities as functions of the radii to solar center. For this discussion, the values should not be considered theoretically deduced values, but rather some values in fair agreement with experiments.

Table 2 Temperatures and electron densities in the quiescent solar corona as a function of distance.

Distance r/R_0 in units of solar radius R_0	Temperature T in degrees Kelvin	Electron densities N_e in cm^{-3}	Distance R/R_0 in units of solar radius R_0	Temperature T in degrees Kelvin	Electron densities N_e in cm^{-3}
1.001	5.70×10^5	7.45×10^8	2.6	2.02×10^6	3.35×10^6
1.002	8.81×10^5	4.73×10^8	2.8	1.92×10^6	2.89×10^6
1.005	1.10×10^6	3.65×10^8	3.0	1.78×10^6	2.54×10^6
1.01	1.27×10^6	2.99×10^8	3.2	1.60×10^6	2.12×10^6
1.02	1.45×10^6	2.38×10^8	3.4	1.29×10^6	1.78×10^6
1.05	1.69×10^6	1.60×10^8	3.6		1.55×10^6
1.1	1.88×10^6	1.03×10^8	5.0		7.36×10^5
1.2	2.06×10^6	5.49×10^7	6.0		1.85×10^5
1.3	2.14×10^6	3.40×10^7	7.0		8.12×10^4
1.4	2.17×10^6	2.29×10^7	8.0		4.45×10^4
1.6	2.19×10^6	1.23×10^7	10.0		1.81×10^4
1.8	2.19×10^6	7.67×10^6	30.0		6.16×10^2
2.0	2.17×10^6	5.85×10^6	60.0		1.23×10^2
2.2	2.14×10^6	4.72×10^6	100.0		3.77×10^1
2.4	2.09×10^6	3.92×10^6	215		6.38

The values serve only as a reference for the discussion and for helping us understand what is going on. However, the temperatures and pressures are consistent with the values observed by Sturrock, Wheatland and Acton [20, 21], and with the pressure in the transition zone as estimated by Vernazza et al. [3]. The values reported in the literature [11-21] depend on time of observation, but during quiescent corona appear to be in reasonable agreement with those in Table 2.

According to Eq. (28), the 50% cut-off wavelength is about 478.5 nm when the temperature is 475,000 K, electron density 10^9 cm^{-3} , and the magnetic field only a few gauss. The cut-off wavelength increases as the temperature increases and the density decreases. At 1.005 solar radii the temperature is about 1,100,000 K, the electron density about $3.65 \cdot 10^8 \text{ cm}^{-3}$, and the cut-off wavelength about 1,833.8 nm. For this estimate the solar radius is assumed to extend to 475,000 K.

The plasma-redshift heating in the upper layers covers the entire solar spectrum and is in excess of the recombination cooling and x-ray cooling. Most of the excess heat transferred to the plasma by redshift of photons will leak by heat conduction into the transition zone.

When we multiply the first term on the right side of Eq. (20) by the right side of Eq. (29) and disregard the second term on the right side of Eq. (20), we have that the plasma-redshift heating is

$$\begin{aligned} \frac{dQ_{heat}}{dt} &= 1.29 \cdot 10^{11} \left(1 - \sqrt{1 - R_0^2/R^2} \right) \cdot 3.326 \cdot 10^{-25} N_e \\ &= 4.3 \cdot 10^{-14} N_e \left(1 - \sqrt{1 - R_0^2/R^2} \right) \text{ erg cm}^{-3} \text{ s}^{-1}, \end{aligned} \quad (33)$$

where the electron density, N_e , is in cm^{-3} . The second term of Eq. (20) and the transformation of the magnetic field energy to heat are most important in the transition zone, as discussed in Section 5.1.

The plasma-redshift heating obtained by Eq. (33) may be compared with the dominant cooling processes, which are due to recombination emissions and x-ray emissions. Sutherland and Dopita [9] have estimated the cooling rate. They find for the temperature range $8 \cdot 10^5 \leq T \leq 1.8 \cdot 10^6$ that the cooling rate is given by $dQ_{heat}/dt \approx 10^{-22} N_t N_e \text{ erg cm}^{-3} \text{ s}^{-1}$, where for solar abundance of helium and trace elements the number density of positive ions is $N_t \approx 0.917 N_e$.

From Table 2, we get for the temperature and the electron density at 1.005 solar radii that the cooling rate is $3.35 \cdot 10^{-14} N_e \text{ erg cm}^{-3} \text{ s}^{-1}$. According to Eq. (33), the redshift heating at the same location is $3.87 \cdot 10^{-14} N_e \text{ erg cm}^{-3} \text{ s}^{-1}$. Thus, the plasma-redshift heating, disregarding the second term in Eq. (20) and the conversion of the magnetic field to heat, is slightly greater than the cooling.

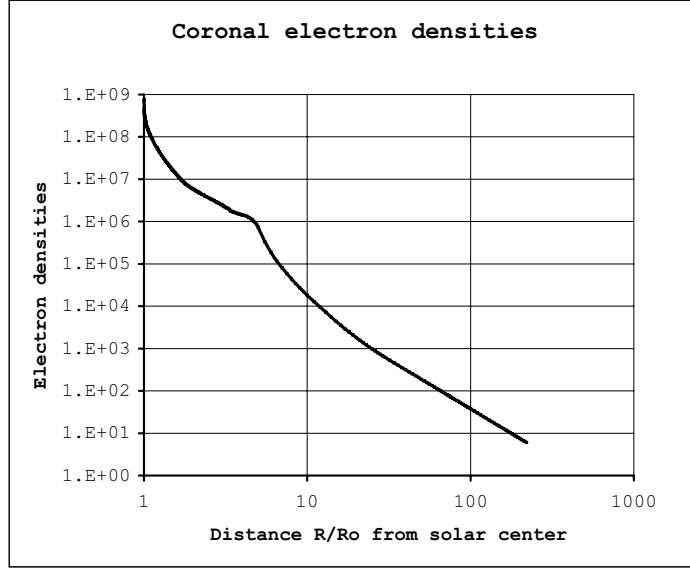


Figure 2: The curve corresponds to $N_e T = 4.75 \cdot 10^{14} \text{ cm}^{-3} \text{ K}$ at the cut-off in the transition zone. The solar wind flux at the distance of the Earth is assumed to be $N_e v_p = 3.2 \cdot 10^8 \text{ cm}^{-2} \text{ s}^{-1}$. The magnetic field in the transition zone is assumed to be 6 gauss, and to decrease nearly inversely with the square of the radius to solar center. The hump around 4 to 5 solar radii is not well defined and is very sensitive to pulsations in the transition zone and the strength of the magnetic field. It is in this example enhanced to remind us that this is an unstable region, where the proton temperature can occasionally drop significantly and cause relatively high densities. Beyond this distance, the solar wind accelerates and the density falls off more steeply.

From Table 2, we get for the temperature and the electron density at 1.1 solar radii that the cooling rate is $0.945 \cdot 10^{-14} N_e \text{ erg cm}^{-3} \text{ s}^{-1}$. According to Eq. (33), the redshift heating at the same location is $2.5 \cdot 10^{-14} N_e \text{ erg cm}^{-3} \text{ s}^{-1}$. The plasma-redshift heating at this location is thus about 2.7 times greater than the cooling. The excessive heating leaks by conduction into the transition zone. These heating estimates disregard the second term in Eq. (20) and the conversion of the magnetic field to heat. The actual heating is, therefore, greater and more heat leaks into the transition zone. This surplus heating over cooling continues to more than about 1.5 solar radii, and the excessive heat leaks by conduction into the transition zone.

At higher temperatures the recombination cooling decreases significantly according Sutherland and Dopita [9]. The plasma-redshift heating then far exceeds the cooling by recombination emissions and x rays. However, because of the lower densities high in the corona (beyond 1.5 solar radii), the cooling from solar wind becomes significant. The lifting of the solar wind in the gravitational field requires energy. Lower in the corona and in the transition zone the gravitational field is stronger, but the high densities dominate the solar wind density, and the energy transferred to the solar wind is an insignificant fraction of the total cooling. High in the corona, the cooling by the solar wind flux is important. This cooling is reduced significantly by the repulsion of diamagnetic moments in the outward decreasing magnetic field, as discussed in Section 5.3. The gravitational cooling by the solar wind, nevertheless, results in a maximum temperature, which is usually between 1.9 and 2.6 million degrees at distances of about 1.8 to 2.0 solar radii. In Table 2 the maximum temperature, about $2.2 \cdot 10^6 \text{ K}$, corresponds to a solar wind flux of $N_p v_p = 3.2 \cdot 10^8 \text{ cm}^{-2} \text{ s}^{-1}$ at the distance of the Earth. The maximum temperature in the quiescent corona varies with the redshift heating, solar wind flux, and the heat conductivity coefficient, which varies with the strength and direction of the magnetic field. Spitzer's conductivity coefficient [26] was used for estimating the values in Table 2.

The temperature profile is obtained by an iteration method. The electron temperature and its variation with height, as shown in Table 2, is similar to that found in the measurements by Wheatland, Sturrock and Acton [20, 21], who examined the temperature in the inner corona using long-exposure Yohkoh images of two regions of quiet corona. Interestingly, for explaining their data they assumed “ad hoc” deposition of energy in the higher layers of the corona. The excess energy then leaked into the transition zone. Their “ad hoc” method for explaining the temperature variations between 1.1 to 1.8 solar radii mimics to some extent the deposition of energy by the plasma redshift. They, of course, could not explain how this heating came about. But their experimentally determined relation is consistent with the predictions of the plasma-redshift theory.

5.3 Solar wind

It has been difficult to explain many of the phenomena associated with the solar wind in the quiescent corona. For example, it has been difficult to explain why the solar wind accelerates outwards. Sheeley Jr. et al. [22] observed “white light images”, which are believed to be associated with the solar wind from quiescent corona, accelerate outwards from a position of about 5 solar radii to about 30 solar radii and beyond. Wang et al. [23] observed similar phenomena closer to the Sun. The outward acceleration of the solar wind continues beyond the position of the Earth, according to Withbroe, the solar wind velocities are higher in the coronal holes [13, 14]. Withbroe estimated the solar wind flux to be usually between about $N_p v_p = 2.7 \cdot 10^8$ and about $3.2 \cdot 10^8 \text{ cm}^{-2} \text{ s}^{-1}$. He also found that the mass flux in the solar wind varies much less than the particle density; that is, when the particle density increases, the velocity decreases.

Some have tried to explain the acceleration as caused by Alfvén waves. However, the velocity $v = B/\sqrt{4\pi\rho}$ of the Alfvén waves at about the distance of the Earth is much lower than that of the observed solar wind. Close to the Earth the magnetic field B is usually less than 0.0001 gauss and the density usually about 5 protons per cubic cm. The mass density including solar abundance of helium is then $1.17 \cdot 10^{-23}$. The corresponding velocity of the Alfvén waves is $8.2 \cdot 10^6 \text{ cm s}^{-1}$, while the measured solar wind velocity according to Gosling [14] usually exceeds $4 \cdot 10^7 \text{ cm s}^{-1}$. As Parker [18] and Spangler and Mancuso [27] have shown, the Alfvén waves are unlikely to be significant for heating of the solar corona.

In the following discussion, we will show that both the plasma-redshift heating and the repulsion of the diamagnetic moments by the magnetic field (see Eq. (B10) of appendix B) are important for explaining the observations.

If the solar wind flux is about $S_{215R_0} = N_p v_p = 3 \cdot 10^8 \text{ cm}^{-2} \text{ s}^{-1}$ at the distance of the Earth, then the corresponding flux at R is $(215R_0/R)^2$ times the flux at $215R_0$. The increase in gravitational potential per cm of this flux is then

$$\frac{dq_g}{dR} = \frac{GM_S \mu m_p}{R^2} \left(\frac{215R_0}{R} \right)^2 S_{215R_0} \approx 2.54 \cdot 10^{-15} \left(\frac{R_0}{R} \right)^4 S_{215R_0} \text{ erg cm}^{-3} \text{ s}^{-1}, \quad (34)$$

where we have assumed 5% abundance of helium in the solar wind, and $\mu = 1.2$ instead of the frequently used factor of 1.4, which corresponds to 10% helium.

At 1.1 solar radii, the gravitational cooling by the solar wind is, according to Eq. (34), about $5.2 \cdot 10^{-7}$, which is about 20% of the plasma-redshift heating alone. The plasma-redshift heating at this location, according to Eq. (33) and Table 2, is 5 times greater or about $2.58 \cdot 10^{-6}$. This estimate disregards the conversion of magnetic field energy to heat, which low in the corona is usually significant. Thus, at this location and below it, the cooling by solar wind is only a small fraction of the plasma-redshift heating, and even smaller fraction of the entire heating. The emission cooling, according to Sutherland and Dopita [9], is $9.7 \cdot 10^{-7}$. The excess heating leaks by conduction in to the transition zone.

At about 1.6 solar radii, the gravitational cooling by the solar wind is according to Eq. (34) about $1.16 \cdot 10^{-7}$. The plasma-redshift heating at this location is according to Eq. (31) and Table 2 also about $1.16 \cdot 10^{-7}$. This estimate disregards the conversion of magnetic field energy to heat, which often may be significant. The radiation cooling at the same location is according to Sutherland and Dopita about $1.4 \cdot 10^{-8}$.

Beyond about 1.6 solar radii, the gravitational cooling by the solar wind dominates the plasma-redshift heating. Nevertheless, the temperature continues to increase and reaches maximum of about 2.2 million degrees at about 1.8 solar radii. Beyond about 5 solar radii the solar wind accelerates although the gravitational cooling exceeds the plasma-redshift heating. For explaining these apparent contradictions, we need to take into account not only direct conversion of magnetic field to heat, but also two important forces.

1. We must take into account that plasma redshift transfers the energy to the electrons, and that the energy-transfer from the electrons to the protons is a very slow process. The light and hot electrons therefore diffuse outwards ahead of the protons and build up an electrical field, which drags the protons outwards or upwards in the gravitational field of the Sun.
2. We must take into account the repulsion of diamagnetic moments by the magnetic field, which is described quantitatively in Eq. (B10) of Appendix B. Low in the corona, this magnetic repulsion force decreases the gravitational cooling significantly. High in the corona, beyond about 5 solar radii, the outward diamagnetic repulsion force exceeds the gravitational attraction force and causes outward acceleration of the solar wind.

The stopping power. The stopping power is about $9.3 \cdot 10^{-11} \text{ erg s}^{-1}$ for a 1000 eV incident electrons penetrating a hot electron plasma with temperature of about one million degrees and an electron density of $N_e = 10^7 \text{ cm}^{-3}$. According to the conventional theoretical estimates, the stopping power is only about $1.2 \cdot 10^{-11} \text{ erg s}^{-1}$. The conventional theory includes energy transfer to the plasma frequency, but not to the very low frequencies corresponding to the root c in Eq. (6). This root is important only in very hot, sparse, non-degenerate plasma. The rate of energy loss of 1000 eV electrons (even according to the conventional theory) is much greater than the rate of redshift heating per electron, as given by Eq. (33), anywhere in the corona and transition zone. The electrons in the solar corona will be thermalized, therefore, and have a Maxwellian energy distribution.

The rate of energy transfer from 1000 eV electrons to protons is much smaller. The shielding effect of the electrons in the plasma prevents all but the highest frequency Fourier harmonics of the incident electrons' field to penetrate to a proton. Møller's (as well as Mott's) hard collision cross-section for stopping of electrons is a very small fraction of the total stopping power. The hard collision term in electron's interaction with protons is even much smaller due to the protons 1836 times bigger mass. The main energy transfer from the electrons to the protons is therefore caused by the electrons' diffusion outwards ahead of the protons. This outward diffusion of the electrons ahead of protons produces an electrical field, which drags the protons outwards. The electron plasma shields the positively charged particles. Their effective charge depends on the density and relative velocity of the electrons to the protons.

Temperature of a plasma. In this context, we should realize that the temperature measurements are usually based on the x-ray production and the ion excitation levels. Mainly the electron temperature, and not the heavy ion temperature, determines both the x-ray production and ion excitations. The temperatures measured by Sturrock et al. [20] and Wheatland et al. [21] are principally the electron temperatures and not necessarily the proton temperatures. The outward forces on the diamagnetic moments, and the outward electrical forces on the protons counteract the gravitational attractions. This reduction in the gravitational attraction corresponds to reduction in the value of G in Eq. (32). The temperature, T , in the exponential term in Eq. (32) is the average temperature and is therefore usually lower than the electron temperature. When the magnetic and electrical forces reduce the gravitational attraction, the temperature, T , inside the brackets in the exponential term must be reduced for maintaining the value of the exponential term.

Magnetic force on diamagnetic moments in the corona. Let us first consider the outward force on each diamagnetic moment created by the outward decreasing magnetic field, as quantified in Eq. (B10) in Appendix B. At a point P in the corona this force is $F = (1/2)mv_{\perp}^2(n/R)$, where

m is the mass of the particle, v_{\perp} its velocity perpendicular to the field, R the distance from solar center, and n is the exponent in the function $B_P (R_P/R)^n$, which gives the radial decrease of the magnetic field B at the location P.

In the transition zone, the electron and the proton temperatures are usually less than or about equal to 500,000 K. The average value of $(1/2) mv_{\perp}^2 = kT \leq 6.9 \cdot 10^{-11}$ erg. Let us assume $n = 3$. We get then that the force on the proton-electron pair is usually less than $6kT/R = 4.1 \cdot 10^{-10}/R$ dyne. The corresponding gravitational force on the proton is about $-3.2 \cdot 10^{-9}/R$ dyne. The repulsion force acting on the diamagnetic moments of a proton-electron is then less than 13% of the gravitational attraction. (However, the magnetic dipoles creating the magnetic field are usually high in the atmosphere. The exponent n could then occasionally be very large. If n were equal to 25, the diamagnetic forces on the proton-electron pair would be $3.5 \cdot 10^{-9}/R$ dyne; that is, greater than the gravitational attraction. More generally, we get that when at this location the value of $n \geq 23$, and when the kinetic energy component of the proton electron pair at the right angle to the magnetic field exceeds $2kT = 1.39 \cdot 10^{-10}$ the magnetic repulsion will exceed the gravitational attraction.)

At a distance of 2 solar radii, the electrons' temperature according to Table 2 is about 2.17 million K, and therefore $kT \approx 3 \cdot 10^{-10}$ erg. The proton temperature may be 25% of the electron temperature. In this region, the magnetic field is likely to decrease with n about equal to 2.1. The diamagnetic repulsion force on the proton-electron pair is then about 49% of the gravitational attraction. For this reason, the solar wind cooling is only 51% of the cooling given by Eq. (34), or $2.59 \cdot 10^{-8}$ erg s $^{-1}$. The emission cooling, according to Sutherland and Dopita [9] is about 13% of this value. The total cooling, $2.91 \cdot 10^{-8}$ erg s $^{-1}$, can be compared with the plasma-redshift heating, which is about $3 \cdot 10^{-8}$ erg s $^{-1}$. The small excess heating leaks by conduction outwards.

The solar wind cooling between about 3 and 5 solar radii is significant and causes instabilities, which are most likely responsible for the formation of the white light images observed by Sheeley Jr. et al. [22]. From about 5 solar radii, they observed the white light images accelerated outwards beyond about 30 solar radii. At about 5 solar radii, the velocities of the white light images were about $2 \cdot 10^6$ cm s $^{-1}$. If this is typical of the proton velocity, the corresponding proton temperature could be very low. The electron temperature could be much higher, as the hot electrons diffuse outward from the hotter layers below. The rate of plasma-redshift heating transferred from the electrons to the protons by means of collisions is small. The electrical field created by the electrons as they diffuse outwards must therefore drag the protons outwards. At 5 solar radii, we set the electrons' temperature at about 1.2 million degrees K. For the electrons, we have then that kT is about $1.66 \cdot 10^{-10}$ erg. The proton's kinetic energy perpendicular to the magnetic field is likely to be only a small fraction of this. The magnetic field is likely to decrease with $n > 2$, for example, $n \approx 2.1$. The diamagnetic force acting on the proton-electron pair is then about $3.5 \cdot 10^{-10}/R$ dyne. The gravitational force acting on the proton-electron pair at 5 solar radii is $6.4 \cdot 10^{-10}/R$ dyne. The diamagnetic force counteracts the gravitational force and reduces the gravitational cooling to 45%. If the solar wind flux at the distance of the Earth is $S_{215R_0} = N_p v_p = 3.2 \cdot 10^8$ cm $^{-2}$ s $^{-1}$, the 45% of cooling given by Eq. (34) is at 5 solar radii equal to $5.9 \cdot 10^{-10}$ erg cm $^{-3}$ s $^{-1}$. According to Sutherland and Dopita [9], the emission cooling is about 10% of this value. The total cooling is then about $6.5 \cdot 10^{-10}$ erg cm $^{-3}$ s $^{-1}$, which is about equal to the plasma-redshift heating given by Eq. (33) and Table 2.

At about 10 solar radii, Sheeley Jr. et al. [22] observed that the white light images had outward velocities of $v \approx 2 \cdot 10^7$ cm s $^{-1}$, which is large compared with $2 \cdot 10^6$ cm s $^{-1}$ at 5 solar radii. When the protons are accelerated outwards between 5 and 10 solar radii, the collision frequency is not adequate to make their velocity distribution isotropic. The diamagnetic moments of the protons at 10 solar radii would then be relatively small. The thermal velocity of the electrons would be more isotropic and their diamagnetic moments large. The electrons would then pull the protons outwards. If the electrons have a thermal velocity of kT equal to about $5 \cdot 10^{-10}$ erg, and the protons and helium about 10% of that, the outward diamagnetic force on a proton for n equal to 2.1 would be about $1.16 \cdot 10^{-9}/R$ dyne. The gravitational attraction force on the protons at this location is about $3.2 \cdot 10^{-10}/R$ dyne. The magnetic repulsion thus exceeds the gravitational attraction by $8.4 \cdot 10^{-10}/R$ dyne. This excess repulsion force on the proton corresponds to outward acceleration of 722 cm s $^{-2}$, which is in the range of 290 to 830 cm s $^{-2}$, observed by Sheeley Jr. et al. [22].

The significance of angular scattering. Eq. (B11) of Appendix B indicates that the angular scattering of the He^{++} -ions is much greater than that of the protons. The velocities of the helium-ions are therefore much more isotropic than that of the protons. The average force on the diamagnetic moments produced by the helium-ions may then be much larger than the corresponding force on the protons. Even the average outward velocity of the helium-ions may then become larger than the corresponding velocity of the protons. This may explain the remarkable observation by Steinberg et al. that helium ions often have velocities that are equal to or even exceed that of the protons [28].

Synopsis. In the transition layer and low in the corona the transformation of magnetic field to kinetic energy and heat is important, as indicated in Appendix B. High in the corona this transformation is less important, because of smaller mutual coupling to the field-generating currents. High in the corona, and especially beyond 5 solar radii, the magnetic repulsion of the diamagnetic moments is important and transfers energy to the plasma. The radial magnetic field must therefore decrease with n greater than 2. When the field decreases and approaches equilibrium with the thermal kinetic energy of the plasma, it bends around due to solar rotation and decreases until the field becomes amorphous.

These examples serve mainly as illustrations of how to use the equations and the theory. The temperature of the protons and the exact variation in the strength of the magnetic field are not known well enough to make exact predictions. However, it appears that the experiments are in rough agreement with both the plasma-redshift theory and the magnetic repulsion theory (see Eq. (B10)), which appear to explain in a simple way phenomena that previously could not be explained.

5.4 Far-reaching solar streamers

During total solar eclipse, far-reaching streamers are seen radiating almost isotropically within the first 3 to 5 solar radii from the Sun. (See Fig. 37, p. 124 of reference [6].) It has been difficult to explain these isotropic streamers. We are inclined to believe that the field lines from dipoles creating the magnetic fields would curve around, and that the field would decrease outwards approximately with $1/(R - R_1)^3$, where R_1 is the distance of the pertinent magnetic dipole from the solar center.

The plasma redshift facilitates explanation of these phenomena. The plasma redshift results in “bubbles” containing hot electron plasmas. The “walls” of the “bubbles” contain slightly colder plasma, which may not be as fully ionized as the inside of the “bubbles”, especially in the transition zone. The electron pressure from the inside on the “walls” of each “bubble” is nearly isotropic. The gravitational field affects the pressure of the protons much more than that of the electrons; the heavier protons inside the bubble and in the walls produce greater pressure at the bottom. The electrical field reduces the vertical pressure difference, but the hotter interior of the bubble will nevertheless create more uniform pressure than the colder plasma in the walls. Consequently, the bubble will be elongated in the vertical direction even at places where the magnetic field initially was horizontal. This bubble structure is rather stable, even when the plasma is fully ionized and reaches far into the corona. The reason is that the plasma redshift is a first-order process while the cooling is second order in density. High in the corona the reduced mutual induction between the currents of charged particles encircling the field lines and the currents creating the magnetic field reduces the conversion of magnetic field to heat. The outward decreasing magnetic field pushes the diamagnetic moments outward and pushes simultaneously the top of the bubble outward, as given by Eq. (B10) in Appendix B. We find, therefore, that the magnetic field radiates nearly isotropically from the Sun and reduces nearly proportional to $1/R^2$, rather than $1/(R - R_1)^3$. The remarkable observations of streamers in solar corona are consistent with predictions of plasma-redshift theory and Eq. (B10) in Appendix B.

5.5 Solar flares

Solar flares come in many sizes and have many forms. At the end of a large solar flare, when a large “bubble” breaks the surface, a hot plasma gushes into the corona and the hot plasma may

reach the Earth, increase auroral activity, influence the magnetic field, and disturb power lines. The plasma-redshift theory facilitates explanations of the flare phenomena.

In Section 5.1, we saw that plasma redshift leads to formation of hot “bubbles” in the upper chromosphere. The spicules consist of colder plasma squeezed between the expanding “bubbles” in the transition zone. The flare phenomena are related to the “bubbles” and the spicules in the transition zone and have similar explanation, but the flares are formed below the spicules region. Usually, the condition for a plasma redshift in deeper layers of the chromosphere and the reversing layers is not present. The temperatures are too low, the densities too high, and the magnetic fields not strong enough for initiating plasma redshift. However, hot gas containing relatively strong magnetic fields can occasionally move up from layers below the photosphere into the chromosphere. As described in Appendix B, the partially ionized plasma cools down when it moves through the photosphere. The B-field then approaches the H-field, which only slowly can transform into heat. The rate of transformation of the magnetic field energy to kinetic energy of the charged particles increases as the plasma temperature increases. At a certain location within this plasma close to the chromosphere, the temperature may be about 20,700 K and electron density about $1.211 \cdot 10^{10} \text{ cm}^{-3}$. (These values are close to the temperature and densities at height of 2154 km in model A by Vernazza et al. [3].) As shown by De La Beaujardire et al. [29], the B-field in a large flare may be in the range of 1000 to 1,600 gauss. Eq. (28) indicates that the 50% cut-off wavelength is then about 70 to 170 nm. This plasma is highly ionized and short wavelength radiation intensity internal in the plasma is high. Because the plasma redshift is a first-order process while the cooling is a second-order process in density, the hot areas have a tendency to get hotter and cold areas colder. A slight imbalance in temperature will therefore concentrate the plasma-redshift heating in a “bubble”, which then becomes much hotter than its surrounding region. Initially, this imbalance is caused mainly by short wavelength light internal to the hot plasma. As the temperature increases the light from the photosphere starts to contribute to the heating in the hot bubble. The heating causes transformation of magnetic field energy to heat, as explained in Appendix B. At higher temperatures, the rate of transformation of the magnetic field to heat increases nearly exponentially. The increase in the diamagnetic moments with the heating causes the B-field to decrease inside the “bubble” volume. This causes an electromotive force that seeks to reduce the currents creating the magnetic field. The corresponding decrease of the magnetic field in the walls of the “bubble” is reduced or even reversed by the return field from the diamagnetic moments inside the “bubble”. The field in the walls has a tendency to intrude into the “bubble” and increase the heating of the intruding plasma particles.

An initial magnetic field of about 1,600 gauss could create a pressure that could balance the thermal pressure in the plasma corresponding to $N_e T \approx 3.8 \cdot 10^{20} \text{ cm}^{-3} \text{ K}$.

It may be difficult to detect the initial formation of the bubble through the layers above, as the short wavelength radiation inside the bubble has usually high optical density. The bubble will expand, preferably along the field lines. When the field is horizontal the bubble may span 100,000 km. The temperature can increase to or exceed 100 million degrees K, and sometimes it could possibly even reach much higher temperatures before the bubble breaks through the surface and the hot plasma erupts into the corona. However, the heat conductivity coefficient becomes very large and will usually prevent these extreme temperatures unless the magnetic field is very strong. The hottest temperatures can nevertheless produce significant amounts of x rays, and even neutrons [29, 30]. Some fusion may take place.

The magnetic heating in the bubble will increase the redshift heating. The high temperatures, large magnetic fields, and high pressure may broaden the photons and increase the rate of plasma-redshift heating in the bubbles to about $8.6 \cdot 10^{-13} \text{ erg s}^{-1}$ per electron. Disregarding the cooling, the rate of temperature increase of the plasma would then be similar to that in Eq. (31) or

$$\frac{dT}{dt} \approx \frac{8.6 \cdot 10^{-13}}{1.9 \cdot \frac{3}{2}k} = 2000 \text{ K s}^{-1}, \quad (35)$$

where k is the Boltzmann constant. The bubble temperature would then reach 100 million degrees K in about 50,000 seconds or about 14 hours. When the bubble becomes hot the rate of transformation of the magnetic field to heat increases, as shown in Appendix B. The last 7 to 10 hours may then be shortened significantly. In the initial stages, much of the recombination cooling does not escape,

but is absorbed or reflected in the walls of the bubble. The rough estimate in Eq. (35) serves only to indicate the order of magnitude.

When the field lines are nearly vertical, we should expect smaller flares because it is easier for the bubbles to expand along the field lines and open up to the corona. The bubbles can also be initiated at smaller field strengths and higher in the atmosphere, which would make the corresponding flares smaller.

Loops and arches. Loops and arches are sometimes seen reaching far into the solar corona. These loops and arches have been difficult to explain; but the plasma-redshift heating helps explain these phenomena.

When a large “bubble” with horizontal field lines approaches the surface, a dome consisting of the “wall” of the bubble may be seen. As the dome rises the wall is likely to split into arches along the field lines, because any weakness caused by ripples or fluctuation will enhance the splitting of the dome along the field lines. When the hot plasma penetrates between the field lines, the redshift heating will push the arches formed in this way apart. The arches are relatively stable structures. The redshift heating is proportional to the density, while the cooling is a second order in density. Inside an arch the cooling dominates and the density inside the arch is higher than that outside the arch. But the pressure inside the arch may be lower than the pressure in the hot sparse plasma outside the arch. The redshift heating outside the arch pushes the sparse plasma on the outside into the arch, while the cold emission-cooled plasma leaks down in both ends of the arch. This structure is relatively stable and can sometimes last for days and stretch far into the corona.

5.6 Plasma redshift of spectral lines and gravitational redshift

Plasma redshifts of solar Fraunhofer lines is significant and requires revision of both Einstein’s gravitational redshift and the standard interpretation of solar redshifts.

5.6.1 Plasma redshift of solar Fraunhofer lines

Redshift of solar lines is small, and the second term on the right side of Eq. (20) is usually significant. Most photon widths are broadened due to the effects of collisions: 1) with neutral atoms, 2) with the Fourier field of charged particles (Stark effect), and 3) with the photon field, which result in stimulated (induced) absorptions and emissions. The photon widths can also be broadened by magnetic fields. The Doppler effect caused by movements in the line-forming elements affects the line width, but not the photon width. The Doppler shifts can be very large in the spicules region; but in the reversing layer and in the photosphere, the Doppler redshifts are nearly equal to Doppler blue shifts. The average Doppler shifts of photospheric lines are usually smaller than those often assumed for explaining the large deviation of the observed shifts from the expected gravitational redshifts.

The broadenings of the widths of the photons vary with temperature and density and therefore with the depth of the line formation in the photosphere and the reversing layers. Usually, a photon’s width varies across the solar disk. It is often significantly smaller close to the limb because of lower density. This then reduces the limb effect, as in the case of the sodium and potassium resonance lines. It is complicated to estimate the broadening effects, as the theories for the different broadenings are often inadequate. It is sometimes necessary, therefore, to rely on experimentally determined values for the Sun. For the relative variations of the collision broadenings of the lower and upper levels of each transition, it is often useful to use as a rough guide the collision excitation functions:

$$Y_L = NT^{1/2} \exp(-E_L/kT), \quad \text{and} \quad Y_U = NT^{1/2} \exp(-E_U/kT), \quad (36)$$

where the E_L and E_U are the energies of the lower and upper levels, and where N and T are densities of the neutral and charged particles and T their temperatures from model C of the solar atmosphere developed by Vernazza et al. [3]. The variations in the functions with height are illustrated in Fig. 3. Besides the excitation functions E_L and E_U , the broadenings depend on electronic configuration, the angular momentum for each level, and transition probabilities for each transition.

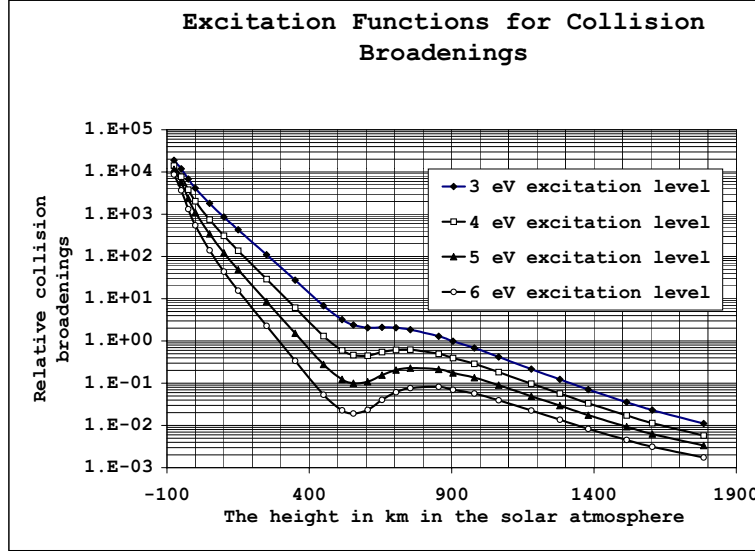


Figure 3: The abscissa gives the height in km above the optical density $\tau_{500} = 1$ in the solar photosphere. The ordinate gives in arbitrary units the excitation function $Y = NT^{1/2} \exp(-E/kT)$ for the collision broadening. The values of the number density N of hydrogen and the temperature T are from model C of Vernazza et al. [3]. The value of the excitation potential E of the energy level in the atom is equal to 3, 4, 5, and 6 eV for the four curves, respectively. The curves indicate how the collision broadening varies with the height of formation. The collision broadening varies also with the transition rate and the angular momentum change for each transition.

These excitation functions show that deep in the photosphere the broadening for each line decreases steeply with increasing height. Analysis of the redshift measurements shows that when the lower excitation potential exceeds about 3.5 eV (and the upper level about 5.8 eV), the collision broadening is usually small, and the photon width is then close to the natural quantum mechanical width, except deep in the photosphere where the temperatures and pressures are high. When the lower excitation potential is less than 3 eV, the collision broadening is often significant even above the temperature minimum in the solar atmosphere.

Weak lines are formed at great depths. When their widths are collision-broadened, the photons have maximum widths at the center of the solar disk. This broadening of weak lines causes increased redshift at the center. Because the lines are weak and formed relatively deep in the photosphere, the broadening decreases sharply with height, as Fig. 3 indicates. We observe therefore a decrease in the redshift as the line of sight moves away from the center of the solar disk and up in the photosphere. For these lines, the observations show that the redshift often reaches a minimum at distances between about 0.4 to about 0.7 solar radii from the center of the solar disk. Beyond this distance the redshift of these weak lines increases towards the limb due to increased path length low in the corona in accordance with the first term, the integral term, of Eq. (20).

Slightly stronger lines are formed higher in the photosphere. These lines often have low excitation potentials and are therefore more easily collision broadened. When they are formed around the temperature minimum in the solar atmosphere, the collision broadening varies less with height. These lines show then a plasma redshift, which increases towards the limb in accordance with the first term of Eq. (20), similar to that shown for the lines listed in Table 3. When at the center the line is formed at or just below the temperature minimum and at the limb just above the temperature minimum, the second term, which is sensitive to variations in the broadening effect, will enhance the limb effect.

Table 3 Solar redshift.

Distance r/R_0 from center of solar disk in units of solar radius R_0	Measurements by Higgs of $(\Delta\lambda/\lambda) \cdot 10^6$	Measurements by Adam of $(\Delta\lambda/\lambda) \cdot 10^6$	Averages of $(\Delta\lambda/\lambda) \cdot 10^6$	Estimates ¹ of Plasma redshift $(\Delta\lambda/\lambda) \cdot 10^6$
0.999				3.12
0.998	3.03	2.67	2.85	(3.03)
0.995	2.83	2.56	2.69	(2.86)
0.990	2.62	2.44	2.53	(2.66)
0.985	2.47	2.35	2.41	(2.53)
0.980	2.36	2.35	2.35	(2.43)
0.975	2.27	2.21	2.24	(2.36)
0.974				2.35
0.970	2.19	2.15	2.17	(2.27)
0.950	1.96	1.96	1.96	(2.08)
0.949				2.04
0.925	1.80	1.77	1.78	(1.84)
0.900	1.70	1.61	1.66	1.72
0.875	1.64	1.48	1.56	(1.60)
0.800				1.40
0.700				1.24
0.600				1.14
0.500				1.08
0.000	1.08	1.08	1.08	1.00

¹ The values in the parentheses are obtained by interpolation.

In case of stronger lines, which at the center are formed close to and slightly above the temperature minimum, the temperature increase may dominate the decrease in density. As the line of sight moves away from the center, the broadening effects may then first increase slowly and reach a low maximum before they decrease again because of reduced density. The redshift of collision-broadened lines formed at this height varies therefore less with the distance towards the limb, as the increase in redshift caused by the first term of Eq. (20) is sometimes compensated by the decrease in the width and the redshift caused by the second term. The lines may then have relatively small center-limb variation. The lines with small center-to-limb effect are then also characterized by having relatively small strength at the limb relative to the line's strength at the center of the solar disk, such as the sodium and potassium resonance lines.

For estimating the redshift, we have used the coronal electron densities shown in Table 2. For the stretch from 3 to 5 solar radii, we used slightly smaller hump, because the average height of this hump is slightly smaller than indicated by Table 2. The redshift given by Eq. (20) is integrated from the cut-off region in the Sun to the observer on the Earth. The integral is rather insensitive to the electron densities variations beyond about 3 solar radii and beyond because of the low electron densities. When the electron densities are relatively large in the transition zone and lower corona, the cut-off region moves up; and when the electron densities are low, the cut-off region moves down. The lower integration limit, therefore, moves up and down with the densities in the cut-off region. The plasma-redshift integral just above the cut-off region varies therefore less than if the cut-off zone did not move up with increase in plasma density. This is the densest region and contributes most to the integral in Eq. (20). The plasma-redshift integral, which uses the average densities, relative to the cut-off, is therefore a relatively good estimate.

The measurements of the redshift are usually made when the solar atmosphere is quiescent, and the average values are usually obtained by integrating over long time periods. The electron densities listed in Table 2 are close to average values for a quiescent corona, because the temperature

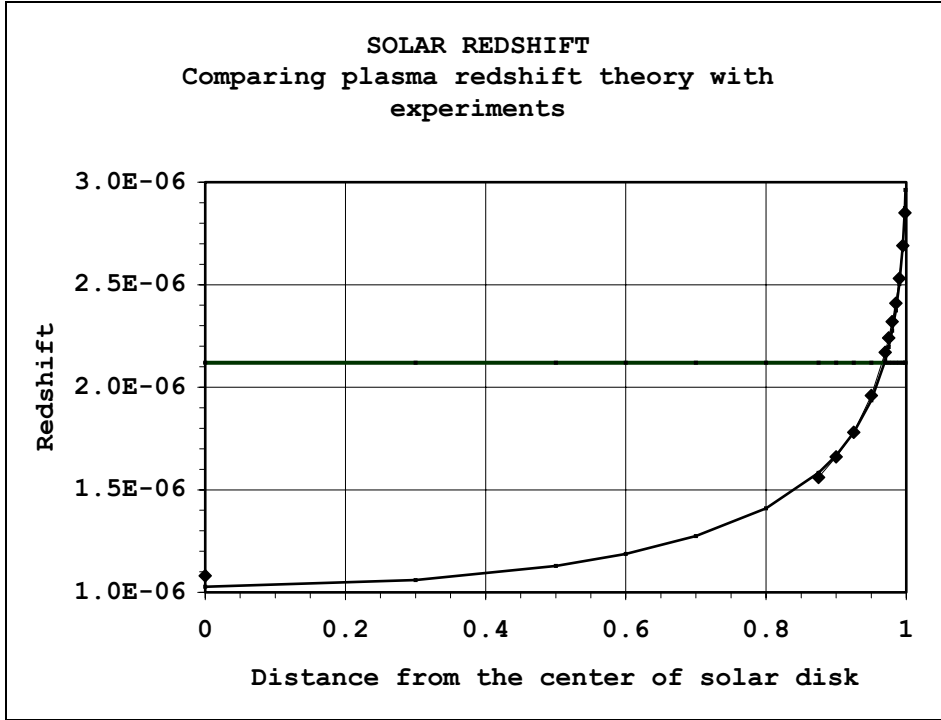


Figure 4: The diamonds show the average redshift measured by Adam [31] and Higgs [32] (see Table 3), while the curve shows the redshift predicted by the plasma-redshift theory when using the coronal electron densities listed in Table 2 and shown in Fig. 2. The horizontal line at $2.12 \cdot 10^{-6}$ shows the redshift predicted by Einstein's classical gravitational theory.

is consistent with the average estimates of Sturrock et al. [20] and Wheatland et al. [21]. For comparison, see the estimates by Newkirk [19], McWhirter et al. [11], and Withbroe [13, 14].

Solar redshift measurements by Adam [31] and Higgs [32] of the 629.78, 630.15, and 630.25 nm lines from Fe-I are listed in Table 3. The ionization potentials of the upper levels are: 4.191, 5.620, and 5.653 eV, and of the lower levels: 2.223, 3.654, and 3.686 eV, respectively, for the three lines. At the center, the formation of these lines is below the temperature minimum; but close to the limb, the formation is above the temperature minimum. The excitation functions mentioned above indicate that the collision broadening of the average of the three lines does not vary much with height for these lines. Estimates of the plasma redshift in the last column are obtained by using the integral term in Eq. (20). This is equivalent to assuming that the average photon widths of these three lines are about equal to the classical width of the photons, and that the collision broadening does not vary much across the solar disk.

In these experiments, the authors made extreme efforts to obtain accurate average redshift for each line at each position all the way to the extreme limit of the solar limb. The steep variation close to the limb requires that the opening angle is very small and the integration time very long. As can be seen from Table 3, the results of Adam and Higgs differ slightly. Such differences are common; and they are understandable when we think of the variation in the electron densities with time; for example, with the sunspot cycle. As Table 3 and Fig. 4 indicate, the agreement between the plasma-redshift theory and the experiments is very good. The redshift varies from center to limb with the electron density integral.

Center-to limb variations. The center-to limb variations may vary slightly from one time to another. The size and frequency of coronal holes vary with the sunspot cycle. Coronal holes are more frequently over the polar region than over the equatorial region. In coronal holes, the electron densities are usually low. The limb effect in the north-south direction will therefore sometimes be smaller than that along the equator. This is consistent with the measurement of the center-to-limb variation of the Fe line 557.6 nm by Brandt and Schröter [33], who found significant difference between center-to-limb redshifts in south-north and east-west directions. Their measurements were made in April 1978 and a few in September 1979. In March the Sun's south pole is tilted about 7 degrees towards the Earth and in September away from the Earth. During the times of observations, there were sunspots at high latitude but very few at low latitude. Brandt and Schröter considered the conventional explanation of possible Doppler shifts. Meridional flows towards the equator could possibly cause the decrease in the redshifts close to the polar region. They rejected that explanation, because they found that the required hypothetical currents of about 250 m s^{-1} were too large and contradicted other observations.

Usually, the redshift increases steeply close to the limb. It is then important that the entrance slit have a small width, preferably less than about 1 arcsec. In the limb region, the line of sight penetrates the spicules region, which is highly turbulent. It is then necessary to use long exposure time to get good averages. Some researchers have not taken this effect adequately into account and find then smaller limb effect. Some of the conventional extrapolations of the redshifts from points far away from the limb to the points close to the limb are invalid, because close to the limb the redshift often increases more steeply towards the limb than that assumed. Frequently, the extrapolations sought to approach Einstein's gravitational redshift at the limb.

Redshifts in active regions. In magnetically active regions, the redshifts are usually found to be greater than the redshifts far away from them [34]. These larger redshifts are often interpreted as due to reduced upward Doppler shifts. The magnetic fields in the active region are expected to reduce the upward movements of photospheric currents. Other researchers explain this increased redshift as due to general down draft in the active regions.

According to Eq. (28), we expect the cut-off region for the plasma redshift to reach deeper into the transition zone over magnetically active region. The magnetic fields over the active region will therefore often increase the redshifts. Concurrently, the magnetic field may reduce the movements in the photospheric layers. However, the Doppler blue shifts should be expected to nearly balance the Doppler redshifts. General down draft is also a possibility, but independent evidence of that is lacking. The magnetic field may reduce the temperature and shift the minimum temperature in the atmosphere, which in turn will affect the distribution in collision broadenings. The shift of the minimum temperature to deeper layers will steepen the increase in collision broadening with depth, which is consistent with the changing tilt of the bisector as observed by Cavallini et al. [34]. The bisector segments close to the continuum are redshifted the most, while the bisector segments closer to the bottom of the line are redshifted less and sometimes blue shifted relative to the regions outside the active regions (most likely due to lower minimum temperature in the active region). According to the plasma redshift theory, this effect and the lowering of the cut-off zone by the magnetic field are the likely causes of the increased redshift in the active regions.

5.6.2 Gravitational redshift

The greatest surprise is that the plasma redshift appears to explain the solar redshift without Einstein's gravitational redshift, as Table 3 and Fig. 4 show. Einstein's gravitational redshift has been proven beyond reasonable doubt in a great many experiments. It follows from reasonable extension of the special theory of relativity to general theory of relativity. The fact that the plasma-redshift theory explains the observed solar redshift of Fraunhofer lines contradicts the generally accepted view that the solar lines are gravitationally redshifted.

However, this apparent contradiction has a simple explanation. The experiments (on the Earth and in space) that appeared to prove the gravitational redshift are not able to detect the blue shift caused photons repulsion by the gravitational field, because the wave packet defining the photons in

these experiments is much too large. Einstein's theory of general relativity (TGR) is entirely in the domain of classical physics. It sometimes, as in these experiments, disregards quantum mechanical effects.

The photons are gravitationally redshifted when emitted in the Sun; but during their travel from the Sun to the Earth, they lose their gravitational redshift, and are not gravitationally redshifted when they arrive on the Earth. The change in frequency, as the photons travel from the Sun to the Earth, is due to increased gravitational potential as the photons travel from the Sun to the Earth. In the quantum mechanical treatment, the photons adjust to the gravitational potential as if they were particles. Thorough analysis consistent with quantum mechanics shows that the photons are actually repelled by the gravitational field. The gravitational field pushes them away from the gravitating body. We may be surprised, because this fact contradicts conventional thinking and what we have been taught. This fact also contradicts Einstein's field equations and the equivalence principle, which surmise that all energy forms are attracted in a similar manner by the gravitational field, because $E = mc^2$. Conventional thinking has surmised without adequate proof that the photons were always attracted like particles by massive bodies. As we will see, correct interpretation of the many relevant experiments shows that the gravitational field repels photons. The repulsion of photons in the gravitational field simplifies explanation of many phenomena. The repulsion of photons to some extent counterbalances the gravitational attraction, makes unnecessary the Einstein's lambda term, and brings stability and harmony to the cosmological perspective, as we will see.

Einstein's thought experiment with an observer in a closed elevator box is interesting and almost correct, but not completely correct. The gravitational field lines are almost parallel, but not completely. In the linear movement of a falling object, the gravitational field has always a gradient, while the inertial field does not. It can be shown that mathematically, a gradient towards a point makes a difference. For the present discussion, we need only recognize that there is a difference between an inertial field and gravitational field directed towards a point.

Let us consider an atom in the Sun. All frequencies of the atom, all the energy levels, and all the frequencies corresponding to the energy differences between two levels in the nucleus or in the electronic configuration are gravitationally redshifted according to Einstein's classical theory of general relativity (TGR). As we bring that atom from the Sun to the Earth, the gravitational redshift of the frequencies disappears. During the travel of the atom from the Sun to the Earth the levels and the frequencies are blue shifted and that blue shift cancels the gravitational redshift (or more exactly, the difference in gravitational redshift in the potentials of the Sun and the Earth). The gravitational redshift depends on the potential energy. We can say that the energy we transfer to the atom by lifting it out of the solar gravitational field is the cause of this blue shift. (In some articles, an incorrect interpretation of the gravitational redshift is given. It is stated that the photons lose energy as they move up the gravitational potential from the Sun to the Earth. This is not the way Einstein saw it. In fact, a maser clock in the Sun would be seen to move at a slower rate than the clocks on the Earth. In the Sun, the frequencies of the photons are slower, like the photon frequencies that would control the maser clocks in the Sun. According to Einstein, the photons do not change frequency as they move from the Sun to the Earth. In his arguments, he considered that light consists of classical electromagnetic waves; that is, that the wave packet for the photons reached from the Sun to the Earth and beyond.)

Photons when treated as quantum mechanical particles behave to some extent the same way as the atoms mentioned above. They are gravitationally redshifted when they are in the Sun; but during their travel to the Earth, their frequencies are blue shifted (like the frequencies of the atom) such that when they arrive on the Earth the photons are not gravitationally redshifted (they have the same redshift as photons from the similar atoms on the Earth). For lifting the atom out of the solar gravitational field, we had to use energy to overcome the gravitational attraction. However, the gravitational field repels the photon. The photon is pushed away, so we do not have to apply energy to bring the photon out of the gravitational field. We may actually assume that gravitational force attracts the photon, as in classical physics; however, then the quantum mechanical repulsion is twice as large. The net result is a repulsion numerically equal but opposite to the classical gravitational attraction.

Einstein argued that equally many waves must arrive on the Earth as leave the Sun. Therefore,

the redshifted photons in the Sun will be redshifted when they arrive on the Earth. This is a classical physics argument applied to infinite train of electromagnetic waves, which is impermissible in quantum mechanics. If the photons reached from the Sun to the Earth, as in classical physics, Einstein could appear to be right. The photons of some masers used in many experiments have this characteristic. They may reach from the Sun to the Earth and well beyond. However, the photons in the visible light are very short, on the order of a few meters. As a measure of their length we can take $\lambda^2/(\Delta\lambda)$, where λ and $\Delta\lambda$ are the wavelength and the photon width. In an undisturbed sodium atom the resonance line has wavelength 589 nm, and a quantum mechanical photon width, which is about the same as the classical photon width 0.0116 pm. The length of the photon is then about 30 m. In the Sun the photon width at the center of solar disk is about 17 times broader, and the length of the photon therefore only about 1.8 m.

The solar light photons during their travel to the Earth have plenty of time to change their frequency and adjust to the gravitational potential field. In contrast, the 14.4 keV photons used in the experiments by Pound and Rebka, Jr. [35, 36], and Pound and Snider [37] did not have enough time (only 75 ns) to change their frequency, as they traveled the distance of only 22.5 m between emitter and absorber in the weak gravitational potential of the Earth. The difference in gravitational potential of the 14.4 keV photons at the position of the emitter and the absorber in the experiments [35-37] is:

$$\Delta E = (\hbar\nu/c^2) 981 \cdot 2250 = 5.67 \cdot 10^{-23} \text{ erg}, \quad (37)$$

where the factor 981 is the gravitational acceleration in the laboratory, and the factor 2250 cm is the height difference. From both the uncertainty relation and the transition theory in quantum mechanics, the minimum transition time between the two states of the photon is:

$$\Delta t \approx \hbar/(2\pi\Delta E) = 1.9 \cdot 10^{-5} \text{ s}, \quad (38)$$

where \hbar is Planck's constant. The wave packet needed to define that small energy difference has a length of about $c\Delta t \approx 5.6 \text{ km}$. The length of the 14.41 keV photon is about $L \approx 2\pi c\tau = 270 \text{ m}$, where $\tau = 143 \text{ ns}$ is the life time of the 14.41 keV transition in the nucleus. During the travel from the emitter to absorber, the photons would usually experience smaller potential difference. Therefore, it is impossible for the photons to adjust to the new potential or to change frequency during their short travel time of 75 ns from the emitter to the absorber in these experiments. On the other hand, the atoms and the nuclei in the emitter and absorber had plenty of time to adjust to the gravitational potential difference. Every transition in quantum mechanics takes time. Photons require time to change from one state to another, even if the states overlap and are continuous. In the experiments [35-37] the photons had no chance to adjust to the gravitational potential, while they moved from the emitter to the absorber. These experiments are inconclusive, in respect to gravitational redshift theory, because they did not make it possible to detect the repulsion or attraction of the photons by the gravitational field.

In the rocket experiments by Vessot et al. [38], the maser photons are too long. Importantly, the potential difference is too small. In the space experiments by Krisher et al. [39], the laser photons (signals) used in the experiment are extremely long. They reach from the Sun to beyond Saturn. None of the experiments proving the gravitational redshift make it possible to detect the relevant gravitational effects on the photon.

Quantum mechanics, in accordance with Bohr's correspondence principle, approaches and becomes identical with the classical mechanics in the limit of macroscopic experiments, and in the limit of slow variation in the gravitational field. A correct quantum mechanically modified TGR does not contradict the classical physics experiments, like the experiments by Pound and Rebka [35, 36], Pound and Snider [37], rocket experiments by Vessot et al. [38], and the space experiments by Krisher et al. [39], because the experiments are inconclusive and do not make it possible to detect a repulsion or an attraction of the photon. In the gravitational deflection experiments by Riveros and Vucetich [40], and in the experiments on the time delay of radar echoes by Shapiro et al. [41], it is important to realize that 50% of the measured effect is due to variation in the speed of light in the gravitational field, and 50% is due to warping of space. The changes in the speed of light, the

warping of space, and the deflection are caused by the mass of the Sun (the star or the galaxy), and are independent of repulsion or attraction of the photon, and independent of any frequency change during time of flight. In these cases, the photon's velocities had to adjust to the gravitational potential during their time of flight. Quantum mechanical analysis of the experiments shows that this is possible.

5.6.3 Results of solar redshift experiments compared with theory

There is thus a fundamental difference between solar redshift experiments and the classical physics experiments that have been assumed to prove Einstein's classical TGR. The solar redshift experiments reveal the repulsion of photons in the gravitational field. The other experiments do not.

It will be argued that the solar redshift experiments have been proven to confirm the gravitational redshift. For example, it will be argued that the elaborate works of Dravins et al. [42] and Dravins [43] have proven beyond reasonable doubt that the difference between the observed redshift and the predicted redshift can be explained as due to Doppler shift in the line forming elements. The analysis by Dravins et al. is supported by many observations. The explanation of shifts of lines as we move from the granules to the intergranular lanes appeared convincing.

Essential premises for the conventional theory by Dravins et al. are:

1. Einstein's gravitational redshift of solar lines when observed on Earth applies.
2. Most of the deviations from the gravitational redshift are due to Doppler shifts.

There is no place for a plasma redshift, which follows from basic laws of physics. For obtaining a match between the assumed velocity distribution and observed C-form of the line median, and for explaining the large blue shifts of most lines at the center of the solar disk relative to the gravitational redshift, Dravins et al. suggested that these observations derive from up-streaming currents of about 1200 m s^{-1} over 75% of the area in the granules and down-streaming currents of about 3600 m s^{-1} over 25% of the area in the intergranular lanes. The actual division between these regions is more gradual and variable. The assumed large asymmetry in the area and velocities between up and down streaming currents was necessary to explain the observations. These assumptions were supported by observation of apparent line shifts in the granules and intergranular lanes. (We will see later when we report on the observations by Miller et al. that the observed shifts in the granules and intergranular lanes are in the wings and not the core of the lines.) It is well known that the observed widths of the Fraunhofer lines exceed the Doppler broadening caused by thermal motion. Vernazza et al. [44] explain the additional broadening as caused by turbulence with velocities on the order of 1 to 1.4 km s^{-1} . But the assumed asymmetry in the flow is not supported by independent evidence.

The predictions of the Doppler shift theory by Dravins et al. are very often the same as the predictions of the plasma-redshift theory. The Doppler shift theory by Dravins et al. explains that weak lines, which are formed deep in the atmosphere, have small redshifts, because the velocities of the up-streaming currents appeared to increase with depth in the atmosphere. (Apart from the observed shifts of the lines, there is no independent verification of increasing velocities with depth. The increasing density with depth would be consistent with decreasing velocities with depth.) As Eqs. (18) and (20) show, the plasma redshift increases with photon width. The plasma redshift predicts that weak lines, which are formed deep in the photosphere, have small redshifts because their photon widths are usually small. The photon width is usually associated with the strength of a line, which is associated with the height of the line's formation in the atmosphere. However, there are important exceptions to this rule. Exceptionally, some weak lines have large photon widths and therefore large plasma redshifts. The Doppler shift theory, on the other hand, predicts small redshifts for the weak lines independent of the photon width.

Pierce and LoPresto [45] found for the Ni I lines a redshift-strength relation similar to that for the Fe I lines. However, for similar equivalent widths the redshift of the Ni I lines was significantly greater than that of the Fe I lines. This is contrary to what is to be expected if the redshift is a function of depth of the line formation as suggested in the theory of Dravins et al. [42]. The observation is in agreement with the prediction of the plasma-redshift theory. For same equivalent

widths, the nickel lines have broader photon widths than the iron lines, because nickel concentration is only about 4% of the iron concentration in the solar atmosphere.

For Ti I lines Pierce and LoPresto [45] found a similar relation, but the discrepancy between the measured redshifts and those expected from the equivalent widths was greater. In the Sun, the concentration of titanium is about 0.4% of that of iron. These observations contradict the conventional theory by Dravins et al., but are consistent with the plasma-redshift theory.

The 3d-4p lines 849.8 and 854.2 nm lines of Ca II have exactly the same upper level (same voltage of 3.15 eV and same angular momentum) as the 393.3 nm resonance line. The relative rate constants and strengths of these three lines are roughly proportional to 1, 9 and 136, respectively. However, the photon widths of the two weaker lines are on the order of or greater than the photon width of the strong 393.3 nm resonance line. The lower levels of the 849.8 and 854.2 nm are easily broadened by Stark effect, as shown by Griem [46], and can be broader than the lower level of the resonance line. St. John [47] measured the center redshift of the strong 393.3 nm resonance-line to be about 1296 m s^{-1} , while Herzberg [48] measured the redshift of the much weaker 849.8 and 854.2 nm lines from the same upper level to be about 1533 and 1933 m s^{-1} , respectively. This is consistent with the plasma-redshift theory, but contradicts the Doppler shift theory by Dravins et al. [42].

Miller et al. [49], who used high spatial resolution technique, about 0.28 square arcsec resolution, measured the redshift and the form of the bisector in the granules and separately in the intergranular lanes. These measurements can be expected to find huge differences in the redshifts. The down streaming currents in the intergranular lanes could result in large redshifts far in excess of the gravitational redshift and the up-streaming currents in the granules could result in large blue shifts. However, the measurements showed that in the core of the line, including the bottom of the line, the redshift and the C-form of the bisector are almost the same (within about 20 m s^{-1}) in the granules and the intergranular lanes. This finding was the case for all three lines investigated (Fe I lines 406.5, 543.4, and 523.3 nm). The wings (not the core) of the lines were redshifted 75 to 200 m s^{-1} in the intergranular lanes as compared with that in the granules. In redshift experiments, the core (and not the wings) of the line defines the redshift.

These observations contradict the assumption by Dravins et al. [42], but are consistent with the plasma-redshift theory. They do not contradict the expectation that the turbulence is significant for broadening of the lines. The turbulence does not appear to affect the redshift of the core of the line, which means that the Doppler redshifts about compensate the Doppler blue shifts. This is consistent with the expectations of many early (before 1960) researchers in this field. Importantly, the core and the vertex of the line determine the observed redshift as usually measured. The redshifts in the wings, 75 to 200 m s^{-1} , may possibly be due to Doppler shifts. However, even if they are, they appear to be much smaller than those expected.

The theory by Dravins et al. [42] explains that the C-form of a line's bisector is due to variation in the upward and downward currents. The assumed larger areas of the upward currents in the photosphere cause the prevailing blue shift relative to the expected gravitational redshift at the center of the solar disk. The plasma-redshift theory explains the C-form of the bisector as caused mainly by the spectrum of photon widths for each line. The collision broadening causes a distribution in the widths of the photons; even without the collision broadening, the widths have a distribution. This distribution in collision broadenings varies with temperatures and densities in the atmosphere, as well as the states of the colliding atoms. The conventional approach of averaging the collision broadenings and the collision shifts is not permissible in the plasma-redshift theory, if our focus is the line form. The plasma redshift, which depends on the photon's width, is independent of the direction of the currents in the line-forming elements. The plasma redshift has a distribution for each line independent of the concurrent Doppler shift. The photons with the largest width are redshifted the most. The fact that Miller et al. [49] observed that the core of the bisector in the granules is about the same as that in the intergranular lanes is consistent with the plasma-redshift theory; however, these observations contradict the Doppler shift theory by Dravins et al. [42].

In the plasma-redshift theory, we often can disregard the collision shift of the lines, because it is usually much smaller than the shift caused by the collision broadening. The collision shift may be on the order of 10% of the collision broadening. The redshift of the wavelength caused by the collision broadening is for the sodium resonance lines about 4 times the broadening, or about $\delta\lambda/\xi = 4\delta\lambda$ for

the 588.995 and 589.592 nm lines of Na I. The collision shift would then be only 2.5% of the redshift caused by the collision broadening. However, if the collision shift is significant, it must be included.

5.6.4 Redshifts of stars

Similar analysis for other stars show that also they must have coronas, especially the hot stars. The redshift heating increases with the fourth power of the temperature as Eq. (30) shows. The redshift heating can then compensate cooling from higher density plasma. This effect of the temperature on the density in the cut-off zone is reduced, because the increased densities lead to increased heights of the cut-off zone. As Eq. (32) indicates, a large radius of a star will usually extend the high-density region of the corona. The intrinsic redshift of a star should therefore increase with the temperature and the size of the star. Crude estimates for Spica leads to an intrinsic redshift of 5 to 10 km s^{-1} . This possibly could explain the K-effect, which shows that large bright stars appear to have large receding redshifts [50].

The observed redshifts of dwarf stars, such as the white dwarf Sirius B, can be explained as plasma redshifts without the conventionally assumed gravitational redshifts, which will have been cancelled by corresponding blue shifts, as the photons move out of the intense gravitational fields. Although the radius of a white dwarf star is small, the large gravitational field results in a dense usually very hot corona. The Stark broadening is exceptionally large in white dwarf stars. The lines are therefore broadened very much by Stark effect and the second term in Eq. (20) is often larger than the first term. The plasma-redshift heating and the magnetic field heating are often large in the transition zone. The heating by the plasma-redshift and the magnetic field can explain the very hot corona of white dwarf stars and their associated intense x-ray emission.

In quasars the measured redshift is useful for characterizing their corona. For the quasar 3C 273 with redshift of 0.158, the electron density integral is $\ln(1.158/3.326 \cdot 10^{-25}) = 4.41 \cdot 10^{23} \text{ cm}^{-2}$. This redshift integral, when combined with the other features, such as the bolometric temperature(s), including x rays and infrared spectrum, can help us to obtain a rough estimates of their absolute magnitude, distance, and even mass. The estimate of a rather simple quasar such as 3C 273 is rather complicated, as it will be necessary to take into account different parts of the spectrum including the x rays, the ultraviolet component, the visual spectrum, the infrared, spectrum, the production and cooling by microwaves, production and cooling of dust emitting infrared radiation, the optical density of the different radiations, the magnetic field, etc. In addition to the usual line broadenings, we may also have that the center-limb effect broadens the observed lines significantly. The plasma redshift is a first order process in the density, while the cooling effects are usually second order in density. This has a tendency to produce cloud formations in the corona, as in the case of the galactic corona. These clouds may result in absorptions lines with smaller redshifts than the emission lines. A crude estimate, based on the assumption that the magnetic field in the corona is small, places the quasar 3C 273 at a distance of about 8 Mpc, while the conventional theory derives a distance of about 680 Mpc. This rough estimate indicates that the absolute magnitude is about -17.6, and the mass is about 50,000 solar masses. The blobs, which move away from the quasar at angular speed of about 0.65 mas per year, would then be moving at a speed of about $3 \cdot 10^4 \text{ km s}^{-1}$.

5.7 Galactic corona

Lyman Spitzer in the 1950's [51] made it plausible that the Milky Way galaxy has a corona. Since then many observations have confirmed this fact. The dispersions in the frequencies of microwaves along the lines of sight from pulsars indicate that the interstellar H II regions within the Milky Way stretch far beyond the Strömgren radii of nearby stars. It has been difficult to explain the required heating of the corona and the heating and the large dimensions of the H II regions [51-58]. The plasma-redshift heating helps explain the observations. Not only does the plasma-redshift heating contribute to the heating of the plasma, but it also increases the electron temperature beyond million degrees. This reduces the density and the cooling. The fully ionized plasma regions can therefore reach far away from the hot stars. The H II regions around stars can retain their high temperature for a long time because of the continuous plasma-redshift heating.

These hot H II regions have often been explained 'ad hoc' as due to past supernovas even when no remnants of a supernova were found, because it was thought that only supernovas could explain the high temperatures. These supernova bubbles were assumed to move out into the corona and supply the needed heating of the corona of our Galaxy [51, 57, 58]. The transition zones to the H II regions and the galactic corona have absorption and emission lines similar to those in the transition to the solar corona. Beyond the transition zone, the hot plasma is usually more difficult to detect; but some lines indicating a million degree temperatures are sometimes observed.

Analyzing the spectrum from the supernova 1987A in the Large Magellanic Cloud (LMC), Pettini et al. [59] found that the 6374.51 Å-line in Fe X caused a pronounced trough in the spectrum. This absorption line is produced preferentially when the electron temperature is about 1.25 million K. If formed at one location, the trough would be relatively narrow. The full width at half maximum (FWHM) would be about 32 km s^{-1} , provided the turbulence is small. The trough stretched from about 210 to about 365 km s^{-1} for a total width of about 155 km s^{-1} [59] (see Section IIIa and Figs. 1 and 2 of that source).

The distance of supernova 1987A in the LMC is about 51 kpc, the galactic longitude about 280 and the galactic latitude about 32 degrees. Its movement along the line of sight is uncertain, as its redshift is a combination of a plasma redshift and a Doppler shift. In the past, we interpreted all shifts as Doppler shifts; and Pettini et al. interpreted the width as due to Doppler shifts in the intervening plasma. In light of the plasma-redshift theory, we realize that most shifts are combinations of the two. We will assume for a moment that the displacement of the beginning of the Fe X absorption, at about 210 km s^{-1} , is mostly due to a Doppler shift caused by the velocity of the solar system relative to the point where the line of sight to the LMC cuts the surface of our Milky Way. Some of the redshifts within our Galaxy will be due to the plasma redshifts in the H II regions. Based on measurements within our Galaxy, the average electron density is about 0.016 [52] to about 0.025 cm^{-3} [54]. For distances of about 2 to 3 kpc, the integrated plasma redshift within our Galaxy is likely to be about 10 to 23 km s^{-1} . The electron temperature of the galactic corona may deviate from the optimum temperature of 1.25 million K for the Fe X line, and would then contribute less to the absorption trough.

We will assume for a moment that the width of 155 km s^{-1} (from 210 to 365) of the trough as observed by Pettini et al. [59] is a rough measure of the plasma redshift along the line of sight in the corona, where the absorption by the 6374.51 Å-line in Fe X is significant. A white light from a supernova could produce such a trough. The light absorbed close to the supernova would have the largest plasma redshift. The light absorbed in the transition zone to the corona would have the smaller redshift, and the lines formed in the H II regions would have redshifts smaller than any part of the trough.

When using Eq. (20) and assuming that the second term on the right side is insignificant, we get that the average electron density along the coronal line segment D is given by

$$z = \frac{155}{3 \cdot 10^5} = 3.326 \cdot 10^{-25} (N_e)_{av} D 3.086 \cdot 10^{21}, \quad \text{or} \quad (N_e)_{av} = \frac{0.50}{D}. \quad (39)$$

If the distance D of the line segment within the corona to the supernova 1987A in LMC is $(51 - 3) = 48 \text{ kpc}$, we get that the average electron density is $(N_e)_{av} \approx 0.01 \text{ cm}^{-3}$, and that the electron column density is $(N_e)_{av} D 3.086 \cdot 10^{21} = 1.6 \cdot 10^{21} \text{ cm}^{-2}$. From Figs. 1 and 2 in reference [59], it appears possible that the absorption trough reaches to about 400 km s^{-1} . The column density would then be about $2 \cdot 10^{21} \text{ cm}^{-2}$.

Pettini et al. [59] believed, however, that absorption trough for the $\lambda = 6374.51 \text{ Å}$ -line stretched only over the range $v_H \approx 215 - 270 \text{ km s}^{-1}$, and that the remaining parts of the absorption trough were due to contamination by telluric lines and diffuse interstellar bands. Pettini et al. did not know the plasma redshift. Their assumption are therefore reasonable. As explained in the following, the high concentration of Fe X is most likely due to ionization by x rays from about $3 \cdot 10^6 \text{ K}$ intergalactic plasma, with an average x-ray energy of 259 eV. These x-rays will deposit their energy in the colder plasma low in the corona and in the transition zone to the corona. The ionization potential of Fe IX is 235 eV, and of Fe X it is 2.62 eV. The x-rays from the intergalactic plasma therefore have about the right energy to create relatively high concentration of the Fe X-ions in the colder plasma, even

in plasma well below $1.25 \cdot 10^6$ K.

In support for the contamination of the line, Pettini et al. point out the difference in the form of the absorption trough in the spectra taken April 9 1987 and July 20 1987 (see Fig. 2 of that source). However, it is more likely that during the 102 days, a colder plasma cloud formed in (or moved into) the line of sight to the supernova thereby enhancing the absorption trough closer to the supernova, as observations on July 20 indicate. Plasma redshift, because it is a first order process, has the tendency to create hot bubbles separated by walls of colder plasma. These walls of colder plasma form and disappear in the line of sight. The walls could also move into or out of the line of sight. Other lines formed in these walls would simultaneously show an increased and decreased strength. Plasma redshift therefore gives a reasonable explanation of the observations.

Pettini et al. [59] assumed the iron concentration to be similar to that in the Sun. They assumed collisional ionization based on thermal equilibrium in the plasma. From the depth and area of the absorption trough, they determined the column density and found a value that corresponds to about $N_H \approx 3.2 \cdot 10^{21} \text{ cm}^{-2}$. Pettini et al. considered several possibilities for explaining this unexpected high value, but concluded that the above-mentioned column density was most likely a reasonable estimate for the corona between our Milky Way and the LMC. However, their assumptions may not be right. The iron concentration may deviate from that in the Sun. The oscillator strength assumed for the line may be inaccurate. For example, the line may be broadened by Stark effect in the hot plasma. A high concentration of Fe X may be produced by the high-energy x rays from about $3 \cdot 10^6$ K hot plasma in intergalactic space (see Section 5.9). As mentioned above, the high-energy x rays from this hot plasma can penetrate, without much attenuation, the fully ionized hydrogen component of the plasma. They are very efficient in ionizing the iron (and other trace elements) in the coronal plasma. At temperatures well below $1.25 \cdot 10^6$ K, this x-ray ionization will make the Fe X concentration appear much higher than if the excitations and ionization were made primarily by the $1.25 \cdot 10^6$ K electron plasma.

If the line is formed within a narrow region with a width of about 55 km s^{-1} , as assumed by Pettini et al., and if the column density is about $N_H \approx 3.2 \cdot 10^{21} \text{ cm}^{-2}$, as they derived, then the pressure would be unreasonably high. For example, if this column density were the integral of the density over 10 kpc or less, the hydrogen density would be $N_H \geq 0.104 \text{ cm}^{-3}$, which when combined with a temperature of $1.25 \cdot 10^6$ K corresponds to an unreasonably high pressure at a distance greater than 8 kpc from the galactic center. Even if the hydrogen density is integrated over the entire distance of 50 kpc to the supernova, the average density of about $N_H = 0.0207 \text{ cm}^{-3}$, would for $1.25 \cdot 10^6$ K correspond to $N_e T = 1.2 N_H T = 3.1 \cdot 10^4 \text{ cm}^{-3} \text{ K}$, which is also too high.

The ionization and heating in the transition zone to the corona would be by the x-rays from intergalactic space, by the heat conduction from the corona, and by the plasma redshift of the galactic light and the CMB. Similarly, the heating of the corona would be by the plasma redshift of the galactic light and the CMB, by the x-rays from intergalactic space, and at the outer edges by the heat conduction from intergalactic plasma.

Peebles [60] (see that source, pages 45-49) using the data of van Albada and Sancisi [61] makes it plausible that the corona of our Galaxy contains significant mass. His evaluation indicates that the coronas of some galaxies contain a halo with a "dark mass" density, which beyond about 5 kpc decreases approximately proportionally to R^{-2} , where R is the distance to the center of the galaxy. For explaining the Tully-Fisher relation for large velocities of distant hydrogen clouds Milgrom [62] suggested modifying Newton's gravitational laws. The evaluation by Bottema et al. [63] was consistent with this suggestion.

According to Eq. (39), the theory of plasma redshift leads to an average plasma density along the line of sight to supernova 1987A, of $(N_e)_{av} \approx 0.01 \text{ cm}^{-3}$ over a distance of about 48 kpc in the corona of the Milky Way. Although this density is about 20 times higher than that usually assumed, it is most likely about right. This average includes the relatively dense plasma in the transition zone. In addition to the relatively high plasma densities made possible by the x-ray ionization and the plasma-redshift heating, we may have significant "cloud" formations caused by the fact that the plasma-redshift heating is a first order in density while the cooling is of higher order in density. The velocities of the ions and electrons close to surface of a galaxy, where the density is relatively large, are likely to be isotropic relative to the local rotational velocity of the plasma. When the

plasma diffuses outwards, its velocity perpendicular to the radius to the center of the Milky Way will remain constant. If that plasma condenses and forms hydrogen clouds at any distance from the galaxy, the velocity of the hydrogen atoms perpendicular to the radius of the galaxy will remain constant and will be roughly equal to the corresponding velocity of the plasma close to the galaxy. This explains the observed constancy of the velocity of the atomic hydrogen perpendicular to the radius as measured by the 21 cm line. The mass of the "clouds" and stars in the corona can be significant. There may therefore not be any need for "exotic dark matter particles" [60] (see p.48 of that source) or for changing the gravitational laws. The plasma redshifts produced by the relatively dense plasma in clusters of galaxies will, when interpreted as Doppler shifts, result in unreasonably large velocities for some of the members of the cluster. Also this misinterpretation of the observations has lead to the "dark matter" hypothesis. The plasma-redshift theory may thus be able to explain the observations without the "dark matter" hypothesis.

We will assume that the light intensity at surface of the Galaxy corresponds to about $n_G 10^{11}$ solar like stars at its center. The factor n_G is most likely between about 1 and 3. The mass of the Milky Way is often estimated to be about $2 \cdot 10^{11}$ solar masses. For a Hubble constant $H_0 = 0.7$, Peebles [60] (see Eq. (3.40) of that source) estimates that inside the distance of the Sun from the galactic center the mass is $1.6 \cdot 10^{11}$ solar masses. The light intensity varies with the direction to the center. For example, it may be greater over the poles (the bulge) of the Milky Way, and it may vary along the surface; for example, it may be larger over the arms. The heating-rate caused by the plasma redshift of the galactic light (GL) is according to Eq. (33)

$$\frac{dQ_{\text{GL}}}{dt} = 2.15 \cdot 10^{-14} n_G 10^{11} N_e \frac{R_0^2}{R^2} = n_G 1.09 \cdot 10^{-24} \frac{N_e}{R^2} \text{ erg cm}^{-3} \text{ s}^{-1}, \quad (40)$$

where N_e is the electron density in cm^{-3} , R the radius in kpc to the galactic center, and R_0 the solar radius in kpc.

In intergalactic space, the average heating rate caused by the plasma redshift of the cosmic microwave background (CMB) radiation will balance approximately the corresponding cooling of the intergalactic plasma caused by emitting the CMB at the original frequency instead of the redshifted frequency. However, because of the higher plasma density in the corona of the Milky Way galaxy, there will be a net heating. As we show in Section 5.9, the energy density in the CMB is about $u_{\text{CMB}} = 4.24 \cdot 10^{-13} \text{ erg cm}^{-3}$. The average energy flux at each location integrated over all directions is then about $c \cdot u_{\text{CMB}} = 1.27 \cdot 10^{-2} \text{ erg cm}^{-2} \text{ s}^{-1}$. For this rough estimate, we can assume that CMB radiations is approximately constant and isotropic. From Eq. (28), we find that at the high temperatures (above about 300,000 K) and low densities in the corona all the frequencies are plasma redshifted. We get then that

$$\frac{dQ_{\text{CMB}}}{dt} = c \cdot u_{\text{CMB}} \cdot 3.326 \cdot 10^{-25} N_e = 4.23 \cdot 10^{-27} N_e \text{ erg cm}^{-3} \text{ s}^{-1}. \quad (41)$$

From Eq. (40) and (41), we see that the heating by the CMB equals the plasma-redshift heating from the galactic light when $R \approx 16\sqrt{n_G}$ kpc. For smaller distances the light from the Milky Way galaxy dominates heating by CMB, and for larger distances the CMB dominates the galactic heating until it becomes about equal to CMB cooling in intergalactic space.

The cooling and heating of the coronal plasma by x rays is important but more complicated. Besides the plasma-redshift heating, we must also consider the excitation heating, the ionization heating, and even the Compton heating by x rays. The average temperature of intergalactic plasma is derived independently in Section 5.9. It must exceed an average temperature of $2.35 \cdot 10^6$ K. It is most likely close to $3 \cdot 10^6$ K. This temperature corresponds to an average excitation of about 259 eV and will therefore ionize a significant amount of Fe IX-ions, which have an ionization potential of about 235 eV, while the ionization potential of Fe X-ions is 262 eV. The high-energy x rays from the intergalactic plasma will penetrate the fully ionized hydrogen component in the intergalactic and coronal plasma and rip off 9 of the electrons in iron in the colder plasma. The intensities of x rays in the intergalactic plasmas with $T \approx 3 \cdot 10^6$ K facilitates a reasonable explanation of the high column density of Fe X measured by Petini et al., confer the remarks below Eq. (39).

For $N_e = 2.27 \cdot 10^{-4} \text{ cm}^{-3}$ and $T = 3 \cdot 10^6 \text{ K}$ in the intergalactic plasma, the x-ray emission is given by

$$\frac{dQ_x}{dt} = a_x 1.426 \cdot 10^{-27} \sum Z_i^2 N_i N_e T^{1/2} \langle g_{ff} \rangle = a_x 2.27 \cdot 10^{-31} \text{ erg cm}^{-3} \text{ s}^{-1}, \quad (42)$$

where the Gaunt factor $\langle g_{ff} \rangle = 1.34$, and $\sum Z_i^2 N_i = 1.33 N_e$. The factor a_x takes into account the x-ray emission due to excitations and ionizations of trace elements. It varies therefore with the concentration of trace elements and with the plasma temperature, which influences the ionization stage of the trace elements. In case of solar abundance and $T = 3 \cdot 10^6 \text{ K}$ the factor a_x is about equal to 7.5 for nonequilibrium (NEQ) cooling, according to Sutherland and Dopita [9].

The plasma redshift determines a maximum absorption length for the x rays of about $R_{z=1} = 1.32 \cdot 10^{28} \text{ cm}$, which is derived from a Hubble constant of $H_0 = 70 \text{ km s}^{-1}$ and an electron density of $N_e = 2.27 \cdot 10^{-4} \text{ cm}^{-3}$, see Section 5.8. The corresponding isotropic flux through each cubic centimeter is obtained by multiplying Eq. (42) by $R_{z=1}$. However, the x-rays can interact in many other ways and will then have shorter absorption lengths. For example, the plasma redshift, which is a first order process while the cooling is second or higher order process in density, has a tendency to create bubble structures with walls of colder plasma. These walls will absorb much of the x rays belonging to the ions of the trace elements. The shorter absorption lengths for these components of the x rays that make up the factor a_x will be reduced and approach 1 when the intensity is integrated over long distances. Even some of the continuum x rays will be absorbed and have shorter absorption length than that determined by the plasma redshift.

If we integrate Eq. (42) over all direction for $R_{z=1} = 1.32 \cdot 10^{28} \text{ cm}$, and divide by speed of light, c , we get that the energy density of the x rays in intergalactic space is

$$u_x = a_x 9.99 \cdot 10^{-14} \text{ erg cm}^{-3}, \text{ and for } a_x \approx 1, \text{ we get } u_x = 10^{-13} \text{ erg cm}^{-3}. \quad (43)$$

When we integrate the emission of x rays over $R_{z=1}$, the a_x - components are reduced greatly compared with the free-free emission components, because of their stronger absorption. We may then sometimes set $a_x \approx 1$. Even some of the remaining energy density, $u_x = 10^{-13} \text{ erg cm}^{-3}$ in the continuum x-rays is slightly absorbed by other processes than the plasma redshift. The fraction $10^{-13} \text{ erg cm}^{-3}$, which is about 23.5 % of the CMB, is likely to be close the upper limit. The x rays and light from the galaxies is likely to increase the average temperature in intergalactic space from $2.35 \cdot 10^6 \text{ K}$ to about $3 \cdot 10^6 \text{ K}$, which corresponds to 27.7 % increase. The conventional absorption length for the free-free emission, without the trace elements, is significantly greater than the $R_{z=1}$.

The column density of electrons over the distance of $R_{z=1}$ is $N_e = 2.27 \cdot 10^{-4} R_{z=1} = 3 \cdot 10^{24} \text{ cm}^{-2}$. The column density in the galactic corona is most likely on the order of or less than 10^{22} cm^{-2} . To the supernova the column density is most likely in the range of $N_e = (1.6 \text{ to } 3.2) \cdot 10^{21} \text{ cm}^{-2}$. Therefore, the plasma-redshift energy deposited in the corona is a very small fraction of the initial energy of both the CMB and the x-ray radiation impinging on the corona. The x rays impinging on the corona, on the other hand, are mostly absorbed by other processes, mainly the photoelectric absorption in the trace elements. Their contribution to the heating of the corona is therefore significantly greater than that of CMB.

As a rough estimate of energy flux, we can take the energy density, $u_x = 10^{-13} \text{ erg cm}^{-3}$, and multiply it by c ; but close to the galaxy, we should in addition multiply by the flux by 0.5, because of one sided irradiation from space. The incident energy flux from all directions close to the galaxy is then on the order of

$$F_{xG} = 0.5 c u_x = 1.5 \cdot 10^{-3} \text{ erg cm}^{-2} \text{ s}^{-1}. \quad (44)$$

The absorption of the x rays is mainly through photoelectric absorption processes. It depends therefore strongly on the ionization stages of the different atoms, mainly the trace elements in and close to the transition zone to the corona, where the plasma temperature is lower. We will assume that in the transition region the product of electron density and temperature is $N_e T = 10^4 \text{ cm}^{-3} \text{ K}$, which corresponds to the pressure often assumed at a distance of 8 to 10 kpc from the galactic center. In the temperature range $0.8 \cdot 10^6$ to $1.3 \cdot 10^6 \text{ K}$ the x-ray cooling rate in plasma with solar abundance of trace elements is about $10^{-22} N_t N_e \text{ erg cm}^{-3} \text{ s}^{-1}$. When we stretch this over

about 1 kpc and integrate the cooling, we get about $0.03 \cdot 10^{-3}$ erg cm $^{-2}$ s $^{-1}$. Just below this region, we assume the same pressure, but the temperature range is $4 \cdot 10^5$ to $8 \cdot 10^5$ K. The x-ray cooling rate is slightly larger or about $1.4 \cdot 10^{-22} N_t N_e$ erg cm $^{-3}$ s $^{-1}$. The cooling integral over 0.5 kpc is about $0.07 \cdot 10^{-3}$ erg cm $^{-2}$ s $^{-1}$. Just below this region, we assume the same pressure, but the temperature range is $2 \cdot 10^5$ to $4 \cdot 10^5$ K. The x-ray cooling rate is slightly larger or about $3 \cdot 10^{-22} N_t N_e$ erg cm $^{-3}$ s $^{-1}$. The cooling integral over 0.2 kpc is about $0.23 \cdot 10^{-3}$ erg cm $^{-2}$ s $^{-1}$. Just below this region, we assume the same pressure, but the temperature range is $1 \cdot 10^5$ to $2 \cdot 10^5$ K. The x-ray cooling rate is slightly larger or about $4 \cdot 10^{-22} N_t N_e$ erg cm $^{-3}$ s $^{-1}$. The cooling integral over 0.1 kpc is about $0.15 \cdot 10^{-2}$ erg cm $^{-2}$ s $^{-1}$.

The summation of these cooling terms in the transition zone and the lower corona is $0.48 \cdot 10^{-3}$ erg cm $^{-2}$ s $^{-1}$. It is about 32% of the x-ray heating given by Eq. (44). The remaining energy flux in Eq. (44) is $1.02 \cdot 10^{-3}$ erg cm $^{-2}$ s $^{-1}$ together with the other heating contributions given by Eqs. (40) and (41) will compensate the cooling in the coronal plasma. The column density of the electron in this transition region is about $N_e = 9.95 \cdot 10^{19}$ cm $^{-2}$ over a distance of 1.8 kpc, or an average of $N_e = 1.8 \cdot 10^{-2}$ cm $^{-3}$. The region $0.4 \cdot 10^6 \leq T \leq 1.3 \cdot 10^6$ K could be considered the lower corona, which stretches over about 1.5 kpc with a column density of $N_e = 5.67 \cdot 10^{19}$ cm $^{-2}$ and with an average density of $N_e = 0.012$ cm $^{-3}$. At these high column densities some of the radiation emitted in the cooling process would be reabsorbed and would then contribute to the heating. We will also have some of the conventional heating by ultraviolet light contribute to the heating low in the transition zone.

Let us for a moment assume that in the corona the pressure is constant and that $N_e T = 10^4$ cm $^{-3}$ K at a distance of about 8 kpc from the center of the Milky Way. Let us also assume for a moment that $T = 1.1 \cdot 10^6$ K. The radiation cooling from the plasma is $10^{-22} N_t N_e$ erg cm $^{-3}$ s $^{-1}$. The integrated energy loss over 48 kpc is then equal to $1.02 \cdot 10^{-3}$ erg cm $^{-2}$ s $^{-1}$, which is equal to the heat energy in Eq. (44) remaining after the losses in the transition zone. The column density of hydrogen $N_e = 1.35 \cdot 10^{21}$ cm $^{-2}$. To this we could add the column density in the transition zone to the Milky Way and in the transition zone to the LMC.

A higher density "bridge" is likely to form between the Milky Way and the LMC. Along the line of sight to the LMC the gravitational potential will increase the density along the line of sight. Also, the LMC will cast a partial shadow and reduce the x-ray intensity from intergalactic space. This lowers the temperature of the plasma between the Milky Way and LMC. The partial shadow will permit enough of the x rays from intergalactic space to find their way around LMC and ionize the Fe-ions in the space between the galaxies. This effect will help explain the unusually high Fe X concentration.

These are only crude estimates and serve merely to illustrate that the x-ray heating from intergalactic space can roughly compensate the cooling in the transition zone and in the corona. In addition to the x-ray heating, we have the plasma-redshift heating from galactic light and the CMB given by Eqs. (40) and (41). As we move away from the Milky Way, the x-ray heating will increase beyond that given by Eq. (44), because the shadow effect of the galaxy decreases with the distance from the galaxy. There are many other heating and cooling processes such as ionization by ultraviolet light and gamma rays.

The temperature and densities will vary with the distance from the galaxy. For example, the gravitational potential will reduce the densities with the distance from the center of the Milky Way. For isothermal conditions at $T \approx 1.25 \cdot 10^6$ K, the density decreases by factor of about 1/e per 9 kpc from the galactic plane [51] (see page 140-143 of that source).

The present estimates show that the coronal densities are about 20 times higher than those estimated by Spitzer [51]. The estimates of the heating requirements are then about 400 times greater than those by Spitzer. The gravitational potential at R kpc from the galactic center is approximately $-n_G 4500/R$ eV. For $n_G = 2$ the potential at R = 100 is about 90 eV, which corresponds to $T = 10^6$ K. The hot plasma high in the corona therefore has escape velocities. The intergalactic space must therefore have significant plasma densities. The large intergalactic plasma densities will be derived independently in Sections 5.8 and 5.9 from the observed redshifts of galaxies.

We can compare the plasma-redshift heating of the galactic light and the CMB radiation with the free-free emission cooling. The cooling by trace elements may be smaller, partly because of reduced

concentration of heavy trace elements and partly because reabsorption of some of the recombination emission stretching over many kpc. The energy emitted in the free-free emission cooling is

$$\frac{dQ_{ff}}{dt} = 1.426 \cdot 10^{-27} \sum Z_i^2 N_t N_e T^{1/2} \langle g_{ff} \rangle \text{ erg cm}^{-3} \text{ s}^{-1}. \quad (45)$$

For solar abundance of trace elements the Gaunt factor is $\langle g_{ff} \rangle = 1.29$ for a temperature of 1.1 million K, but for insignificant concentration of trace elements the Gaunt factor is closer to 1.4. This continuum x-ray cooling is about $2 \cdot 10^{-24} N_t N_e$, where $N_t \approx N_e$ refers to the positive ion. When equating the cooling given by Eq. (45) with the summation of the heating given by Eqs. (40) and (41), we get

$$N_e \approx \frac{n_G \cdot 0.55}{R^2} + 1.65 \cdot 10^{-3} \text{ cm}^{-3}. \quad (46)$$

For $n_G = 1$ and for R equal to 8, 16, and 40 kpc from the galactic center, we get that the values of N_e are equal to 0.0102, 0.0038 and 0.0020 cm⁻³, respectively. For $n_G = 2$ the values of N_e are 0.019, 0.0059, and 0.0023 cm⁻³, respectively. In the colder regions the x rays, mainly from intergalactic space, will ionize the trace elements. These colder regions will increase the average density significantly.

According to Sutherland and Dopita [9] the local continuum x-ray cooling at $1.1 \cdot 10^6$ K is about 3% of the total local x-ray cooling in plasma with solar abundance of trace elements. The x rays from intergalactic space appear essential for explaining the Fe X concentration observed by Pettini et al. [59].

As is to be expected from a nearly static universe derived in the following sections, it turns out that the x-ray intensity from intergalactic space entering the corona of the Milky Way is about equal to the electromagnetic energy, including the light intensity, leaving the Milky Way. The electromagnetic energy, including the light, emitted into space is absorbed in the intergalactic plasma and is then transformed by means of the corresponding plasma heating to x rays, which then enter and are absorbed in the corona of the Milky Way. When we in this way equate the galactic light emission with the energy flux in Eq. (44), we get that the radius of the Milky Way's corona is roughly $R \approx 47\sqrt{n_G}$ kpc. If $n_G = 2$, we get that the radius of the corona is $R \approx 66$ kpc. Actually, some of the x-ray intensity is reflected back into space together with the emission of some of the x rays produced in the corona. These radiations will be emitted out into space and will then contribute to the luminosity of the Milky Way. This effect will increase slightly the effective radius of the Milky Way.

Effect of magnetic field. We have disregarded the repulsion of the diamagnetic moments in a divergent magnetic field. The repulsion requires that the energy density, of the magnetic field be greater than the kinetic energy density of the particles, which corresponds to $H \approx 10^{-5}$ gauss. According to Clarke et al. [64], the magnetic field in a few extended regions (10 kpc) of the intracluster plasma is about $5 \cdot 10^{-6}$ to 10^{-5} gauss. The corresponding energy density in these few clouds with detectable magnetic fields is then comparable, as is to be expected (see Appendix B), to the kinetic energy density. It is therefore not clear if the diamagnetic repulsion is significant.

At places where the magnetic field is relatively strong, most likely close to the surface of the galaxy, the field would facilitate the outward streaming of the plasma. It could then deposit significant energy into the plasma, and the densities would increase beyond the above estimates. The magnetic repulsion could possibly facilitate outflow of hydrogen from the Galaxy, which could contribute to a too high density of hydrogen in the galactic corona, which in turn leads to subsequent precipitation of hydrogen into clouds. However, clear evidence for such effects from magnetic fields is lacking.

Cloud formation in the galactic corona. The plasma-redshift heating is first order in density while the cooling is second order in density. This disparity produces instabilities. The hot low-density regions become hotter and the cold high-density regions colder. This fact has some similarities to stability of loops and arches in the solar corona mentioned at the end of Section 5.5. The phenomena are also related to the formation of the spicules in the transition to solar corona and to the formation

of flares. The imbalances caused by the plasma redshift and the cooling could also explain the relative stability of hydrogen clouds; that is, the fact that the plasma redshift in the hot regions has a tendency to push the hot plasma into the colder regions such as arches in the solar corona or clouds in the galactic corona.

Within the corona of the Milky Way Galaxy, we have many clouds, including the clouds in the Leading Arm of the LMC, in the bridge between the Large and Small Magellanic Clouds, and in the Magellanic Stream, which trails the Clouds in our Milky Way corona [65, 66]. The pressure in the hotter and sparser plasma outside a cloud could be higher than the pressure inside it. The pressure in the hotter plasma outside a cloud could then push the hot plasma into the cloud and cause it to grow, or the outside pressure could more or less balance the pressure in the cloud and cause the cloud to be relatively stable.

When the temperature in the cloud's surface decreases, the emission cooling increases and the redshift heating decreases. This instability may cause the plasma to cool to a very low temperature. The rate of cooling has several relative minima, which depend on the concentration of the trace elements. The cooling rate usually has a relative minimum around 20,000 K. A relatively large fraction of the cloud's surface may then have a temperature around 20,000 K. The density is then about 50 times greater than that at 1 million K. Other minima are lower, and the center of the cloud could be much colder and density higher, while the surface of the cloud will be warmer due to collisions and x rays. The mass contained in a cloud may be significant. Putman [66] estimates that the Magellanic Bridge between the two Magellanic Clouds may contain about 100 million solar masses; and the Leading Arm may contain 10 million solar masses [65].

If the plasma contains magnetic field, the field lines will concentrate in the cloud as the hot plasma outside the cloud pushes the plasma into the cloud, similar to that in the relatively stable arches in the Sun's corona. The cloud may then often have a tendency to form structures or filaments that are elongated like the clouds in the Leading Arm and in the Magellanic Stream [65, 66]. Kazès et al. [67] searched for the Zeeman effect in clouds and detected only one with about $11.4 \cdot 10^{-6}$ gauss, which indicates that the magnetic field energy density is usually small or only about equal to the kinetic energy density in the surrounding hot plasma.

Some clouds could form far away from the Galaxy, even in intergalactic space. It has been difficult to explain the cloud formation and the structures observed, but the plasma redshift with its tendency to create instabilities hot "bubbles" between colder regions gives a natural explanation of the observed phenomena.

The redshifts within the galaxies. Clusters of galaxies are often shown as having an elongated distribution in the radial direction (z-direction); for example, Virgo cluster, and Coma cluster ("Finger of God" pointing at us) are elongated significantly in the radial direction (see Fig. 3.6 in reference [60]). Now we are inclined to interpret this elongation in the radial direction as caused by plasma redshift. As the line of sight penetrates the relatively dense plasma between galaxies in the cluster, the redshift increases and causes the objects at the back of the cluster to have relatively large plasma redshifts. This explanation applies also to the anomalous redshift of the Centaurus cluster (see Fig. 5.4 of reference [60]). The observed redshifts are significantly larger than the redshifts expected from the Tully-Fisher relation for determining the distances. Sometimes, the distances can be determined independent of the redshift. The excessive redshifts are usually assumed to be due to Doppler shifts. This misconception may then lead to excessive intracluster velocities, which then lead to assumption of "dark matter" for explaining the dynamics. The plasma redshift may thus resolve: 1) the dark matter problem, 2) the problem of preferential elongation of galaxy clusters along the line of sight, and 3) the anomalous redshift of some members in the Centaurus cluster.

In the transition zone to the corona, and at the surface of the clouds formed in the corona, the temperatures may be too low and densities too high for the cut-off condition given by Eq. (28) to be fulfilled for the 21 cm H I line. The redshift of the 21 cm line may then be slightly smaller (and the blue shift larger) than the redshift (blue shift) of lines in the visual spectrum. This tendency, although a small effect, is seen in Table 3 of reference [77].

Positrons. Positrons will increase the redshift heating without contributing much to the x-ray cooling. Positrons are formed by gamma rays with energy in excess of 1.02 MeV. Many processes can form positrons, such as decay of nuclei and of pions. Aharonian and Atoyan [68] make a case for the importance of high-energy inelastic proton interaction for explaining the gamma-ray emission in the range of 10^8 to 10^{11} eV in the galactic disk. These interactions must also apply to intergalactic space. The high-energy protons may result in formation of pions and electron-positron pairs in intergalactic space. Such processes will contribute to the heating of intergalactic plasma. In the intergalactic sparse plasma, the hot positrons would have a long lifetime [69]; and according to Gould [70], the x-ray intensity produced by a 5 million K electron-positron plasma is reduced by factor of $v^2/c^2 \approx 10^{-3}$ when compared to the x-ray intensity in an electron-proton plasma at the same temperature.

The large intensity of positron annihilation radiation in the galactic center was clearly demonstrated by Purcell et al. [71] and Kinzer et al. [72]. Dermer and Skibo [73] have found that there appears to be a “fountain” of positrons streaming into the galactic bulge of the Milky Way. They suggest that the positrons are injected within about 100-200 pc of the galactic center and are carried up by the hot gas to annihilate in the polar regions of the galaxy at heights mostly within a few kpc. Other galaxies and quasars are likely to be rich sources of electron-positron pairs. The background x-ray spectrum of Trombka et al. [74] shows clearly a hump corresponding to the annihilation photons in the x-ray background. However, it is possible that most of the annihilation radiation is due to point sources, and is not from a dispersed intergalactic plasma.

It appears possible that the positrons with the electrons will diffuse into intergalactic space far away from the galaxies, due to their low gravitational potential relative to the protons. The positron-electron plasma might then fill most of the intergalactic space with the proton-electron plasma confined mainly to the corona of galaxies. The positrons would produce a plasma redshift similar to that of the electrons. The x-ray cooling would be much smaller, but the annihilation radiation should be pronounced. If we are to be able observe the annihilation radiation, the radiation must be able to penetrate the relatively dense plasma around the galaxies. It should be detectable although the intensity is weakened by the absorption and scattering. Annihilation radiation from intergalactic plasma has not been firmly established, as most of the observed annihilation radiation has been traced to point sources. It is unlikely, therefore, that even far away from the galaxies a positron-electron plasma replaces the proton-electron plasma. Future research should, nevertheless, consider this possibility.

Observations of x rays from galactic corona. The Draco cloud is located at $(l, b) \approx (90^\circ, +39^\circ)$ and at a distance in excess of 300 pc. Borrows and Mendenhall [75] observed that the Draco cloud decreased the x-ray intensity from the corona behind it. The shadow covered x rays in the range below about 0.4 keV. This shadow appears to be a footprint of the 1 to 4 million degree hot coronal and intergalactic plasma. Both Herbstmeier et al. [76], and Wakker and Woerden [77] give examples where the intermediate and high-velocity clouds throw a shadow in the 250 eV region. The shadows indicate that also beyond the high-velocity clouds the plasma temperature may reach about 2 to 3 million degrees.

Synopsis. The simplified examples above serve only as a point of reference and for illustration. The actual facts may deviate significantly from the assumed values. For example, the light and x-ray intensities from the galactic center may not be isotropic. Close to the axes and in the “bulge” of the Milky Way Galaxy, the light and x-ray intensities as well as the magnetic field may be relatively larger than at lower latitudes. Even in case of such a modification, the plasma-redshift heating, together with x-ray heating and conduction heating from intergalactic plasma would predict a galactic corona with greater densities than those usually assumed.

The light intensity equal to $n_G 10^{11}$ Suns in Eq. (40) is arbitrary and serves only as a point of reference. It appears, however, that the heating by plasma-redshift of galactic light and CMB, and by the x rays from the intergalactic plasma are needed for explaining the high densities deduced from the observations by Pettini et al. [59]. The intergalactic plasma is heated by plasma redshift

of intergalactic light, as will be discussed in Section 5.8 and 5.9.

The conventional explanation, which assumes that supernovae supply the heating to both the H II regions within the Milky Way and to its corona, is inadequate for explaining the observations. The past estimates have usually assumed a value of $N_e T \approx 500 \text{ cm}^{-3}\text{K}$ instead of the above estimated value of $N_e T \approx 10,000 \text{ cm}^{-3}\text{K}$ at a distance of 10 kpc from the galactic center. The required heating by supernovae [51] was about 0.25% of the present estimates, which are based on the plasma-redshift heating. The higher densities predicted by the plasma-redshift theory appear essential for explaining the observations.

5.8 Cosmological redshift

We have until now used Eqs. (18) and (20) for small redshifts. For large cosmological redshifts, we must use the expression on the left side of Eq. (18) with the natural logarithm $\ln(1+z)$. For the cosmological redshifts, the first term on the right side in Eq. (20) is usually large compared with the second term on the right side. In Eq. (18), we can usually in the extended plasmas of space set $F_1(a) = 1$, because the intergalactic plasma is usually very hot and the electron density very low. We can also set $\gamma = \gamma_0$, because the redshifts are relatively large compared with the initial photon width. From Eq. (18), we get then for large redshifts that

$$\ln(1+z) \approx 3.326 \cdot 10^{-25} \int_0^R N_e dx. \quad (47)$$

If the electron density is nearly constant, the right side is proportional to R , and we get that

$$R = \frac{\ln(1+z)}{3.326 \cdot 10^{-25} N_e} = \frac{3.007 \cdot 10^{24}}{N_e} \ln(1+z). \quad (48)$$

From Eq. (48), we derive the average electron density (or the sum of electron and positron density) in intergalactic space provided the plasma redshift explains the entire cosmological redshift. The redshift is $z = H_0/c$ when the integration distance R is one Mpc, that is, $R = 3.086 \cdot 10^{24} \text{ cm}$. Press [78] has evaluated statistically the different estimates of Hubble constant H_0 and finds that it is most likely between 72 and 77 $\text{km s}^{-1} \text{Mpc}^{-1}$. Initially, we will therefore often set the Hubble constant equal to the average $74.5 \text{ km s}^{-1} \text{Mpc}^{-1}$. We get then from Eq. (47) that

$$\begin{aligned} \ln(1+z) &= \ln\left(1 + \frac{H_0}{3 \cdot 10^5}\right) \approx \frac{H_0}{3 \cdot 10^5} = 3.326 \cdot 10^{-25} (N_e)_{av} 3.086 \cdot 10^{24}, \text{ or} \\ (N_e)_{av} &= \frac{H_0}{3.077 \cdot 10^5} \approx \frac{74.5}{3.077 \cdot 10^5} = 2.42 \cdot 10^{-4} \text{ cm}^{-3}, \end{aligned} \quad (49)$$

which shows that the average number density of the electrons (or the sum of electrons and positrons) is equal to $(N_e)_{av} = 2.42 \cdot 10^{-4} (H_0/74.5) \text{ cm}^{-3}$.

The Compton scattering reduces the number of photons that reach the observer from a distant supernova. The reduction in light intensity, I , is given by

$$I = \frac{I_0 \cdot \exp(-a(R) - bN_e R - 2bN_e R)}{R^2}, \quad (50)$$

where the factor $\exp(-a(R))$ accounts for the absorption and scattering by grains, mostly Galactic and host galactic extinctions. The factor $\exp(-bN_e R)$ accounts for reduction in bolometric light intensity due to the plasma redshift. The cross section for the plasma redshift is $b = 3.326 \cdot 10^{-25} \text{ cm}^2$. The factor $\exp(-2bN_e R)$ is due to Compton scattering. The cross section $2b$ for the Compton scattering is twice the cross-section b for the plasma redshift. From Eqs. (47) and (50) we get

$$I = \frac{I_0 \exp(-a(R))}{(1+z)^3 R^2}. \quad (51)$$

We have so far disregarded the Raman scattering on the plasma frequency. The electron-plasma is in thermodynamic equilibrium, and the photons energy loss in Raman scattering should therefore usually equal the energy gain. However, the Raman scattering causes small angular scattering, which for very distant small objects, like the distant supernovas, could be significant. The effect of this small angular scattering depends on how the observed light intensity is integrated.

For a single Raman scattering the deflection angle is about equal to $\alpha = \omega_p/\omega$, where $\omega_p = 5.64 \cdot 10^4 N_e^{1/2} \approx 878$ Hz is the plasma frequency in intergalactic space, and $\omega \approx 2\pi \cdot 10^{15}$ Hz for the observed 300 nm photons. For the large redshifts of space, the photon width is equal to the classical photon width. We get then from Eq. (7) that the cross section for Raman scattering on the plasma frequency is $(\omega/\omega_p) 3.326 \cdot 10^{-25}$ cm². The number of interactions during photons travel over a distance R is then about $(\omega/\omega_p) 3.326 \cdot 10^{-25} N_e R$, where product of electron density and the distance can be obtained from Eq. (48). For a supernova with redshift $z = 0.97$, the number of interactions is then about $(\omega/\omega_p) \ln(1+z) = (\omega/\omega_p) 0.678$. The scattering angle after many interactions is a gaussian distribution with an average of

$$\theta = \sqrt{\frac{\omega_p}{\omega} \ln(1+z)}; \text{ and } R\theta \approx \frac{3.007 \cdot 10^{24}}{N_e} \left(\frac{\omega_p}{\omega}\right)^{1/2} (\ln(1+z))^{3/2}, \text{ or} \\ R\theta \approx \frac{7.14 \cdot 10^{26}}{\sqrt{N_e \omega}} (\ln(1+z))^{3/2}. \quad (52)$$

For $z = 0.97$, the angle is $\theta \approx 3.08 \cdot 10^{-7}$ and the distance $R\theta \approx 3.23 \cdot 10^{20}$ cm. At large distances, the angular spread may exceed the size of the supernova. The method of light intensity measurements may then not include all the scattered light, because the peak of the light intensity at the center of the image will be reduced and scattered out to larger angles. It may sometimes be difficult to distinguish the supernova light from the background, which may include scattering from other stars in the host galaxy. The short wavelengths are scattered slightly less than the long wavelengths. This difference could affect the evaluation. If any of the scattered light is not included, the star will appear dimmer. Density fluctuations will increase the angular scattering, and other effects may also play a role. We will in the following assume that the measurements include correctly the scattered light. (We can for example measure the light-intensity background from the galactic region containing the supernova before, or well after the supernova explosion.)

Increase of an object's observed magnitude by δm is defined, as a decrease of the light intensity by $10^{-0.4\delta m}$, and the absolute magnitude M of an object is its magnitude at 10 parsec. We have then from Eq. (51) that the object's observed magnitude is given by

$$m = 5 \log R + 1.086a + 7.5 \log(1+z) - 5 \log(10p) + M, \quad (53)$$

where the distance R to the star is in the unit of parsec, and $p = 1$ pc, and $a = a(R)$ is defined below Eq. (50). In this equation, we insert R from Eq. (48) and change the units for R from cm to parsec. We get then the relation between magnitude and plasma redshift

$$m - 1.086a = 5 \log \left(\frac{3.007 \cdot 10^{24} \ln(1+z)}{3.086 \cdot 10^{18} N_e} \right) + 7.5 \log(1+z) - 5 + M, \text{ or} \\ m - 1.086a = 5 \log(\ln(1+z)) + 7.5 \log(1+z) + 5 \log \left(\frac{3.007 \cdot 10^{24}}{3.086 \cdot 10^{18} N_e} \right) - 5 + M. \quad (54)$$

This equation may be compared with the conventional equation (see Eq. (23) of reference [79]), which is based on the big bang and expansion of the universe, but disregards both possible acceleration and deceleration of this expansion

$$m - 1.086a = 5 \log(z) + 5 \log(1+z) + 5 \log \left(\frac{10^6 c}{10^5 H_0} \right) - 5 + M. \quad (55)$$

The third term on the right side of Eq. (54) is equal to the third term on the right side of Eq. (55), because of Eq. (49). In these equations, c is in cm s⁻¹, H_0 in km s⁻¹ Mpc⁻¹, and N_e in cm⁻³.

Table 4 The variation in $-\Delta m_d$ with the redshift z as defined in Eq. (56).

z	$-\Delta m_d$						
0.1	0.0008	0.6	0.0200	1.1	0.0496	1.6	0.0820
0.2	0.0030	0.7	0.0254	1.2	0.0560	1.7	0.0885
0.3	0.0062	0.8	0.0312	1.3	0.0624	1.8	0.0951
0.4	0.0102	0.9	0.0371	1.4	0.0689	1.9	0.1016
0.5	0.0149	1.0	0.0433	1.5	0.0754	2.0	0.1081

We may subtract Eq. (55) from Eq. (54) and get that difference in expected magnitude is

$$\Delta m_d = 5 \log \left(\frac{\ln(1+z)}{z} \right) + 2.5 \log(1+z). \quad (56)$$

For z equal to: 0.5, 1.0, and 2.0, we find Δm_d is: -0.0149 , -0.0433 , -0.1081 , respectively; see Table 4. If a redshift less or equal to $z = 0.5$ is used to determine the magnitude-redshift relation, the deviations at larger z -values would be reduced significantly and make it still more difficult to distinguish between two radically different theories.

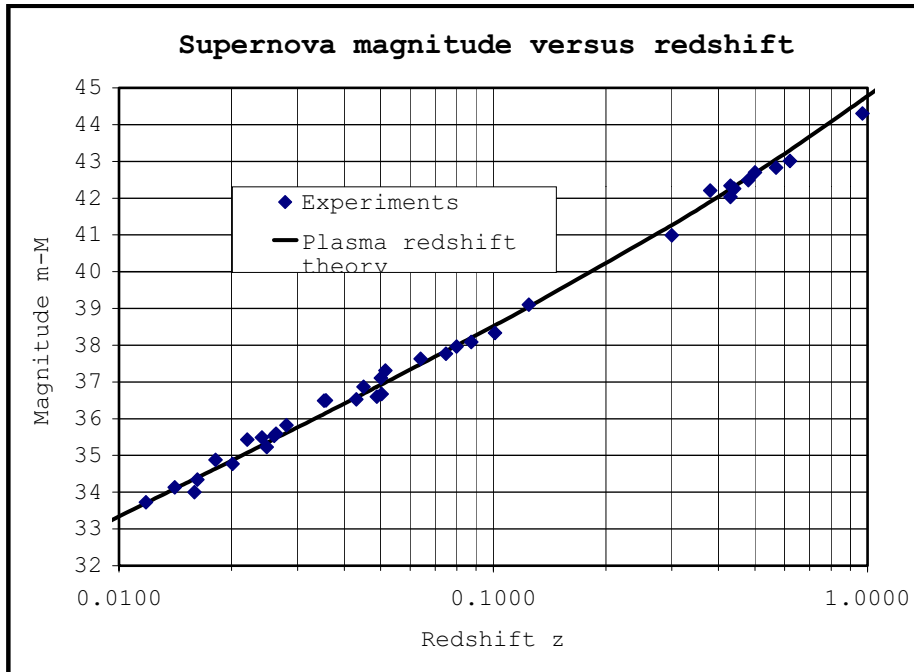


Figure 5: The magnitude $m-M$ of supernovas versus their redshifts z . The experimental points, indicated with diamonds, are from Riess et al. [82] (see in particular Tables 6 to 10 of that source). The curve shows the theoretical predictions of the plasma redshift theory Eq. (54) for a Hubble constant of $H_0 = 65.23 \text{ km s}^{-1} \text{ Mpc}^{-1}$.

The observations of supernovas by Perlmutter et al. [80, 81] and Riess et al. [82, 83] are consistent with Eq. (54) as Fig. 5 shows. The electron density in the third term of Eq. (54) is determined by the Hubble constant as shown in Eq. (49). The best fit to all the experiments is obtained for $H_0 = 65.23 \text{ km s}^{-1} \text{ Mpc}^{-1}$. *The observations clearly confirm the plasma-redshift theory.* Most

supernovas are within a galaxy. A galaxy usually has a corona, which adds to its redshift. Therefore, nearby supernovas tend to be above the line, while distant supernova will more often be below the line. The observations are also in agreement with Eq. (55). However, in Eq. (55), we have assumed that the expansion neither decelerated nor accelerated. In the big bang scenario, this is not a reasonable assumption. The masses in the universe are expected to slow the expansion or decelerate the expansion. There is a possibility for continued expansion force, which would decrease the deceleration or even accelerate the expansion. The deceleration of the expansion, due to an attraction of the masses, would reduce the expansion with increasing time. In the long past the stars would then be moving apart faster than in the recent past. For a given redshift, a distant star would be closer and therefore brighter, and the magnitude m smaller than if there were no deceleration. Perlmutter et al. [80, 81] and Riess et al. [82, 83] have considered these different possibilities. When they assumed reasonable deceleration, the distant supernovas were dimmer than expected. Only if the acceleration approximately compensated the deceleration, as in Eq. (55), was there a reasonable fit. We see thus that while the experiments confirm the plasma-redshift theory, they can only fit the big bang hypothesis if an expansion force approximately compensates the attraction of the masses in the universe.

If the plasma redshift explains the cosmological redshift, then there is no need for big-bang hypothesis or cosmological-expansion hypothesis. In his static model of the universe, Einstein introduced Λ to counter the gravitational attraction. Its meaning has been modified in the scenario of big bang and expanding universe and several lambdas have been introduced to explain the contradictions with experiments.

The gravitational repulsion of photons (which was deduced from the solar redshift experiments) counteracts the gravitational attraction of matter. The more matter concentrates, the more is converted to photons, which are repelled and if energetic enough can reform matter in a continuous renewal process lasting forever. The plasma-redshift theory leads, thus, to a self-regulating static universe, without the need for Einstein's Λ , without the need for a big bang, without need for dark matter, without the need for black holes, as we will see.

5.9 Cosmic microwave background radiation

The cosmic microwave background (CMB) radiation has a spectrum and intensity corresponding to a radiation from a thermal blackbody cavity with temperature of 2.736 ± 0.017 K (see Eq. 6.1 of reference [60]). This radiation, which is isotropic, is often been mentioned as a strong proof for the big bang hypothesis. It has been difficult to find any other reasonable explanation for it.

We saw in Section 5.8 that the plasma redshift, which follows from basic axioms of physics, could explain the cosmological redshift. From the Hubble constant we determined the electron density to be

$$(N_e)_{av} = 2.27 \cdot 10^{-4} \left(\frac{70}{H_0} \right) \text{ cm}^{-3}. \quad (57)$$

The value of the Hubble constant, H_0 , estimated by Press [78] and used in Eq. (49), is likely to be too large, because he did not take in to account the intrinsic redshifts of galaxies. We have in this case, therefore, used a Hubble constant of 70 as more representative. Even this estimate may be too large as Fig. 5 indicates. If we correct for the intrinsic redshifts of galaxies, the Hubble constant is possibly about $H_0 \approx 63 \text{ km s}^{-1} \text{ Mpc}^{-1}$.

The electrons in intergalactic space will scatter the photons and create thereby a blackbody cavity with a radius equal to one Compton scattering length, which is given by

$$R_C = \frac{1}{6.652 \cdot 10^{-25} \cdot (N_e)_{av}} = \frac{4.625 \cdot 10^{29}}{H_0} = 6.61 \cdot 10^{27} \left(\frac{70}{H_0} \right) \text{ cm}. \quad (58)$$

The radiation within the cavity can be scattered many times and will be very uniform and isotropic. The redshift distance for $z = 1$ is twice as long as the Compton scattering length, or

$$R_{z=1} = \frac{1}{3.326 \cdot 10^{-25} (N_e)_{av}} = 1.32 \cdot 10^{28} \left(\frac{70}{H_0} \right) \text{ cm}. \quad (59)$$

When analyzing absorption and emission of the radiation by microscopic dust particles in space, we often get a temperature of the dust that is reasonably close to that of the cosmic microwave background. However, such microscopic dust particles, needles, and whiskers have resonances, which make it impossible to obtain the smooth spectrum of the microwave background without the blackbody cavity.

Kirchoff, when establishing the relation between thermal radiation and energy density, u , in a cavity, found that $u = E^2/(8\pi) + H^2/(8\pi)$ was independent of the materials in the walls of the cavity. Many processes, including the radiation from accelerated and oscillating point charges and dipoles, create the electromagnetic radiation field. The Fourier harmonics of the transversal electromagnetic field around the moving particles always have a significant intensity in the low-frequency components. In the spectrum of the Fourier harmonics integrated for all particles, the intensity of the low frequency components will dominate. We do not know, and we do not need to know the exact value of the kinetic energy of the particles in intergalactic space or the intensity spectrum of their Fourier harmonics, nor the details of the radiation emission. According to Kirchoff, we have a blackbody cavity.

In the laboratory experiments, the radiation temperature of the blackbody cavity is equal to the temperature of the particles. This is not necessarily the case in dilute plasma where Compton scattering on the electrons serves to define the cavity. As we show towards end of Section B1 in Appendix B, in an extended plasma, we must have equipartition between kinetic energy density, the energy density of the magnetic field, and the energy density of the electrical field. We can have temporary and local fluctuations, but such systems that are out of balance will then move towards equilibrium.

From Stefan-Boltzmann law, we have that the CMB corresponds to an energy density of

$$u = aT_B^4 = 4.24 \cdot 10^{-13} \text{ erg cm}^{-3}. \quad (60)$$

The temperature of the CMB is as mentioned above assumed to be $T_B = 2.736$ K. As shown towards the end of Section B1 in Appendix B, we have in quasi-equilibrium that

$$p = NkT = u/3 = 1.413 \cdot 10^{-13} \text{ dyne cm}^{-2}, \quad (61)$$

where N is the particles' number density and T their temperature. If the energy density of the photons is mainly due to the CMB, and if the intergalactic plasma has solar abundance, we have that the average temperature T per particle would be

$$T = \frac{u}{3Nk} = \frac{aT_B^4}{3 \cdot 1.917 (N_e)_{av} k} = 2.35 \cdot 10^6 \left(\frac{70}{H_0} \right) \text{ K}. \quad (62)$$

The average electron density, $(N_e)_{av} = 2.27 \cdot 10^{-4} (H_0/70) \text{ cm}^{-3}$, is obtained from Eq. (49).

As mentioned in Section 5.7, the average energy density of the x rays in intergalactic space may be about 23.5 % of the energy density in the CMB radiation. Most of that x-ray intensity is from the plasma, and the x-ray heating will then balance the x-ray cooling. Peebles [60] (see in particular Eq. (5.143) of that source) estimated for a Hubble constant of $H_0 = 70 \text{ km s}^{-1} \text{ Mpc}^{-1}$ that the average luminosity density from the brightest galaxies is about $9.12 \cdot 10^{-33} \text{ erg s}^{-1} \text{ cm}^{-3}$. When we multiply this value by $R_{z=1}$ and divide by c , we get $4.01 \cdot 10^{-15} \text{ erg cm}^{-3}$ for the energy density of the light in intergalactic space from the brightest galaxies. This is only about 0.95 % of the CMB. But Peebles [60] (see his remarks below his Eq. (5.168) of that source) also indicated that the average light luminosity in intergalactic space could be 10 times higher, corresponding to about 9.5 % of the energy density in the CMB. The average temperature per particle could then be as high as about 1.33 times that derived in Eq. (62), or $3.13 \cdot 10^6$ K. Due to the uncertainty, most likely on the order of 30 %, in the x-ray and light intensities, we will usually assume that the average temperature in intergalactic space is:

$$T_{av} \approx 3 \cdot 10^6 \left(\frac{70}{H_0} \right) \text{ K}. \quad (63)$$

When analyzing the phenomena in the transition zone to the solar corona in Section 5.1, the solar flares and arches in Section 5.5, and the galactic corona in Section 5.7, we saw that the plasma redshift has a tendency to create large hot “bubbles” with relatively cold plasma in the “walls” of the “bubbles”. We expect to see similar phenomena in intergalactic space, where the “bubble” surfaces or the “walls” may have temperatures similar to that in the transition zone to the galactic corona, while the temperatures of the interiors of the “bubbles” could be high. In large “bubbles” the temperatures may approach 10 million K. The increase in Spitzer’s thermal conductivity coefficient will limit the high temperatures, and the x-ray intensity will counteract the decrease in the temperature in the walls of the bubbles. These bubble structures will naturally have a tendency to build walls or bridges between galaxies (see the discussion in Section 5.7 about the bridge between the Milky Way and the LMC). It is likely that the magnetic field will influence the structures and be aligned with the walls. This “bubble” structure in intergalactic space will affect statistical variance in the measurements of the average redshift versus distance, or the determination of the average value of the Hubble constant.

The radiation emission is usually closely related to the absorption coefficient. In sparse hot plasma of intergalactic space, the absorption coefficient (excluding the plasma-redshift absorption) for the continuum spectrum of the emitted x rays is very small. Therefore, if the conventional absorption length determined the radius of the blackbody cavity, the x-ray intensity would be very large. Based on this argument many physicists will object that the high densities deduced by the plasma-redshift theory are much too high and would lead to much too high x-ray intensities. It is therefore important to realize that not only the radius, R_C , of the black body cavity, but also the new absorption length, the plasma-redshift distance, $R_{z=1}$, are small compared with the conventional absorption length.

The average mass density of the plasma in intergalactic space is

$$\rho = \frac{1.4}{1.2} (N_e)_{av} m_p = \frac{1.4}{1.2} \frac{H_0}{3.077 \cdot 10^5} 1.67 \cdot 10^{-24} = 4.44 \cdot 10^{-28} \left(\frac{H_0}{70} \right) \text{ g cm}^{-3}. \quad (64)$$

The average mass density derived in Eq. (71) is about 48 times larger than the maximum of the conventionally assumed mass density, which for $H_0 = 70$ is: $\rho_{crit} = 1.88 \cdot 10^{-33} H_0^2 \approx 9.21 \cdot 10^{-30} \text{ g cm}^{-3}$. For this critical density value, see in particular Eq. (5.67) of [60]. To the density in Eq. (64), we should add the average of the additional mass density of the coronal plasma around the galaxies and galaxy clusters, and the average mass density of stars in any form, including quasars, neutron stars, dwarf stars, and planets, and of neutral gas and dust particles. These additional masses are usually estimated to be a small fraction of the mass estimate in Eq. (64).

If, however, most of the intergalactic space were filled with electron-positron plasma the density in intergalactic space would be small. When we add the density of the electrons and positrons to that of conventionally assumed density (Peebles [60], see Eq. (6.27) and Table 20.1 in that source), we get about

$$\rho_0 = \rho_{ep} + \rho_B = 2.1 \cdot 10^{-31} \left(\frac{H_0}{70} \right) + 3.7 \cdot 10^{-31} \left(\frac{H_0}{70} \right)^2 \approx 5.8 \cdot 10^{-31} \text{ g cm}^{-3}. \quad (65)$$

The fact that the gravitational field repels the photons causes fundamental changes in Einstein’s field equation. Because of the equivalence of kinetic mass and energy in the special theory of relativity, and because of the equivalence principle in GTR, it is conventionally assumed that the gravitational field attracts any form of mass and energy. The failure of this assumption in case of photons causes us to be more critical, and to suspect that other forms of energy may also be exempted. We will assume, nevertheless, that the assumption that gravitational field attracts all forms of energy remains valid except for photons, which are repelled by the gravitational field. The repulsion of photons means that the energy density of all photons corresponds, in some respect, to a negative mass density. Estimates of the photons energy density indicate that the negative mass density is most likely an insignificant fraction of the density estimates given by Eqs. (64) and (65). The modification of Einstein’s classical physics field equations is then most likely small.

According to Møller [84] (see Eq. 12.121 of that source), the classical field equations and Einstein's static model lead to

$$\frac{1}{R^2} = \frac{4\pi G\rho}{c^2}. \quad (66)$$

As is usually done, we assume that the gravitational constant is a constant, and that the velocity of light is a constant. We get then for the average mass density given by Eq. (65), that the curvature radius is about $R \approx 4.3 \cdot 10^{28}$ cm. Had we used the much higher density given by Eq. (64), the curvature radius would be $1.55 \cdot 10^{27}$ cm. These values for the radius in the curvature are deduced here only for reference. Many physicist will now object that the high densities derived in Eq. (64) are much too high as they lead to much too small curvature radius in accordance with Eq. (66).

Einstein accepted Newton's phenomenological equations for gravitational attraction of masses and extrapolated their use to infinity. He was concerned about the fact that this extrapolation for a static infinite universe leads to infinite gravitational potential. His equations, however, lead to a space curvature given by Eq. (66), which alleviates the problem of infinite gravitational potential. We should realize that such extrapolations of Newton's gravitational laws are based on classical physics assumptions, and that we have no observations justifying such extrapolations. Nor do we have any reliable theory for gravitational attraction at very large cosmological distances. In the classical physics it is surmised that somehow the gravitational field is able to transfer to a particle the strength and direction of the gravitational field, even when the field is extremely weak at very large cosmological distances. Simultaneously with this extremely weak gravitational attraction, the hot particles in stars and intergalactic plasmas are being bombarded by other particles that change their directions and rotations. According to the uncertainty relation in quantum mechanics, it is then likely that the direction and strength of the gravitational field will not have the time to manifest itself between the collisions. The hot particles are likely to exchange rotational, vibrational and translational energy with the Fourier harmonics of the field from surrounding particles before the extremely weak gravitational field can assert itself, both in respect to direction and potential energy. Rough estimates based on the uncertainty principle, the gravitational potential, the collision frequency, collision cross section, and temperature indicate that the extrapolation of Newton's equation for gravitational attraction to very large cosmological distances is without foundation in theory or any observation. A rudimentary analysis of these phenomena indicates that the high temperatures of the attracting and the attracted body or ion can reduce the gravitational attraction. Demonstration of this important effect will be left for another time. For the present discussion, we use only that there is no experimental evidence supporting the extreme extrapolation of Newton's phenomenological equations to large cosmological distances.

The velocity of light, c , is not a constant, as it varies with the gravitational potential. The experiments by Shapiro et al. [41] have proven that the velocity of light varies with the gravitational potential and therefore with the mass density distribution. Related and well-confirmed observations are also bending of light by gravitational lenses, both of which indicate that velocity of light varies with the gravitational potential. These changes in the velocity are due to very small ripples in the gravitational potentials. Thus, in spite of the invalidity of Eq. (66) and the gravitational redshift, some aspects of the TGR are still intact.

Photons as they move through space cannot communicate instantaneously with distant galaxies, but they can communicate with the local gravitational field. It is possible that photons velocity is affected by masses through the pressure they cause in a somewhat similar way that speed of sound waves at the bottom of the ocean are affected by local pressure and density. Accordingly, the velocity of light in the laboratory and within the solar system is likely to be influenced by the mass distribution within our Galaxy and within the cluster of galaxies to which it belongs, and not only the average cosmic mass density. In a more thorough evaluation, we would have to modify the field equations and allow for: the repulsion of photons, the fading of the gravitational field effect with distance, the temperature, the particle configuration, and the particle's surroundings. For deriving a proper equation to replace Eq. (66), we would have to take into account the variations in the density from one place to another, and we would have to explore more thoroughly if the repulsion of photons applies to other particles or fields than photons. Evaluation of these many possibilities is better left for a separate article.

The Hubble constant must be reevaluated in light of the plasma-redshift theory. We have seen that the density around a galaxy is usually greater than that in intergalactic space. Each galaxy will then usually have a significant intrinsic redshift. Usually, the Hubble constant is based on redshifts to objects with known luminosity in nearby galaxies. These redshifts include the plasma redshift along the line of sight through the interstellar space and galactic corona of our own Milky Way, and they include the analogous plasma redshifts that are intrinsic to the observed galaxy. The determinations of the Hubble constant in the past are then biased towards large values. For example, the redshift to Coma cluster with an average receding velocity of $7,000 \text{ km s}^{-1}$ [60] includes the intrinsic redshift of the Milky Way Galaxy and the Coma cluster. We have seen that the intrinsic plasma redshift of the Milky Way is likely to exceed $c z = 150 \text{ km s}^{-1}$. The average electron density around the Coma cluster is larger and its intrinsic plasma redshift may exceed 300 km s^{-1} . The receding velocity of $7,000 \text{ km s}^{-1}$ to the Coma cluster would then be less than $6,550 \text{ km s}^{-1}$ and the value of $H_0 \approx 74.5$ would be reduced to less than about $H_0 \approx 70 \text{ km s}^{-1} \text{Mpc}^{-1}$. This example is used for illustration only. Good determination of Hubble constant requires perusal of many more data.

The space geometry, the velocity of light, the bending of light, and the time retardation close to heavy bodies is affected by the TGR in the conventional way. There will be variations in the density from one place to another, as observations of galactic clusters indicate, and there will be some fluctuations with time. However, these variations and fluctuations are damped, because the more matter concentrates, the more will be transformed to photons to regenerate matter at another place.

The soft x-ray shadows made by Draco cloud and the high velocity clouds in the galactic corona [75, 70, 71] mentioned in Section 5.7, are consistent with an average temperature of about 2.35 to 3.1 million K for the intergalactic electron-proton plasma, as well as, the about 4.5 to 4.9 million K for electron-positron plasma, which has insignificant x-ray intensity. However, the low intensity of x rays from positron-electron plasma in intergalactic space could not explain the ionization of the galactic corona. That fact together with lack of annihilation radiation excludes it from being a major component. The spatial temperature distribution in the intergalactic space may often deviate significantly from the average, and it may fluctuate with time. In clusters of galaxies, the temperatures and plasma pressure may exceed the averages. When a line of sight to an object grazes along the sides or over the poles of a galaxy, the object is likely to have larger redshifts than the redshift along a line of sight to similar object at the same distance but not grazing the galaxy. This should include observations of globular clusters in our own Galaxy when the line of sight passes above the galactic poles. The observed redshift will always be a combination of the Doppler shift and the plasma redshift.

The hot high-density plasma in galactic clusters may shift slightly the brightness temperature of the CMB radiation. When we in the CMB eliminate the dipole component caused by the motion of the observer station relative to an assumed isotropic component, we should find a slight correlation between the ripples in CMB and the direction to close clusters, provided the plasmas in these clusters (such as Coma and Virgo clusters) have temperatures and pressures above the average. The correlation is likely to be detectable in the high frequency region above 300 MHz in the CMB. Higher temperatures in these directions would not necessarily mean that our Milky Way is moving towards these clusters. The dynamics within these clusters must also be reevaluated in the light of the fact that the observed shifts are a combination of the plasma redshift and the Doppler shift.

6 Repulsion of photons

In Section 5.6, the redshifts of the solar lines are explained as due to the plasma redshift. The good fits between the predicted plasma redshifts and the observed shifts indicate that the Fraunhofer lines, when observed on the Earth, are not gravitationally redshifted. We explained that the photons are gravitationally redshifted in the Sun; but that the gravitationally redshifted photons in Sun are blue shifted as they travel from the Sun to the Earth. This blue shift cancels the gravitational redshift.

The solar redshift experiments can and did detect the gravitational repulsion of photons. In quantum mechanics, the frequencies of photons behave like the frequencies of particles, that is,

the frequencies increase with the gravitational potential. When an atom moves from the Sun to the Earth, its gravitationally redshifted energy levels and frequencies are blue shifted such as to cancel their gravitational redshift. In a forthcoming paper Brynjolfsson [85] shows that a simple and natural extension of the classical TGR to quantum mechanics leads to gravitational repulsion of the photons, which causes their blue shift as they travel from the Sun to the Earth. This change in frequency is closely related to the increase in velocity of light with the gravitational potential.

The transition from quantum mechanics to classical mechanics is in accordance with Bohr's correspondence principle. In the classical limit, therefore, the quantum mechanically modified theory of general relativity becomes observationally identical to the classical theory, and can explain the outcome of the experiments in references [35-40] as well as [40,41].

Realizing that gravitational field repels photons, we find it likely that just before black hole limit, the matter is converted to photons, which must be repelled from the brink of the black hole limit and should according to well known laws of physics reform matter at a distance from the black hole limit when photon energy is large enough. Considering the pressure and the kinetic energy, the photons could have energy far exceeding the pair-production. Although this is a natural extrapolation, we should consider if any observation supports this extrapolation.

Narayan [86] finds that accreting black holes (or more correctly, objects which he believes are accreting black holes) almost always emit a substantial fraction of their luminosity in hard x rays and gamma rays. The spectrum of the rays can be approximated by a power-law with a photon index α_N as

$$N_E dE \propto E^{-\alpha_N} dE, \quad (67)$$

where the index is usually in the range of 1.5 to 3. He also notes:

1. Electron-positron annihilation features have been seen only in black hole candidates.
2. Relativistic jets of active galactic nuclei and x-ray binary jets are all unambiguous signatures of black holes.

It is more likely that such high-energy jets are emitted from a brink of a black hole limit, if the gravitational field pushes the photons outwards, instead of attracting them.

At the center of a neutron star, the density greatly exceeds that of the atomic nucleus, as pointed out by Ruderman [87]. The transition from hadronic matter to quark-gluon matter may well occur at the center of the "neutron" stars (or a neutron star like object), as pointed out by Olive [88]. We don't know at what density such a phase transition occurs, but it may occur before the "black hole limit". We know from high-energy laboratory experiments that heavy ion collisions lead to many very unstable particles, which may quickly decay into high-energy photons, which may create particle pairs. It appears possible that close to "black-hole limit", we not only have the formation of electron-positron pairs, but at higher energies also proton-antiproton pairs and higher-mass particles. It appears to me far-fetched to think that only the accumulation of the entire mass in the universe could lead to such a condition, and recreation of matter.

At the brink of a black hole limit at the center of a galaxy the kinetic energy of the mass particles is very high and will exceed the rest energy of most of the particles, which is reduced by the gravitational redshift factor. Laboratory experiments show that when the particle's kinetic energy exceeds the rest energy the particles can transform into photons. The high-energy photons, which are repelled and gain energy as they are pushed away from the "brink of a black hole limit", can recreate matter at a distance from the center. Even if the kinetic energy were removed, the gravitational pressure of nuclear matter is likely to increase the potential energy of its subunits and their excited states could emit high-energy photons. The condition for the formation of proton-antiproton pairs is there and the formation of elements could possibly be made to fit the observations, just as the big bang scenario was made to fit the formation and concentration of the elements.

This possibly could explain not only the electron-positron formations, which, according to Narayan [86], are an unambiguous signature of a black hole, but also why a large amount of hydrogen, which according to Burton [89] streams outward from the center of our Milky Way galaxy. This center is believed to contain a black hole.

Burton [89] points out that the redshifts of the 21 cm line from the region around the center of the Milky Way galaxy show that a tremendous amount of hydrogen moves at high speed away from the galactic center. The flux of total gas flow is on the order of 1 to 2 solar masses per year. The plasma redshift would modify slightly the flow diagrams used by Burton [89] and simplify the interpretation of the observed flow.

For example, along the line towards the center of the Galaxy, the electron density causes a significant plasma redshift. When we take the plasma redshift into account, the velocities of the hydrogen streaming towards us from the center would be greater than those reported by Burton. Analogously, the velocities of the hydrogen streaming away from us on the other side of the center would be smaller than those reported by Burton. In fact, reasonable numbers for the plasma redshift would make the observed asymmetrical flow, as reported by Burton, become more symmetrical. An average electron density in the mid plane of about 0.02 cm^{-3} (an average of 0.016 from reference [52] and 0.025 from reference [54]) over 6.5 kpc from observer towards the hydrogen at 1.5 kpc from the center results in a plasma redshift of 40 km s^{-1} , which when added to the observed 53 km s^{-1} for the arm close to the center gives an average of 93 km s^{-1} . On the other side of the galactic center the plasma redshift is greater as the line of sight passes through the hot high-density area closer to the nucleus. The average electron density in that region may be on the order of 0.08 cm^{-3} over 3 kpc. The corresponding plasma redshift is about 74 km s^{-1} , which together with the 40 km s^{-1} reduces the observed velocity of 210 km s^{-1} away from the center to about $[210 - (74 + 40)] = 96 \text{ km s}^{-1}$. The actual outward flow would then be nearly symmetrical at about 95 km s^{-1} . This outflow is lower than the average outflow $(53 + 210)/2 = 131 \text{ km s}^{-1}$ without the plasma redshift. Importantly, the plasma redshift indicates that the outflow of hydrogen from the center is approximately symmetrical and very large.

The plasma redshifts assumed in this example are uncertain, and better numbers can be obtained by analyzing the entire set of data. However, such a modified analysis would not change the essence of the prior conclusion that a tremendous amount of hydrogen appears to be streaming away from the center of the Galaxy.

Burton mentions that Oort [90, 91] suggested a particular interpretation of the observed velocity flow around the nucleus, which was worked out by van der Kruit [92]. In this interpretation the galactic nucleus ejected gas at high velocity and at an angle of 25 to 30 degrees with respect to the galactic plane. This material would then return to the plane at a few kpc from the center.

In light of the repulsion of the photons by the gravitational field, we are inclined to suggest that the high-energy photons from transformation (annihilation) of nuclear matter are ejected mainly along the vortex-axes at the brink of the "black hole". In both ends of the vortex, the high-energy photons would gain energy as they move outwards, and if photon energy exceeds the rest mass energy, they can recreate matter. (The ratio of photon energy and rest mass energy is independent of the gravitational potential in the modified TGR.)

Initially, when very little matter covers up the ends of the vortex, we observe two jets, one from each end, beaming far away from many objects believed to be black holes. We will first see "knots" or "lumps" on the beams or jets, because, as is well known from laboratory experiments and theory, matter enhances the transformation rate of photons to particle pairs. When more and more hydrogen is formed and covers up the ends of the vortex (sometimes one end of the vortex before the other), the jets will shorten, and we see a bulge form over the vortex.

When the density in the bulge increases, the protons that are formed will diffuse from the axes of the vortex, and the recombination-emission cooling would result in neutralization of the hydrogen, which would then, due to gravity, leak down to the center plane at some distance, but close to the nucleus. It is natural for systems affected by the plasma redshift to form structures of colder streams separated by redshift-heated spaces in between. As mentioned under the discussion of the spicules in the transition zone to the solar corona, and the discussions about the structures in the solar corona and the galactic corona, such structures are relatively stable, because the regions with sparse density will be hotter and the plasma-redshift heating relatively greater than in the denser regions. The hydrogen would then flow down from the bulge into the center plane, and then outwards into the relatively stable arms of the galaxy, the way Oort saw it. Due to the tendency of the plasma redshift to create "bubble" structures, a relatively hot redshift-heated plasma will separate the arms. The

arms structures of the galaxies have been difficult to understand, but the plasma-redshift heating helps explain the arm structures.

Presently, this scenario should be considered only a working hypothesis. However, both the plasma-redshift theory and the gravitational repulsion of photons appear helpful in explaining in a simple way these remarkable and difficult to explain observations.

7 Possible future experiments

I have failed to conceive of a reliable and practical laboratory experiment for testing the pertinent theorems. The plasma redshift may play an important role in future designs of fusion experiments, because of its unique feature of transferring heat energy to a fully ionized plasma. In such experiments, it is important to use the fact that the initial plasma-redshift, as given by Eq. (18), is proportional to the photon width. The source of the light used should therefore be designed to produce large photon widths, for example, by use of light sources at high pressures and high temperatures. In hydrogen fusion experiments; we could make use of plasma-redshift heating, but it would be difficult to test quantitatively the different relations. The fusion equipment are usually too small and the plasma often not in thermodynamic equilibrium, which would make it difficult to measure conclusively small plasma redshifts. I have therefore opted to use different astronomical observations for testing the predictions of the theory.

We should be able to confirm the plasma redshift by observing the shifts of spectral lines of stars as they graze the limb of the Sun during solar eclipse by the moon. The spectral lines from the stars should be redshifted slightly as the line of sight to each star grazes the limb of the Sun. The plasma redshift should increase as the stars approach the solar limb. The relatively large fluctuations in the electron densities may require observations of many lines from many stars for the purpose of getting a statistically valid value. It is then important to select a time period when the solar corona is quiescent and without major eruptions. The effect from intense light scattering from the corona must be reduced as much as possible to allow observations close to the limb. Use of a narrow focus on the star will reduce the background of the scattered light.

Comparison of the plasma-redshift theory with the observed redshift of the Fraunhofer lines, see Fig. 4, shows that the lines are not gravitationally redshifted when observed on the Earth. This lack of gravitational redshift, when observed on the Earth, indicates that the gravitationally redshifted photons in the Sun are blue shifted, as they travel to the Earth. For confirming the blue shift of photons during their time of flight in a different way, we could modify the laboratory experiment reported by Pound and Rebka [35, 36] and Pound and Snider [37]. This modification could entail increasing the height difference from 22.5 m to about 700 to 1000 m. The absorption of the low energy photons, such as 14.4 keV photons from ^{57}Fe , in any gas including helium over the height of 1000 m is large. A large evacuated cylinder between emitter and absorber must then replace the helium filled plastic cylinder in the experiments by Pound et al. It is also necessary to increase the source strength and the sensitivity of the detector, which together with the vacuum cylinder will increase the cost of the experiment significantly. Use of existing structures, such as, mines, boreholes, caves, or cliffs, for building the large about 1 km evacuated steel cylinder, may possibly facilitate the design and reduce the cost. We should also consider use of higher frequency gamma rays than the 14.41 keV from ^{57}Fe . For example, the 23.87, 27.72, and 73.0 keV gamma rays from ^{119}Sn , ^{129}I , and ^{193}Ir , respectively, all have higher frequencies and could make it possible to reduce the height difference. In case of iridium, however, the short half life, 31 h, of ^{193}Os would often make its use difficult.

We could also modify the experiments in reference [38] by increasing the height and length of the rocket path, and by increasing the frequency used. However, laser photons are coupled; they are on the top of each other. We do not know what effect the coupling has on the gravitational interaction, and we would have difficulty, therefore, in interpreting any experiment using laser photons.

8 Summary and conclusions

We have deduced from conventional axioms of physics a new cross section for interaction of photons with a hot electron plasma. This important cross section, plasma redshift, has been overlooked in the past; most likely, because it is usually insignificant, and because it cannot be detected in conventional laboratory experiments. The plasma redshift is important only in a very hot and low-density electron plasma. The cross section is given by Eq. (18). In this equation, the oscillator strength function, $F_1(a)$, is given by Eq. (14), and the numerical values are shown in Table 1. It is small for large values of a , but becomes significant as a decreases. We have that for a equal to: 0.344, 1.163, and 2.671 the oscillator strength function is 90%, 50%, and 10%, respectively, of its full value. Instead of the parameter a , we can use the cut-off wavelength defined by Eq. (15). The 50% cut-off wavelength is given by Eq. (16) and when magnetic fields are significant by Eq. (28), which gives the relation between the cut-off wavelength for the plasma redshift, the electron temperature, electron density, and the magnetic field.

The plasma redshift of photons results in transfer of very small quanta to the plasma. This does not change the direction of the photons significantly. The photon's energy loss by plasma redshift is in some respect analogous to a charged particle's energy loss by Cerenkov radiation. The energy lost by the photons is immediately absorbed in the electron plasma and results in significant heating. As shown in Sections 5.1 to 5.5, the plasma-redshift heating together with the magnetic heating contributes significantly to the heating of the solar corona and to the heating responsible for many observable and interesting phenomena in the solar atmosphere.

In Section 5.1, we use Eq. (28) to show that the cut-off wavelength for plasma redshift of photons predicts well the onset of the plasma-redshift heating in the transition zone to the solar corona. The 50% cut-off wavelength is about 500 nm when the temperature is about 500,000 K, the electron density about $N_e = 10^9 \text{ cm}^{-3}$, and magnetic field less than 10 gauss. These values correspond to about the middle of the transition zone to solar corona. For shorter wavelengths, the cut-off wavelength reaches deeper into the transition zone, while for the longer wavelengths, the cut-off reaches higher. The cut-off zone reaches deeper into the transition zone as the magnetic field increases. For example, the cut-off wavelength in the above example increases by 130% when the magnetic field increases from 10 to 100 gauss.

In Section 5.1, we also show how the plasma redshift together with transformation of magnetic field to heat, as described in Appendix B, facilitates explanation of the spicules in the transition zone to the corona. Without the plasma-redshift theory, the formation of the spicules has been difficult to explain.

In Sections 5.2, 5.3, and 5.4, about the solar corona, the solar wind, and the solar streamers, we find that the plasma-redshift theory together with the theory for conversion of magnetic field to heat, as described in Appendix B, is consistent with many observations that have been difficult to explain. In Section 5.2, we show that above the cut-off zone, the plasma redshift exceeds the emission cooling and the excess heat leaks by conduction into the transition zone. Gradually, the gravitational cooling by the solar wind exceeds the plasma redshift heating and results in maximum temperature at about 2 solar radii. The repulsion of the diamagnetic moments, as described by Eq. (B10), reduces this gravitational cooling by the solar wind. At about 5 solar radii, the magnetic repulsion force exceeds the gravitational attraction. This results in outward acceleration of the solar wind. Due to Eq. (B11), this kind of acceleration of the heavier ions, such as helium ions, can sometimes be greater than that of the protons. The plasma redshift transfers its energy to the electrons. This causes the electron temperature often to exceed the proton temperature. This also affects the solar wind phenomena in Section 5.3. The explanation of solar streamers, described in Section 5.4, is related to the explanation of the spicules in Section 5.1. This explanation includes the effect of magnetic repulsion of the diamagnetic moments.

In Section 5.5, we demonstrated that the plasma-redshift theory is helpful in explaining solar flares. It is shown that for large magnetic fields, the plasma redshift can be initiated in the chromosphere. The plasma redshift heating can then also initiate conversion of the magnetic field energy to heat. The heating that results from plasma redshift and the magnetic conversion can then initiate many hitherto unexplained phenomena, including the flares, loops and arches.

In Sections 5.6.1, we compare the theory with the solar redshift experiments. In Section 5.6.2, we discuss the gravitational redshift and how the observations lead to repulsion of photons, and in Section 5.6.3, we focus on the comparison of the present and conventional explanations of the solar redshift. We find that the plasma redshift explains significant fraction of the observed redshifts of the solar Fraunhofer lines. It leads thereby to the conclusion that the solar lines are not gravitationally redshifted when observed on the Earth. For the evidence, see for example Table 3 and Fig. 4. It is concluded that while the photons in the solar spectrum are gravitationally redshifted when in the Sun, as predicted by Einstein's classical TGR, the photons are usually not gravitationally redshifted when they arrive on the Earth. The photon's frequencies are blue shifted during photon's time of flight from the Sun to the Earth somewhat analogously to the atom's frequencies when the atom is moved from the Sun to the Earth. This does not conflict with any of the experiments that have been assumed to have proven the gravitational redshift, because these experiments, due to quantum effects, were unable to detect if the photons were attracted or repulsed by the gravitational field. The solar redshift experiments can discern if the photons are attracted or repulsed, and these experiments show clearly that the photons are pushed outward from the Sun by the gravitational field. This conclusion does not conflict with the results of the experiments reported in references [35-39].

In Section 5.6.4, we mention that as in case of the solar corona, the plasma redshift appears to be able to explain in a reasonable way the relatively large redshifts of many bright astronomical objects including the redshifts of quasars. The details of this explanation, however, were not pursued in the present paper, because the extrapolations from solar corona appear plausible. Detailed calculations are necessarily elaborate, and require often extrapolation from known facts. Such extrapolations introduce uncertainties. For example, we don't know much about the intensity and structure of the magnetic field in quasars. We also don't know if the corona of a quasar and therefore their plasma redshift is isotropic.

In Section 5.7, we find that the plasma redshift predicts and can explain the observed coronas of galaxies, including our own Milky Way Galaxy. It leads also to hot intergalactic plasma filling the intergalactic space, as the kinetic energy of the particles exceeds their gravitational potential energy.

In Section 5.8, we show that the plasma redshift can explain the entire cosmological redshift, if the average electron density or the summation of electron and positron densities in intergalactic space is

$$(N_e)_{av} = (N_{ep})_{av} \approx 2.27 \cdot 10^{-4} \left(\frac{H_0}{70} \right) \text{ cm}^{-3}. \quad (68)$$

The agreement between the theory and experiments is good. The recently discovered dimming of distant supernovae is predicted by the plasma-redshift theory. No expansion or contraction of the universe is needed to explain the observations.

In Section 5.9, we show that the plasma-redshift theory can also explain the cosmic microwave background. The agreement between theory and observations is again good. It is found that if the intergalactic space is filled with electron-proton plasma, the average temperature per particle in intergalactic space is

$$(T)_{av} \approx (2.35 \text{ to } 3.1) \cdot 10^6 \left(\frac{70}{H_0} \right) \text{ K}. \quad (69)$$

The upper limit of (T_{av}) includes contributions from the CMB, the x-rays, and the intergalactic light.

The corresponding average density in intergalactic space is estimated to be about

$$(\rho)_{av} \approx 4.44 \cdot 10^{-28} \left(\frac{H_0}{70} \right) \text{ g cm}^{-3}. \quad (70)$$

The average density in the universe is then about 48 times higher than the density usually assumed for a closed universe when the $H_0 \approx 70 \text{ km s}^{-1} \text{ Mpc}^{-1}$. The plasma redshift leads thus to a much higher density in intergalactic space than that conventionally assumed.

Some experts in the field will object that the high density and high temperature in space will result in an x-ray intensity that is too high. Closer scrutiny shows, however, that the predicted

x-ray intensity is consistent with observations. This is because redshift length (the inverse of plasma-redshift absorption) is many times shorter than the usually assumed absorption length (the inverse of conventional x-ray absorption coefficient). The integral of x-ray luminosity degraded by the Compton scattering and the plasma redshift over the redshift distance results in modest x-ray intensity. This soft x-ray intensity is nevertheless significant for maintaining uniform ionization in space and it helps ionize the corona of galaxies and other objects. This soft x-ray background from intergalactic plasma does not contradict the observations that find that most of the harder x rays from intergalactic space are due to point sources.

The softer x-ray intensity is due mostly to relatively colder filaments between huge bubbles heated by the plasma redshift. Like in the transition zones to the solar and galactic coronas, the bubble structure is due to the fact that the plasma redshift is first order process in density, while the cooling processes are usually second order in density.

Some experts will also object that the high density in space will lead to too large a curvature of space. Repulsion of photons means that Einstein's field equations will have to be modified. This modification is most likely small, although fundamentally very important. However, Einstein's extrapolation of Newton's phenomenological equation for gravitation to very large distances and even to infinity has no experimental support and is most likely incorrect. Distant collisions by hot electrons (and other particles) with a proton particle (and other particles) will change the angular momentum of the proton and transfer energy to it, before the gravitational potential change can assert itself, as the hot proton rotates and moves around. Quantum mechanical theory requires a finite time for the proton to interact with the gravitational field. Even with the high densities of Eq. (64), the space could be flat as most observations indicate.

It is remotely possible, that large parts of the intergalactic space contain significant density of electron-positron plasma, while only close to the galaxies the intergalactic space is filled with electron-proton plasma, the average electron-positron density in intergalactic space would equal the electron density in electron proton plasma. The average temperature in pure electron-positron plasma in intergalactic space is then about

$$(T_{ep})_{av} \approx (4.5 \text{ to } 4.9) \cdot 10^6 \left(\frac{70}{H_0} \right) \text{ K.} \quad (71)$$

The corresponding average density, including the electron-proton plasma in and around galaxies, hydrogen clouds, and all star-like objects would be about

$$(\rho_{ep})_{av} \approx 5.8 \cdot 10^{-31} \left(\frac{H_0}{70} \right) \text{ g cm}^{-3}. \quad (72)$$

The positrons have a very long lifetime in the hot sparse intergalactic space. Nevertheless, if the positron density is significant, the annihilation spectrum should be observable. While annihilation spectrum from point sources, including the center of Milky Way, is significant, there appears to be no evidence supporting significant annihilation spectrum in the cosmic background (apart from the point sources). The intergalactic plasma consists therefore most likely mainly of electron-proton plasma.

In Section 6, we show that the blue shift and the repulsion of photons as they move out of solar gravitational field are supported by other important observations. It was concluded in Sections 5.6.2 and 5.6.3 that the plasma redshift could explain the observed redshift of solar Fraunhofer lines without the gravitational redshift, which was expected from the classical theory of general relativity (TGR). It was concluded that the photons are gravitationally redshifted while in the Sun; but as the photons travel from the Sun to the Earth their frequencies are blue shifted such as to cancel their gravitational redshift. The quantum mechanically modified TGR leads to repulsion of photons in the gravitational field. This unexpected result contradicts fundamental assumption in physics and in TGR that gravitational field attracts all forms of mass and energy. The equivalence of mass and kinetic energy in special theory of relativity, means that according to equivalence principle also the kinetic mass of the photon, $m = h\nu/c^2$, should be attracted by the gravitational field. Section 6 serves to show that, independent of the solar redshift experiments, other evidence supports the contention that the photons are repelled in the gravitational field.

It is argued that the repulsion of photons removes the need for black holes, which are fictions created by extrapolating Newton's phenomenological equation beyond their experimental foundation. It is more likely that matter, instead of being sucked into a black hole, is transformed to photons at the brink of a black hole, or at a vortex at a center of a large neutron star like object. The photons are then repelled by the gravitational field and can reform matter, such as electron positron pairs and proton antiproton pairs and other particles at a distance in the usual way known from the laboratory experiments. This scenario is an extrapolation of the repulsion of photons that was indicated by the solar redshift experiments. This extrapolation requires more experimental support.

The experimental evidence for the correctness of this extrapolation is found in the intense positron annihilation spectrum detected close to the galactic center, and in the large amount of hydrogen observed streaming away from galactic center. The repulsion of photons and transformation of a matter at the center of galaxies (and quasars) bring a self-regulating stability into our cosmological perspective. Although it was not discussed in Section 6 (because the evidence is not clear), the gravitational repulsion of photons may also facilitate explanation of the large amount of energy released in supernova explosions.

The plasma redshift appears to eliminate five major deficiencies in Einstein's cosmological model for a static universe:

1. Plasma redshift can explain the cosmological redshift.
2. Plasma redshift can explain the cosmological microwave background.
3. Plasma redshift resolves the Olbers' paradox. If starlight were not attenuated, as it traveled through intergalactic space, the sky would be bright as the stars in an infinite universe. The attenuation of the light intensity by the plasma redshift and the Compton scattering of light by intergalactic electrons resolves this problem.
4. Einstein's cosmological model has significant instability, which is caused by the tendency of matter to concentrate due to gravitational attraction. Plasma redshift, when compared with solar redshift, leads to repulsion of photons and to renewal of matter at the center of galaxies and quasars. The eternal renewal of matter removes this gravitational instability.
5. In Einstein's static model of the universe, the stars will run out of energy and will have a finite lifetime. Plasma theory leads to repulsion of photons. A reasonable extrapolation of that finding is that matter is continuously renewed at the centers of galaxies and quasars. As shown in Section 6, the observations support this extrapolation.

Plasma redshift, which is based on fundamental and basic physics, leads thus to fundamental changes not only in gravitational theory, but also in our cosmological perspective.

The problem of ever-increasing time and ever-increasing entropy is resolved when we realize that we are usually observing only one half of the material-photon cycle. We usually focus on the physical changes from particle creation of material through its changes (which define the time) towards annihilation, while often disregarding the other half of the time cycle, the creation of photons and their transformation to matter in an ever lasting renewal process at the centers of the galaxies, and most likely at the centers of quasars.

Acknowledgements I am indebted to my colleague Dr. Chia-P. Wang, Weston, MA for his comments when reviewing this paper.

Appendix A

A1 Fourier spectrum of photons in dielectrics

We think of an atom free of external forces emitting a photon as it decays exponentially from an excited state with a lifetime of $\tau = 1/\gamma$. The energy difference between the two states corresponds

to a cyclic frequency $\omega_0 = 2\pi\nu_0$. Using gaussian (cgs) system of units, we have in a homogeneous electron plasma with the permeability $\mu = 1$, and the dielectric constant ε , that electrical field E_y and the magnetic field H_z of a photon moving in the x-direction can be Fourier analyzed and we get at the point $(t, x) = (t, 0)$ that

$$E_y(t, \varepsilon) = \int_{-\infty}^{\infty} \frac{E_y(0, 1)}{2\pi\varepsilon(\gamma/2 + i(\omega - \omega_0))} \exp(i\omega t) d\omega, \quad (\text{A1})$$

and for the magnetic field, we have analogously that

$$H_z(t, \varepsilon) = \int_{-\infty}^{\infty} \frac{E_y(0, 1)}{2\pi\sqrt{\varepsilon}(\gamma/2 + i(\omega - \omega_0))} \exp(i\omega t) d\omega. \quad (\text{A2})$$

A2 Equation of motion for electrons

In the following we will consider a simple case of an isotropic and uniform plasma without any constant magnetic field and with permeability $\mu = 1$. (The effect of the magnetic field is considered in Section 4 of the main paper.) At the position of $x = 0$, the equation of motion for a plasma electron acted upon by the electrical field's Fourier component, $(A/\varepsilon) \exp(i\omega t)$, may be approximated by

$$m\ddot{r} + \alpha\dot{r} - \beta m\ddot{r} + m\omega_q^2 r = e\frac{A}{\varepsilon} \exp(i\omega t), \quad (\text{A3})$$

where \dot{r} , \ddot{r} , and \dddot{r} are the first, second and third time derivative of the complex radius r in the oscillation of the electron with charge e and mass m in the electrical Fourier field harmonic with electrical field amplitude A/ε and the frequency ω . The first term on the left side is the acceleration of the electron in the field; the second term on the left accounts for the collision damping; the third term on the left accounts for the emitted radiation damping when the electron is accelerated; and the fourth term accounts for any “elastic” force that binds the electron to a certain equilibrium position. This binding of the electron is characterized by its “eigenfrequency”, ω_q .

According to classical electromagnetic theory, the damping constant β in the ground state of a free electron (not bombarded with the surrounding electrons in an electronic plasma) is given by

$$\beta = \beta_0 = \frac{2}{3} \frac{e^2}{mc^3} = 6.266 \cdot 10^{-24}. \quad (\text{A4})$$

The validity of Eq. (A3), specifically the third term, the radiation damping term, has often been questioned in the literature. The problems raised can be traced to the fact that we do not have a reliable model of the electron structure. [93 - 98]

As shown by Dirac [97] already in 1938, it is reasonable to assume that this form of the equation is valid, as it leads to correct quantum mechanical results. We can expect deviations as shown by Hartemann and Kerman [98], when the radiation intensity becomes extremely high or when the wavelength approaches the classical electron radius. These limits are well beyond the application of intensities and photon energies in focus of the present article.

In general, the force, $F(\omega, \varepsilon)$, acting on an electronic oscillator differs from the average field, which is $(A/\varepsilon) \exp(i\omega t)$. We have more generally that

$$F(\omega, \varepsilon) = \frac{A}{\varepsilon} \exp(i\omega t) + k4\pi P(\omega), \quad (\text{A5})$$

where $P(\omega) = N_e e r(\omega)$ is the polarization when N_e is the electron density and $r(\omega)$ the solution of Eq. (A3). In an amorphous isotropic matter, we can usually set the shielding factor $k = 1/3$. More generally this shielding factor, k , is a complex tensor. In a fully ionized plasma without magnetic fields, we have that $\omega_q = 0$, and $k = 0$. The effects of magnetic fields complicate the calculations. Their effects are treated in Section 4 of the main paper.

When the electron is bound, we can set the collision damping $\alpha = 2/\tau$, where τ is the time between collisions. The collisions with electrons and ions together with the collisions with neutral atoms are important for determining the width of the emissions and absorption lines. In fully ionized plasmas, where $\omega_q = 0$, the collision fields of the free electrons and ions can be Fourier analyzed and can be considered a part of the external fields affecting the third term in Eq. (A3). We can then set $\alpha = 0$, and replace the classical damping term, $(\alpha + \beta_0 \omega^2)$, by the quantum mechanical damping term, $\beta \omega^2$, which in hot plasmas is much greater than the classical radiation damping, $\beta_0 \omega^2$, as shown in Section 3.

The value of the damping for free electrons in the classical theory cannot be used to predict the damping constants nor the transition probabilities in transitions between highly excited plasma states. In a hot sparse plasma, the Fourier field of the surrounding fast electrons and ions can make $\beta \gg \beta_0$. The reason for this greater value is principally due to the collision fields. In the present classical calculations, we use the notation β rather than β_0 to draw attention to the fact that β , due to the fields from collision broadening, can be much larger than the usually assumed classical value. The quantum-mechanical treatment in Section 3 of the main paper explains this.

In Eq. (A3), we have neglected the magnetic field force

$$\frac{\dot{r}}{c} e \frac{A}{\sqrt{\varepsilon}} \exp(i\omega t), \quad (\text{A6})$$

because it is very small for low-energy photons of light, and because in the first approximation it does not perform any work. Its main component is at right angle to the velocity, \dot{r} , along the incident electrical photon field, and at right angle to the magnetic photon field H_z . Its main component is thus opposite to the photon's pressure on the electron. This force is thus responsible for the loss and change of momentum of the photon, as it is deflected and its energy attenuated.

A solution to Eq. (A3) is

$$r = \frac{e}{m} \frac{A/\varepsilon}{\{\omega_q^2 - \omega^2 + i(\alpha + \beta\omega^2)\omega\}} \exp(i\omega t). \quad (\text{A7})$$

To this solution, we may add the solutions of the homogeneous differential equation, that is, the solutions

$$\Delta r = (C_1/\alpha) + [C_2 \exp(-k_1 t) + C_3 \exp(k_1 t)] \exp(t/2\beta), \quad (\text{A8})$$

where

$$k_1 = \sqrt{\frac{\alpha}{\beta} + \frac{1}{4\beta^2}}. \quad (\text{A9})$$

However, we can disregard these last mentioned solutions, which have been discussed by Dirac [97].

The polarization is given by

$$P(\omega) = N_e e r, \quad (\text{A10})$$

where N_e is the number of plasma electrons per cm^3 , e the electronic charge, and where r , the displacement of each of the electrons, is given by Eq. (A7). The dielectric constant is defined as

$$\varepsilon(\omega) = 1 + 4\pi \frac{P(\omega)}{(A/\varepsilon) \exp(i\omega t)}, \quad (\text{A11})$$

When in this expression for the dielectric constant, we insert Eqs. (A7) and (A10), we get

$$\varepsilon = 1 + \frac{4\pi N_e e^2 / m}{\{\omega_q^2 - \omega^2 + i(\alpha + \beta\omega^2)\omega\}} = 1 + \frac{\omega_p^2}{\{\omega_q^2 - \omega^2 + i(\alpha + \beta\omega^2)\omega\}}, \quad (\text{A12})$$

where

$$\omega_p = 2\pi\nu_p = \sqrt{\frac{4\pi N_e e^2}{m}} = 5.642 \cdot 10^4 \sqrt{N_e}, \quad (\text{A13})$$

is the cyclic plasma frequency.

If we write the complex dielectric constant on the form $\varepsilon = (n - i \cdot \kappa)^2$, we get from Eq. (A12) that

$$\frac{2n\kappa\omega}{\varepsilon\bar{\varepsilon}} = \frac{(\alpha + \beta\omega^2)\omega_p^2\omega^2}{(\omega_q^2 + \omega_p^2 - \omega^2)^2 + (\alpha + \beta\omega^2)^2\omega^2}. \quad (\text{A14})$$

We have deduced this form for later use in calculating the attenuation of the photons in a plasma.

A3 Time average of the Poynting vector

The Poynting vector is $\mathbf{S} = c(\mathbf{E} \times \mathbf{H})/4\pi = c(E_y)_{\mathfrak{R}}(H_z)_{\mathfrak{R}}/4\pi$, where the last expression is in the direction of the x-axis, and where the subscript \mathfrak{R} means the real value of the indexed quantity. For obtaining the time average \bar{S} of the Poynting vector at $x = 0$ and at $t = 0$, we insert the Fourier transforms for E_y and H_z for the photon pulse with a decay time $\tau = 1/\gamma$ and integrate. We get

$$\bar{S} = \frac{c\gamma}{4\pi} \int_{-\infty}^{\infty} \frac{A(\omega, 0)}{\varepsilon} d\omega \int_{-\infty}^{\infty} \frac{A(\omega', 0)}{\sqrt{\varepsilon}} d\omega' \int_{-\infty}^{\infty} \exp(i(\omega + \omega')t) dt. \quad (\text{A15})$$

The last integral is the Dirac delta-function, $2\pi\delta(\omega + \omega')$. We can then set $\omega' = -\omega$, and the corresponding function of $-\omega$ equal to the complex conjugate function of ω . We add the complex conjugate of the average Poynting vector and divide by 2, and get¹

$$\bar{S} = \frac{c\gamma}{4} \int_{-\infty}^{\infty} \left[\frac{1}{\sqrt{\varepsilon\varepsilon}} + \frac{1}{\sqrt{\varepsilon\varepsilon}} \right] A(\omega, 0) \bar{A}(\omega, 0) d\omega. \quad (\text{A16})$$

The bar over the quantity means the complex conjugate. We have also that

$$\frac{1}{\sqrt{\varepsilon\varepsilon}} + \frac{1}{\sqrt{\varepsilon\varepsilon}} = \frac{2n}{\varepsilon\bar{\varepsilon}}; \quad (\text{A17})$$

and when we for the Fourier transforms insert expressions from Eqs. (A1) and (A2), we get

$$\bar{S} = \frac{c\gamma}{4} \int_{-\infty}^{\infty} \frac{2n E_y^2(x = 0, t = 0, \varepsilon = 1)}{\varepsilon\bar{\varepsilon} 4\pi^2 (\gamma^2/4 + (\omega - \omega_0)^2)} d\omega, \quad (\text{A18})$$

where E_y is the amplitude of the electrical field at $x = 0$, $t = 0$, and $\varepsilon = 1$; and $\omega_0 = 2\pi\nu_0$ is the center frequency of the photon in vacuum². If we in the above deduction include the variation with x , we get

$$\bar{S} = \frac{c\gamma}{4} \int_{-\infty}^{\infty} \frac{2n E_y^2(x = 0, t = 0, \varepsilon = 1)}{\varepsilon\bar{\varepsilon} 4\pi^2 (\gamma^2/4 + (\omega - \omega_0)^2)} [\exp(-2\kappa\omega x/c)] d\omega. \quad (\text{A19})$$

We will normalize the Poynting vector \bar{S} at $x = 0$ to the average energy flux of one photon, $\hbar\omega_0 = h\nu_0$, per second and per cm^2 in vacuum, where h is the Planck constant; that is, we set

$$\frac{cE_y^2(x = 0, t = 0, \varepsilon = 1)}{8\pi^2} \gamma = \hbar\omega_0 \frac{\gamma}{2\pi}. \quad (\text{A20})$$

We get then that in dielectric medium, the Poynting vector corresponding to a flux of one photon per second and per cm^2 at the distance x from the source is

$$\bar{S} = \hbar\omega_0 \frac{\gamma}{2\pi} \int_{-\infty}^{\infty} \frac{n}{\varepsilon\bar{\varepsilon}} \frac{[\exp(-2\kappa\omega x/c)]}{(\gamma^2/4 + (\omega - \omega_0)^2)} d\omega, \quad (\text{A21})$$

where ω_0 is the center frequency of the photon in vacuum.

¹It is easily verified that the Poynting vector is also equal to the product of energy density and the light velocity in the medium.

²It can be shown that the form of these equations in the mks (rationalized) system of units is identical to their form in cgs system.

A4 Photon's energy loss in a plasma

We will consider an electronic plasma, where the magnetic permeability is equal to one. When we differentiate with respect to x the average Poynting vector \bar{S} as given by Eq. (A21), we get the decrease in photon energy flux per cm,

$$\frac{d\bar{S}}{dx} = -\hbar\omega_0 \frac{\gamma}{2\pi c} \int_{-\infty}^{\infty} \frac{2\kappa\omega n}{\varepsilon\bar{\varepsilon}} \frac{[\exp(-2\kappa\omega x/c)]}{\left(\gamma^2/4 + (\omega - \omega_0)^2\right)} d\omega. \quad (\text{A22})$$

When we then insert Eq. (A14) into Eq. (A22) and set $x = 0$, we get

$$\frac{d\hbar\omega_0}{dx} = -\frac{\hbar\omega_0\gamma}{2\pi c} \int_{-\infty}^{\infty} \frac{\omega_p^2(\alpha + \beta\omega^2)\omega^2}{\left[(\omega_q^2 + \omega_p^2 - \omega^2)^2 + (\alpha + \beta\omega^2)^2\omega^2\right]} \frac{d\omega}{\left\{\gamma^2/4 + (\omega - \omega_0)^2\right\}}, \quad (\text{A23})$$

which gives the photon's energy loss per cm at $x = 0$ due to the “frictional” forces resisting the forward movement of the photon.

The expressions in the denominator have 8 complex roots. The four roots in the upper plane are:

$$\omega = \left\{ \begin{array}{ll} a & = +\sqrt{\omega_{qp}^2 - \frac{(\alpha + \beta\omega_{qp}^2)^2}{4}} + i\frac{(\alpha + \beta\omega_{qp}^2)}{2} \\ b & = -\sqrt{\omega_{qp}^2 - \frac{(\alpha + \beta\omega_{qp}^2)^2}{4}} + i\frac{(\alpha + \beta\omega_{qp}^2)}{2} \\ c & = \qquad \qquad \qquad + i\left(\frac{1}{\beta} + \alpha + \beta\omega_{qp}^2\right) \\ d & = +\omega_0 \qquad \qquad \qquad + i\frac{\gamma}{2} \end{array} \right\}. \quad (\text{A24})$$

For integrating Eq. (A23), we use complex integration. We select a path along the x-axis from $-\infty$ to ∞ and then along a semicircle in the upper half-plane from $+\infty$ to $-\infty$. The integral along the semicircle is equal to zero. The integral along the x-axis is therefore equal to $2\pi i$ times the sum of the residues in the poles in the upper half-plane. Of the four poles in the upper half-plane, one pole, corresponding to the root d in Eq. (A24), is due to the roots of the expression inside the braces in the denominator of Eq. (A23), while the remaining three poles are due to the roots of the expression inside the brackets in the denominator. It is of interest to keep these contributions separate, because the different roots correspond to distinct interactions.

The root d would exist even when the dielectric constant is equal to one. This root corresponds to the conventional Compton scattering. It is due to interactions of the photon with individual electrons. It is due to high frequency Fourier components around the center frequency ω_0 of the photon for which the dielectric shielding is usually unimportant.

The three remaining roots in the upper plane are of different character. They are due to the expression in the first pair of brackets, and to the dielectric constant not being equal to one. Conventional calculations usually disregard these roots. They correspond to photons energy losses, which are due to collective interactions of the photon field with the plasma electrons. As the photon with its associated virtual photon field penetrates and disturbs the plasma, it leaves behind a wake of collective oscillations, which carry away the energy given up by the photon to the plasma. Two of the three roots, the roots a and b in Eq. (A24), correspond to Stokes scattering or Raman scattering or resonance scattering, where the frequency, $\omega_{qp} = \sqrt{\omega_q^2 + \omega_p^2}$, is the frequency that causes the Stokes scattering. As can be seen, the absorption frequency ω_{qp} differs slightly from the eigenfrequency ω_q . (In unionized matter the absorption frequency has a slightly different form).

The imaginary root c in Eq. (A24) is of a different nature. This root, which is important only in a hot sparse plasma, has not been considered before. It corresponds to energy loss in what we will call “plasma redshift” of the photon as it penetrates a hot electron plasma. In a hot sparse plasma, the collision damping, α in Eq. (A23), is very important. When $\omega_q = 0$, we can equate the

collision field with the Fourier harmonics of the fast moving electrons. As shown in Section 3 of the main paper, the quantum mechanical damping term $\beta\omega^2$ in the plasma oscillations then replaces the classical damping term $(\alpha + \beta_0\omega^2)$, where $\beta_0\omega^2$ is the classical radiation damping.

In this article, the focus is on the plasma redshift, because the Stokes scattering and the Compton (Thomson) scattering are well known and have been estimated accurately by others, for example, by Heitler [1]. We can then in the following simplify the Stokes scattering term and set $\omega_q = 0$.

When evaluating the integral of Eq. (A23), we will assume that the following six conditions are fulfilled:

- 1) $\omega_q = 0$;
- 2) $\alpha = 0$;
- 3) $\beta \gg \beta_0 = 6.266 \cdot 10^{-24}$;
- 4) $\beta\omega_p \ll 1$;
- 5) $\omega_0 \gg \omega_p$;
- 6) $\gamma \ll \omega_0$.

As we will see, these conditions are usually fulfilled for the plasmas of main interest in this article.

The four roots in the upper plane of the denominator are then:

$$\omega = \left\{ \begin{array}{l} a = +\omega_p + i\frac{\beta\omega_p^2}{2} \\ b = -\omega_p + i\frac{\beta\omega_p^2}{2} \\ c = \quad \quad + i\left(\frac{1}{\beta} + \beta\omega_p^2\right) \\ d = +\omega_0 + i\frac{\gamma}{2} \end{array} \right\}. \quad (\text{A25})$$

The roots “a” and “b” are very close to the real axis, while the root “c” is purely imaginary. In hot, sparse plasmas β is small, although it is very large compared with β_0 .

The results of the integration on the right side of Eq. (A23) is then

$$\begin{aligned} \frac{d\hbar\omega_0}{dx} &= -2\pi i \frac{\hbar\omega_0\gamma}{2\pi c} [\text{Res}(a) + \text{Res}(b) + \text{Res}(c) + \text{Res}(d)] \\ &= -\frac{\hbar\omega_0\gamma\omega_p^2}{c\omega_0^2} \left[\frac{1}{4} + \frac{1}{4} + \frac{1}{2} \frac{\left(1 - 1/(\beta\omega_0)^2\right)}{\left(1 + 1/(\beta\omega_0)^2\right)^2} + \frac{\beta_0\omega_0^2}{\gamma\left(1 + (\beta_0\omega_0)^2\right)} \right]. \end{aligned} \quad (\text{A26})$$

We use the notation γ for the actual quantum mechanical width of the incident photon, while the classical photon width is given by

$$\gamma_0 = \beta_0\omega_0^2 = \left(\frac{2}{3}\frac{e^2}{mc^3}\right)\omega_0^2 = 6.266 \cdot 10^{-24}\omega_0^2.$$

Eq. (A26) can then be written on the form

$$\frac{d\hbar\omega_0}{dx} = -\hbar\omega_0 6.65 \cdot 10^{-25} N_e \left[\frac{\gamma}{2\gamma_0} + \frac{\gamma}{2\gamma_0} \frac{\left(1 - 1/(\beta\omega_0)^2\right)}{\left(1 + 1/(\beta\omega_0)^2\right)^2} + \frac{1}{1 + (\beta_0\omega_0)^2} \right]. \quad (\text{A27})$$

The first term inside the brackets corresponds to Stokes scattering (or Raman scattering). It corresponds to the collective scattering on the plasma frequency. In the quantum mechanical treatment of highly excited plasma, some of the oscillator strengths are negative while others are positive. The incident photon can then absorb and emit a plasma frequency photon, and thereby increase or decrease its energy to $\hbar(\omega_0 + \omega_p)$ or $\hbar(\omega_0 - \omega_p)$. In thermodynamic equilibrium, the two processes will average out. There will be an equal number of positive and negative oscillator strengths. However, when one is observing very distant supernovae, the narrow beam geometry may scatter some of the photons enough to remove them from the observed intensity.

The second term inside the brackets of Eq. (A27) corresponds to the plasma redshift. This interaction has not been discovered before. Usually, the collision damping α has been disregarded and the damping $\beta\omega^2$ equated with $\beta_0\omega^2$. This term was then insignificant as $\beta_0\omega_0 \ll 1$. However, in Section 3 of the main paper, we show that in a hot sparse plasma the damping in the plasma

oscillations is $\beta\omega^2$, which then replaces the classical damping term $(\alpha + \beta_0\omega^2)$, where $\beta_0\omega^2$ is the classical radiation damping. We may then have that $\beta\omega_0 > 1$, provided the plasma is very hot and sparse. The required conditions for experimental determination have not been present in the laboratory experiments. There are thus good reasons why this interaction has neither been theoretically nor experimentally discovered before. The energy loss in the plasma-redshift scattering is all absorbed in the plasma. It is about 50% of the total Thomson (Compton) scattering. For $\beta\omega_0 < 1$, the plasma-redshift term can be slightly negative, but the corresponding blue shift are usually insignificant. This occurs mostly in relatively cold and dense plasmas. However, in hot, sparse plasmas, the value of β can be very large and $\beta\omega_0 > 1$. The second term inside the brackets is then important for explaining many astrophysical phenomena. In Section 3 of the main paper, we use quantum-mechanical treatment to estimate β . We can then see how β varies with the temperature and the density of the plasma and the condition for $\beta\omega_0 > 1$. In Section 4 of the main article, we show how the magnetic field affects β .

Most of the plasma-redshifted photons are not scattered out of the path in the narrow beam geometry, because the individual energy losses are so small. The angular scattering of the photons is therefore so small in intergalactic space (smaller than the angular scattering on the plasma frequency) that it does not affect the observed intensity of the distant stars and supernovae.

The fourth term, the Compton scattering term, is calculated assuming that $\beta \approx \beta_0$ for incident photons with relatively high frequencies $\omega_0 = 2\pi\nu_0$. That is, we assumed that in accordance with the conventional Compton (Thomson) scattering the photons interact with individual electrons, and not coherently with several electrons in the plasma. If the incident photon's frequency is very low, the plasma electrons may act collectively in the field of the incident photons (confer Rayleigh scattering on atoms). Compton scattering is then affected.

The recoil energy in the Compton scattering, which is absorbed in the plasma, is for $\hbar\omega_0 \ll mc^2$ only an insignificant fraction of the incident photon energy. However, the scattered photons are usually removed from the narrow beam observation of a star. The Compton scattering causes then dimming of the distant stars and galaxies, as shown in Section 5.8.

Appendix B

B1 Conversion of magnetic field energy to heat in a plasma

The diamagnetic moments in closed shells of atoms are small. But at high temperatures the atoms are ionized and form a plasma. The electrons and the ions in a magnetic plasma encircle the magnetic field lines and produce thereby large diamagnetic moments with direction opposite the magnetic field. These large diamagnetic moments in the plasma often cause the **B**-field to be significantly smaller than the **H**-field. For simplifying the analysis, it is usually assumed in the following that the cyclotron frequency is much larger than the plasma frequency.

An increasing magnetic field induces rotational electrical field, which accelerates the electrons and the ions as they encircle the field lines; that is, the increasing field increases the velocities of the electrons and ions, and therefore the plasma temperature. From Maxwell's theory, we have, using gaussian (cgs) system of units, that

$$\nabla \times \mathbf{E} = -\frac{1}{c} \frac{\partial \mathbf{B}}{\partial t} = -\frac{\mu}{c} \frac{\partial \mathbf{H}}{\partial t} - \frac{\mathbf{H}}{c} \frac{\partial \mu}{\partial t}, \quad (B1)$$

where $\nabla \times \mathbf{E}$ is the rotational electrical field created by the change in the magnetic induction $\mathbf{B} = \mu\mathbf{H}$ with time t . In the plasma μ is less than 1, and when **H** increases μ could decrease or increase; but let us assume for a moment that μ is constant. Then when **H** increases, the **B**-field increases proportional to the **H**-field, and the rotational electrical field transfers energy to the encircling charged particles producing diamagnetic moments.

If the **H**-field is constant while we transfer heat to the plasma, the **B**-field will decrease; and if the plasma emits heat while the **H**-field is constant, the **B**-field will increase and approach the

H-field. If μ is constant, the work performed on a particle with charge e encircling the field lines is for one revolution

$$\oint e\mathbf{E} \cdot d\mathbf{r} = e \int \int (\nabla \times \mathbf{E})_n df = -\frac{e}{c} \frac{\delta \mathbf{B}}{\delta t} \pi r_{\perp}^2 = -\frac{e}{c} \frac{\mu \delta \mathbf{H}}{\delta t} \pi r_{\perp}^2, \quad (B2)$$

provided the rate of change in the field is so slow that it can be considered constant during one revolution of the particle. The radius in the cyclotron movement at right angle to \mathbf{B} is $r_{\perp} = v_{\perp}/\omega = v_{\perp}/(2\pi\nu)$, where v_{\perp} is the velocity of the particle perpendicular to the \mathbf{B} -field. When $\partial\mathbf{B}/\partial t$ and $\partial\mathbf{H}/\partial t$ are positive, the work is positive and the particle's energy increases.

However, μ is usually not a constant in a plasma. For example, when the heating by the plasma redshift increases the temperature and the kinetic energy of the charged particles in the plasma, the diamagnetic moment may increase from \mathbf{M} to $\mathbf{M} + \Delta\mathbf{M}$. For constant \mathbf{H} -field the induction may then decrease from $\mathbf{B} = \mathbf{H} - 4\pi\mathbf{M}$ to $\mathbf{B} - \Delta\mathbf{B} = \mathbf{H} - 4\pi(\mathbf{M} + \Delta\mathbf{M})$.

The mutual inductance between the diamagnetic moments and the currents that create the \mathbf{H} -field may sometimes be small. The plasma redshift results in a hot bubble surrounded by colder plasma. When the plasma redshift increases, the temperature in the hot bubble increases, and the \mathbf{B} -field in the hot bubble decreases. But that decrease in the \mathbf{B} -field results often in a corresponding increase in the \mathbf{B} -field in the colder surroundings, the walls of the hot bubble. The coupling between the initial diamagnetic moment in the hot bubble and the more distant currents creating the \mathbf{H} -field is then reduced significantly.

Let us for a moment assume that these distant currents are constant and therefore the \mathbf{H} -field is constant; and let us see if we can quantify some of these changes. When we multiply Eq. (B2) by the number of turns per second $\nu = \omega/2\pi$, we get that the energy gained per second is

$$\frac{\partial A}{\partial t} = -\frac{\partial \mathbf{B}}{\partial t} \frac{e}{c} \nu \pi r_{\perp}^2, \quad (B3)$$

where for e positive the number of turns is positive when the rotation vector is opposite to the direction of the \mathbf{B} -field. The force from a magnetic induction field \mathbf{B} on the moving particle with charge e and velocity \mathbf{v} is $\mathbf{F} = e(\mathbf{v}/c) \times \mathbf{B}$, which leads to $\vec{\omega} = -e\mathbf{B}/mc$, as shown in Eq. (B4).

The work ∂A in Eq. (B3), which is transferred to the particle, increases its kinetic energy as the \mathbf{B} -field decreases due to the plasma-redshift heating. The increase is proportional to the rate of change in the field \mathbf{B} . The kinetic energy also increases with the diamagnetic moments. In a fully ionized plasma, the radius r_{\perp} in a particle's orbit around the field-lines is not a constant during the increase or decrease in \mathbf{B} . We can also show that the particles usually make great many turns before being affected significantly by collisions in sparse plasmas of our main interest.

Our present interest is to focus on the particle's interactions with large magnetic fields. We can equate the centripetal force with the centrifugal force and get

$$\left| \frac{ev_{\perp}B}{c} \right| = \left| \frac{mv_{\perp}^2}{r_{\perp}} \right| \quad \rightarrow \quad |r_{\perp}| = \left| \frac{mv_{\perp}c}{eB} \right| = \left| \frac{mr_{\perp}\omega c}{eB} \right| \quad \rightarrow \quad \vec{\omega} = -\frac{e\mathbf{B}}{mc}. \quad (B4)$$

The last expression is obtained by keeping track of the directions of the different vector quantities.

From Eqs. (B3) and (B4), we get

$$\partial A = mv_{\perp}dv_{\perp} = -\partial B \frac{e}{c} \nu \pi r_{\perp}^2 = -\partial B \frac{e}{c} \frac{eB}{2\pi mc} \pi \frac{m^2 v_{\perp}^2 c^2}{e^2 B^2}; \text{ or } 2 \frac{dv_{\perp}}{v_{\perp}} = -\frac{dB}{B}, \quad (B5)$$

which when integrated gives

$$v_2^2 B_2 = v_1^2 B_1, \quad (B6)$$

where B_1 and v_1 are the lower and B_2 and v_2 are upper integration limits for the field \mathbf{B} and for the particle's velocity v_{\perp} perpendicular to the induction field \mathbf{B} .

We can simplify the analysis by assuming that the field \mathbf{H} is constant and that the number density of particles is constant. We multiply Eq. (B6) by $m/2$ and by $H/(8\pi)$, and integrate over

the different particles. We get

$$\frac{HB_2}{8\pi} \sum \frac{mv_2^2}{2} = \frac{HB_1}{8\pi} \sum \frac{mv_1^2}{2}, \text{ or}$$

$$\frac{\sum \frac{mv_2^2 - mv_1^2}{2}}{\frac{HB_1 - HB_2}{8\pi}} = \frac{\sum \frac{mv_1^2}{2}}{\frac{HB_2}{8\pi}}. \quad (\text{B7})$$

When we apply this equation to the reversing layers of the Sun, we find that the initial energy density $HB_1/(8\pi)$ of the magnetic field is usually much larger than the charged particles' kinetic energy density $\sum mv_1^2/2$ perpendicular to the field (which is $2/3$ of the total kinetic energy density). At an optical density of $\tau_{500} = 1$ at 500 nm in the solar photosphere, the electron density is about $N_e = 6.4 \cdot 10^{13} \text{ cm}^{-3}$ and the temperature about $T = 6420 \text{ K}$. The kinetic energy density in charged particles' movements perpendicular to the field is then about $\sum mv_1^2/2 \approx 114 \text{ erg cm}^{-3}$. In and above the photosphere the field is sometimes about 1000 gauss and the energy density in the field is then about $40,000 \text{ erg cm}^{-3}$. Higher, at an optical density of $\tau_{500} = 2.64 \cdot 10^{-7}$, the electron density is about $N_e = 2.4 \cdot 10^{10} \text{ cm}^{-3}$ and temperature about $T = 21,000 \text{ K}$. The kinetic energy density is then about $\sum mv_1^2/2 \approx 0.114 \text{ erg cm}^{-3}$. We have for large fields that $B \approx H$. Even when the field is only 100 gauss, its energy density is about 400 erg cm^{-3} . Therefore, the kinetic energy density of the charged particles is often much smaller than the energy density of the field. Often, the initial ratio on the right side of Eq. (B7) (the lower equation) is therefore very small. When the field energy in the denominator on the left side of Eq. (B7) (the lower equation) decreases by a small amount, the numerator on the left side is very small; that is, a very small fraction of the field energy is transformed into kinetic energy.

We see thus that the magnetic field energy cannot transform easily into kinetic energy unless something else, such as the heating ΔQ from the plasma redshift contributes to the heating. When the magnetic field's fluctuations decrease the field, only a small fraction of the field energy transforms into kinetic energy or heat due to the small ratio on the right side of Eq. (B7). The field would then bounce back to nearly its initial value. In solar atmosphere plasma redshift creates hot plasma "bubbles", which lead to increased plasma redshift and reduced cooling, which therefore leads to high temperatures in the "bubble". This increase in temperature facilitates transformation of the magnetic field energy to heat. At high temperatures, the rate of transformation then increases exponentially, and may lead to explosive phenomena such as large flares in the Sun.

If the decrease in the magnetic field energy is to equal the increase in kinetic energy or heat, the left side of Eq. (B7) must be close to 1. When by some means heat energy ΔQ is transferred to the plasma, the temperature will increase and a larger fraction of the magnetic energy is transformed into heat. When during the field fluctuations the field energy decreases, less of the field energy will then bounce back. We can write $\Delta Q = T \Delta S$, where ΔS is the entropy density of the plasma and field. We will assume that initially the field energy density is high relative to the kinetic energy density. When we then introduce heat ΔQ the particles entropy will increase and the field energy decrease. But as we approach equilibrium, $HB_2/(8\pi) = \sum 3mv_2^2/4$, the entropy reaches its maximum and the transformation ceases. In a similar way, if the kinetic energy is initially greater than the field energy, small fluctuations induce the system either to increase the field energy or to reduce the kinetic energy of the system.

The aggregate of a plasma and a magnetic field, thus, requires for a equilibrium that the magnetic field energy about equals the kinetic energy component perpendicular to the field, provided that chemical potentials are in balance; that is, when these chemical potentials neither release or absorb heat.

The Fourier harmonics of the fields produced by moving and accelerating particles in a cavity of matter create a spectral energy density given by $u_\omega = (E_\omega^2 + H_\omega^2)/(8\pi)$, where E_ω and H_ω are the electrical and magnetic field components with frequency ω . The integrated electromagnetic energy density is $u = \int_0^\infty u_\omega d\omega$. This energy density is created mainly by the accelerated charges and dipoles. This electromagnetic field is the source of the blackbody radiation from blackbody cavity. In plasmas, we may have magnetic fields with energy densities that far exceed the energy densities of the particles' thermal motions.

The electrical field interacts more easily with the charged particles and the atoms through excitations and ionizations. Therefore, when a plasma with the fields moves up through the photosphere from a position deep under the solar photosphere, the electrical field can quickly interact and adjust to the decrease in temperature, while the magnetic field, as shown by Eq. (B7), has difficulty transferring its energy to the particles when the plasma cools abruptly in the photosphere. In the reversing layers of the Sun, we can therefore for a while have large magnetic fields, but rather normal electrical fields. The electrical and magnetic fields are coupled; and the fields become equal, as we approach the equilibrium over huge dimensions of black body cavity. The total pressure p of the electromagnetic energy is equal to $u/3$, where u is the total electromagnetic energy density. In a quasi equilibrium, we must have that the electromagnetic pressure is about equal to the pressure in the plasma. We get then that $p = NkT = u/3$, where N is the total number density of particles and k is Boltzmann constant. The kinetic energy density is then $(3/2)NkT = u/2$; that is, *we have equipartition between the kinetic energy, the electrical field energy, and the magnetic field energy*. This is principally valid as an average over the huge dimensions of a black body cavity, and not necessarily over smaller dimensions where the plasma may not be in equilibrium with the fields.

Like the paramagnetic moments and the ferromagnetic moments, the diamagnetic moments are coupled. This coupling seeks to direct all the diamagnetic moments in the same direction. When the diamagnetic moments are small as they are in atoms, the thermal motion usually dominates the coupling; and the direction of the magnetic moments is not aligned. However, when the diamagnetic moment \mathbf{M} is large, the energy $MH/2$ in some external field, \mathbf{H} , may become larger than the kinetic energy fluctuations. Just outside the periphery of the domain containing the diamagnetic moments the induction field \mathbf{B} becomes stronger. The magnetic moments, both perpendicular and along to the field lines, can then align and gradually build up huge domains. While the diamagnetic moments align along the field lines, they will reduce the \mathbf{B} -field within the domain and thereby reduce the field energy within the domain.

While these equations are deduced assuming a hot sparse plasma, they are to some extent valid for diamagnetic moments of hot material with temperatures in excess of any paramagnetic and ferromagnetic Curie point, such as that of the hot interior of the Earth. This possibly explains why the Earth has a magnetic field with large secular variation and even reversals, [99] like the magnetic fields in the Sun. The Moon and Mars, most likely with relatively cold interior, have very small magnetic fields.

B2 Repulsion of diamagnetic moments

Sometimes, we also must consider that diamagnetic moments are pushed away in a direction of a decreasing field. For example, the diamagnetic moments of protons and electrons are pushed away from the Sun, because of the outward decreasing magnetic field. When we divide Eq. (B3) by $\partial R/\partial t$, the velocity along the field lines, we get the outward force, F , on the magnetic moment, which is

$$F = \frac{\partial A}{\partial R} = -\frac{\partial B}{\partial R} \frac{e}{c} \nu \pi r_{\perp}^2 = -\frac{\partial B}{\partial R} M = -\frac{\partial B}{B \partial R} \frac{1}{2} m v_{\perp}^2. \quad (\text{B8})$$

We have made use of that the diamagnetic moment is given by

$$M = \frac{e \nu \pi r_{\perp}^2}{c} = \frac{e \nu \pi v_{\perp}^2}{c \omega_c^2} = \frac{e v_{\perp}^2}{2 c \omega_c} = \frac{m v_{\perp}^2}{2 B}.$$

Close to a point P we use Eq. (B6) and set $v_{\perp}^2 = v_P^2 (B_P/B)$, where B_P is the value of the \mathbf{B} -field and v_p the value of the particle velocity at right angle to the field at the point P. From Eq. (B8) we get then that the outward force at P is

$$F_P = \frac{\partial (1/B)}{\partial R} \frac{1}{2} m v_P^2 B_P. \quad (\text{B9})$$

If the field at P decreases outward as $B = B_P (R_P/R)^n$, we get

$$F_P = \frac{n}{2} \frac{m v_P^2}{R_P}, \quad (\text{B10})$$

We see from this equation that the force pushing the diamagnetic dipole outwards from the Sun is independent of the magnetic field strength at P (because when the field decreases the diamagnetic moment increases); but the force depends on n ; that is, the force depends on how fast the field decreases with R . When $n(mv_P^2/2)$ of the particle exceeds the numerical value of its gravitational potential, the particle will be pushed away from the Sun. This uses energy and the magnetic field will decrease until it becomes amorphous.

In thermal equilibrium the velocity distribution is often isotropic, and the average kinetic energy component $mv_P^2/2$ perpendicular to the field lines is $2/3$ of the average of the total kinetic energy of the particles. However, as the protons accelerate outwards in sparse plasma of the outer corona, the scattering cross section may not be large enough to make the velocity distribution isotropic. The velocity perpendicular to the field may be nearly constant as the velocity along the field lines increases. The average value of $mv_P^2/2$ perpendicular to the field at the point the P may then be much smaller than $2/3$ of the average total kinetic energy.

As a rough guide, we can use Rutherford formula for the angular scattering cross section $\sigma(\theta)$ for elastic scattering in the center of mass system, which is valid in the classical limit for proton temperatures well below $2.8 \cdot 10^8$ K. We have then that

$$\frac{d\sigma(\theta)}{d\Omega} = \frac{Z_1^2 Z_2^2 e^4}{4m^2 v^4 \sin^4 \frac{\theta}{2}}, \quad (\text{B11})$$

where $d\Omega = 2\pi \sin\theta d\theta$ and θ the scattering angle; the mass $m = m_1 m_2 / (m_1 + m_2)$ is the reduced mass of two particles with masses m_1 and m_2 and charges $Z_1 e$ and $Z_2 e$, respectively; and v is their relative velocity. This equation shows that the scattering is larger for multiply charged ions. Eq. (B11) serves only to indicate the trend. In the laboratory system the total cross section is the same, but variation with θ is slightly different, and good estimates require also that we take into account the shielding effects. In a plasma with 5 to 10% He^{++} -ions and 95 to 90% H^+ -ions, the velocities of the helium ions will become isotropic before the proton ion. The average of the outward accelerating force on the helium ion can then be greater than that on the proton. The average velocity of helium ions can even become equal to or slightly greater than that of the protons.

References

- [1] W. Heitler. *The Quantum Theory of Radiation*, 3rd d. Oxford Clarendon Press, 1954
- [2] R. J. Gould. ApJ. **285** (1984) 275
- [3] J. E. Vernazza, E. H. Averett, and R. Loeser, ApJ. Suppl. Series **45** (1981) 635
- [4] P. A. Sturrock, *Plasma Physics*, Cambridge University Press 1994. ISBN 0 521 44350 4
- [5] U. Feldman, I. E. Dammasch, K. Wilhelm, ApJ. **558** (2001) 423
- [6] H. Friedman. *The Astronomers Universe*, (Balatinus Books, New York, 1990)
- [7] J. V. Hollweg, ApJ. **257** (1982) 345
- [8] M. L. Goodman, ApJ. **503** (1998) 938
- [9] R. S. Sutherland and M. A. Dopita, ApJ. , Supplement Series **88** (1993) 253
- [10] H. Holweger, Astron. Astrophys. **10** (1971) 128
- [11] R. W. P. McWhirter, P. C. Thonemann, R. Wilson, Astron. & Astrophys **40** (1975) 63
- [12] G. L. Withbroe, ApJ. **325** (1988) 442
- [13] G. L. Withbroe, ApJ. **337** (1989) L49

- [14] J. T. Gosling, Annual Review of Astronomy and Astrophysics, **34** (1996) 35
- [15] J. B. Zirker, Solar Physics **148** (1993) 43
- [16] H. Zirin, Solar Physics **169** (1996) 313
- [17] R. A. Frazin, and P. Janzen, ApJ. **570** (2002) 408
- [18] E. N. Parker, ApJ. **372** (1991) 719
- [19] G. Newkirk, Jr., Annual Review of Astronomy and Astrophysics **5** (1967) 213
- [20] P. A. Sturrock, M. S. Wheatland, L.W. Acton, ApJ. **461** (1996) L115
- [21] M. S. Wheatland, P. A. Sturrock, L. W. Acton, ApJ. **482** (1997) 510
- [22] N. R. Sheeley, Jr. et al. ApJ. **484** (1997) 472
- [23] Y.-M. Wang et al. ApJ. **508** (1998) 899
- [24] D. A. Falconer, R. L. Moore, J. G. Porter, G. A. Gary, T. Shimizu, ApJ. **482** (1997) 519
- [25] R. L. Moore, D. A. Falconer, J. G. Porter, S. T. Suess, ApJ. **526** (1999) 505
- [26] L. Spitzer, *Physics of fully ionized gases* (New York Interscience, 1962)
- [27] S. R. Spangler, S. Mancuso, ApJ. **530** (2000) 491
- [28] J. T. Steinberg, A. J. Lazarus, K. W. Ogilvie, R. Lepping, J. Byrnes, Geophys. Res. Lett. **23** (1996) 1183
- [29] J.-F. De La Beaujardire, R. C. Canfield, H. S. Hudson, J.-P. Wülser, L. Acton, T. Kosugi, S. Masuda, ApJ. **440** (1995) 386
- [30] R. J. Murphy, G. H. Share, K. W. DelSignore, X.-M. Hua, ApJ. **510** (1999) 1011
- [31] M. G. Adam, Mon. Not. R. astr. Soc. **119** (1959) 460
- [32] L. A. Higgs, Mon. Not. R. astr. Soc. **121** (1960) 421
- [33] P. N. Brandt, E. H. Schröter, Solar Physics **79** (1982) 3
- [34] F. Cavallini, G. Ceppatelli, A. Righini, Astron. Astrophys. **143** (1985) 116
- [35] R. V. Pound, G. A. Rebka, Jr., Phys. Rev. Lett. **3** (1959) 439; ibid. **3** (1959) 554
- [36] R. V. Pound, G. A. Rebka, Jr., Phys. Rev. Lett. **4** (1960) 337
- [37] R. V. Pound, J. L. Snider, Phys. Rev. Lett. **13** (1964) 539
- [38] R. F. C. Vessot et al., Phys. Rev. Lett. **45** (1980) 2081
- [39] T. P. Krisher, D. D. Morabito, J. Anderson, Phys. Rev. Lett. **70** (1993) 2213
- [40] C. Riveros, H. Vucetich, Phys. Rev. D. **34** (1986) 321
- [41] I. I. Shapiro et al. Phys. Rev. Lett. **26** (1971) 1132
- [42] D. Dravins, L. Lindgren, Å. Norlund, Astron. Astrophys. **96** (1981) 345
- [43] D. Dravins, Ann. Rev. Astrophys. **20** (1982) 61
- [44] J. E. Vernazza, E. H. Averett, and R. Loeser, ApJ. Suppl. Series **30** (1976) 1
- [45] A. K. Pierce, J. C. LoPresto, Solar Phys. **196** (2000) 41

- [46] H. R. Griem, *Spectral line broadening by plasmas*, Academic Press, New York, and London, ISBN 0-12-302850-7, 1974
- [47] C. E. St. John, ApJ. **67** (1929) 195
- [48] L. Herzberg, Can. J. Phys. **38** (1960) 853
- [49] P. Miller, P. Foukal, P. Keil, Solar Phys. **149** (1984) 33
- [50] H. Arp, *Seeing Red: Redshifts, Cosmology and Academic Science*, published by Apeiron Montreal, Quebec, 1998, ISBN 0-9683689-0-5
- [51] L. Spitzer, Jr., J. P. Ostriker, *Dreams, Stars, and Electrons: Selected writings of Lyman Spitzer Jr.* Princeton University Press, Princeton, New Jersey, 1997
- [52] R. J. Reynolds, ApJ. **372** (1991) L17
- [53] R. J. Reynolds, D. P. Cox, ApJ. **400** (1992) L33
- [54] J. M. Cordes, J. M. Weisberg, D. A. Frail, S. R. Spangler, M. Ryan, Nature **354** (1991) 121
- [55] G. C. Gómez, R. A. Benjamin, D. P. Cox, Astron. J. **122** (2001) 908
- [56] B. D. Savage and D. Massa, ApJ. **314** (1987) 380
- [57] D. P. Cox, R. J. Reynolds, Ann. Rev. Astron. Astrophys. **25** (1987) 303
- [58] R. A. Chevalier, W. R. Oegerle, ApJ. **227** (1979) 398
- [59] M. Pettini, R. Stathakis, S. D'Odorico, P. Molaro, G. Vladilo, ApJ. **340** (1989) 256
- [60] P. J. E. Peebles, *Principlees of Physical Cosmology*, Princeton University Press, ISBN 0-691-01933-9, 1993
- [61] T. S. van Albada, R. Sancisi, Phil. Trans. R. Soc. London **A320** (1986) 447
- [62] M. Milgrom, ApJ. **270** (1983) 365
- [63] R. Bottema, J. L. G. Pestaña, B. Rothberg, R. H. Sanders. Astron. Astrophys. **393** (2002) 453
- [64] T. E. Clarke, P. P. Kronberg, and H. Böhringer, ApJ. **547** (2001) L111
- [65] M. E. Putman, B. K. Gibson, Publ. Astron. Soc. Aust. **16** (1999) 70
- [66] M. E. Putman, Publ. Astron. Soc. Aust. **17** (2000) 1
- [67] I. Kazès, T. H. Troland, R. M. Crutcher, Astron. Astrophys. **245** (1991) L17
- [68] A. Aharonian, and A. M. Atoyan, Astron. Astrophys. **362** (2000) 937
- [69] R. J. Gould, ApJ. **344** (1989) 232
- [70] R. J. Gould, Phys. Rev. A **23** (1981) 2851
- [71] W. R. Purcell, et al. ApJ. **413** (1993) L85
- [72] R. L. Kinzer, W. R. Purcell, W. N. Johnson, J. D. Kurfess, G. Jung, J. Skibo, Astron. & Astrophys, Suppl. **120** (1996) 317
- [73] C. D. Dermer, and J. G. Skibo, ApJ. **487** (1997) L57
- [74] J. I. Trombka, et al. ApJ. **212** (1977) 925
- [75] D. N. Borrows, J.A. Mendenhall, Nature **351** (1991) 629

- [76] U. Herbstmeier, U. Mebold, S.L. Snowden, D. Hartmann, W. B. Burton, P. Moritz, P. M. W. Kalberla, R. Egger, *Astron. Astrophys.* **298** (1995) 606
- [77] B. P. Wakker, H. Van Woerden, *Ann. Rev. Astron. Astrophys.* **35** (1997) 217
- [78] W. H. Press, Understanding data better with Bayesian and global statistical methods. In *Unsolved Problems in Astrophysics*, Ed. J. N. Bahcall and J. P. Ostriker, Princeton University Press, Princeton, NJ, ISBN 0-691-01607-0.
- [79] A. Sandage, *ApJ.* **133** (1961) 355
- [80] S. Perlmutter, et al. *ApJ.* **483** (1997) 565
- [81] S. Perlmutter et al., *Nature* **391** (1998) 51
- [82] A. G. Riess, et al., *Astron. Journal* **116** (1998) 1009
- [83] A. G. Riess, et al., *ApJ.* **504** (1998) 935
- [84] C. Møller, *The Theory of Relativity*, 2nd ed., Oxford University Press 1972, Delhi, Bombay, Calcutta, Madras, SBN 19 560539
- [85] A. Brynjolfsson, To be published
- [86] R. Narayan, Accretion flows around black holes. In *Unsolved Problems in Astrophysics*, Ed. J. N. Bahcall and J. P. Ostriker, Princeton University Press, Princeton, NJ, ISBN 0-691-01607-0
- [87] M. Ruderman, In and around neutron stars. In *Unsolved Problems in Astrophysics*, Ed. J. N. Bahcall and J. P. Ostriker, Princeton University Press, Princeton, NJ, ISBN 0-691-01607-0
- [88] K. A. Olive, *Science* **251** (1991) 1194
- [89] W. B. Burton, The large-scale distribution of neutral hydrogen in the galaxy. In *Galactic and Extragalactic Radio Astronomy*; pp. 82-117. Ed. by G. L. Verschuur, and K. I. Kellermann, ISBN 0-387-06504-0, Springer Verlag, New York, Heidelberg, Berlin, 1974
- [90] J. H. Oort, *Nonstable phenomena in “Galaxies.”* Proc. IAU Symp. No 29. Yerevan: Izd-vo Akademii Nauk Armianskoi SSR, (1966) 41.
- [91] J.H. Oort, *Nuclei of galaxies*; ed. D.J.K. O’Connell, North Holland Publishing Co., Amsterdam, (1971) 321
- [92] P. C. van der Kruit, *Astron. & Astrophys.* **13** (1970) 405
- [93] W. K. H. Petoskey and M. Phillips, *Classical Electricity and Magnetism*, (Addison-Wesley Publ. Co., Inc., Reading, MA 1956; see in particular Chapters 19 - 21
- [94] J. D. Jackson, *Classical Electrodynamics*, John & and Sons, Inc., New York, London, 1972; see in particular Chapter 17
- [95] F. Rohrlich, *Classical Charged Particles*, Addison-Wesley, Reading, MA, 1965, (see in particular Chapters. 6 and 9).
- [96] F. Rohrlich, *The Theory of the Electron*, The-first Joseph Henry lecture, read before the Society May 11, 1962. <http://philsoc.org/1962Sprin/1526transcript.html>.
- [97] P. A. M. Dirac, *Classical theory of radiating electrons*, Proc. of the Roy. Soc. London, Ser. A, Math. and Phys. Sci. **167** (1938) 148.
- [98] F. V. Hartemann, A.K. Kerman, *Phys. Rev. Lett.* **76** (1996) 624
- [99] A. Brynjolfsson, *Phil. Mag.*, Suppl. **6** (1957) 247